2005

Synthesis and characterization of nanostructured aluminas

Weihua Deng
Iowa State University

Synthesis and characterization of nanostructured aluminas

by

Weihua Deng

A dissertation submitted to the graduate faculty

in partial fulfillment of the requirements for the degree of

DOCTOR OF PHILOSOPHY

Major: Chemical Engineering

Program of Study Committee:
Brent H. Shanks, Major Professor
Kurt Robert Hebert
Dennis R. Vigil
Shang-Yi Victor Lin
Kristen P. Constant

Iowa State University

Ames, Iowa

2005

Graduate College
Iowa State University

This is to certify that the doctoral dissertation of

Weihua Deng

has met the dissertation requirements of Iowa State University

Signature was redacted for privacy.

Major Professor

Signature was redacted for privacy.

For the Major Program

Table of Contents

Abstract

In the work, mesoporous aluminas were produced by nonionic supramolecular templating and characterized to determine the stability of their physical structure during extended calcination at elevated temperatures. The effect of synthesis temperature on the physical structure of these materials and the resulting thermal evolution from synthesized aluminum hydroxide to transitional alumina was studied using thermogravimetric analysis. A high resolution multiple quantum magic angle spinning NMR spectroscopy method was used to determine quantitatively the evolution of the aluminum coordination during the thermal processing. The mesoporous alumina exhibited high stability upon prolonged heating, which is essential for their future applications in catalytic chemistry.

Using surfactant-mediated synthesis, aluminas with hierarchical nanopores were produced. The structures were found to be stable to the thermal removal of the surfactant. Synthesis factors affecting the morphology of hierarchically structured alumina material were discussed and a parameter space in which macropores could be obtained was determined. Based on the results from a parameter study and the similarity of the process to the macropore formation on anodized aluminum surface, a mechanism in which the interaction of water and aluminum alkoxide droplet played a important role was proposed to explain the structural organization for the material at multiple length scales.

Acknowledgements

First and foremost, I would like to express my sincere thanks to my major professor, Dr. Brent H. Shanks, for his encouragement, guidance, and support over my study and research in Chemical Engineering at Iowa State University.

To my committee members, Dr. Hebert, Dr. Vigil, Dr. Lin, and Dr. Constant, I thank you for your helpful discussion and services.

I am deeply grateful to my parents, my wife, Dongmei, and my daughter, Victoria, without whose love, encouragement and support, I could not have done this study.

I would also like to thank my group members, my friends who helped me and encouraged me these years.

Chapter 1. Introduction and Literature Review

1.1. Introduction

Catalysis is fundamental to the present technology for the manufacture, utilization and processing of crude oil and other chemical raw materials [1,2]. Heterogeneous catalysts frequently used in the petroleum refining operations are generally multi-functional catalysts where hydrogenation reactions occur on impregnated metal centers, whereas hydrogenolysis reactions involve interactions with the support and its acidic sites. The acidity function can be provided either by a zeolite, aluminum, or aluminosilicates, or their mixtures. The proper pore geometry and pore size distribution, together with an appropriate combination of hydrogenation and bond-breaking functions, are necessary to provide a catalyst with the appropriate sites and site accessibility, which is controlled by the pore size of the catalyst, for the desired hydrotreating properties such as activity, selectivity and stability [3,4].

Alumina is frequently used in the generic identification of any of the several crystalline forms of aluminum oxide (Al_2O_3), aluminum trihydroxide ($Al(OH)_3$), aluminum monohydroxide (AlOOH) and some aluminates. There are 27 materials referred to as "alumina" [5], which differ one form another in their crystalline and chemical structure. The properties of these forms are influenced both chemically and physically by the properties of precursor hydroxide forms and subsequent processing steps.

Under thermal treatment, different aluminum precursor hydroxides give different thermal evolution routes. Given in Figure 1-1 is a schematic description of the derivations

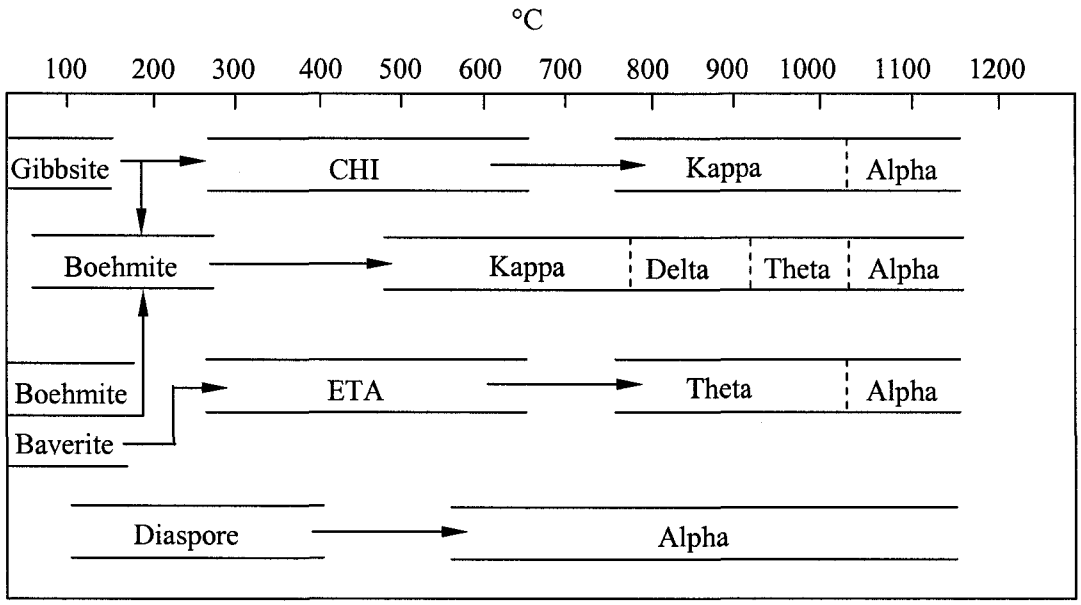

Figure 1-1. Transformation sequence for aluminum hydroxide precursors [6].

for the initial precursor alumina hydroxide forms. The γ-form of alumina, which has many catalytic applications, can be obtained from boehmite (aluminum monohydroxide) or pseudoboehmite by means of calcination. Subsequent transformations to δ-, θ-, α-form of alumina occur during additional thermal treatment. Although it transforms to boehmite under hydrothermal conditions, bayerite (aluminum trihydroxide) mainly changes to η-form of alumina and then θ-, α-form of alumina under calcination as shown in Figure 1-1.

Alumina has long been used in industry as a catalyst or catalyst carrier as well as an adsorption medium. Activated alumina, which refers to alumna with high surface area and high chemical activity, has been successfully used in many processes such as the dehydration of alcohol, petroleum hydrodesulfurization, the Claus reaction and the dehydrogenation of butane. Since the pore size of traditional alumina contains a significant range of micropores [7] and no well-defined pore structures exist, it is hard to extend the application of aluminas

to more reactions or the fields where molecular recognition (shape selective) of high-molecular-weight chemicals is desired. A major problem related to the use of traditional alumina catalyst is the deactivation by coke formation and pore plugging that hinder the diffusion of reactant and product in and out of catalyst pellets. It is well known that the larger the contribution of micropore to surface area and the wider the pore size distribution, the greater the enhancement in the deactivation rate. Therefore, the synthesis of mesoporous alumina with well-defined pore structure and narrow pore size distribution is of great industrial interest.

The invention of supramolecular templating technique [8,9] made it possible to improve the textural properties of traditional alumina and hence, extend its industrial applications. The focus of this work was the synthesis, characterization and morphology control of mesoporous alumina materials. Firstly, in this chapter, the literatures on the mesoporous material research started by Mobil scientists in 1992 are reviewed in a sequence of mesoporous silica, mesoporous alumina and morphology control of these materials. In Chapter 2, syntheses of mesoporous aluminas with desired physical properties using a nonionic templating methodology are described. Several factors affecting the properties of final products are discussed and moreover, characterization of thermal stability under elevated temperatures for the materials is presented.

Controlling particle morphology of mesoporous material provides not only opportunities to improve its diffusive properties and hence enhances mesopore accessibility, but also insights into the understanding of similar processes that are frequently observed in biomineralization. Using a surfactant mediating method, a hierarchically structured alumina that features the existence of regular arrays of macropores of several hundreds of nanometers

in size was synthesized. In Chapter 3, synthesis and characterization of a hierarchically structured alumina are presented. By investigating the effect of different reaction variables on the formation of this material, a parameter space in which the hierarchical structure could be obtained is determined.

Compared to the synthesis of hierarchically structured aluminas, elucidating the formation mechanism of the material is more difficult because of elusive properties and a high reactivity of aluminum tri-*sec*-butoxide – the aluminum precursor for the final products. It was found that the hierarchically structured aluminas even could be synthesized by hydrolyzing aluminum alkoxide solely in water without the assistance of surfactant and co-solvent. This indicates that formation of the hierarchical structure for the materials at macro length sale originates from an interaction between aluminum alkoxide and water. In Chapter 4, based on the experimental results from a parametric study and the similarity of this process to macropore formation on the surface of anodized aluminum, a formation mechanism is proposed to account for the structural organization of this material at both meso and macro length scales.

Finally, synthesis of a high-order hierarchically structured alumina by a nanoparticle assembly method is described in Chapter 5. This material, having well defined structures at three length scales, was the first one ever reported for the mesoporous alumina material. Its development provides new insights into the understanding of formation of hierarchically structured materials.

1.2. Supramolecular templating

According to the definition of IUPAC [10], the materials that are extensively used in catalysis and adsorption can be divided into two categories: microporous (pore size < 20Å) and mesoporous (20Å < pore size < 500Å) solids. Most of the shape-selective reactions used by the industry involve catalysts containing zeolite having pore size around 0.5nm. This size is sufficient to accommodate a broad spectrum of small molecules of industrial interest. However, the usefulness of current heterogeneous catalysts in processing high-molecular-weight hydrocarbons is limited by the pore size of the zeolite and by the pore geometry of the catalyst carrier. A considerable synthetic effort has been devoted to developing a framework with pore sizes within the mesoporous range, the largest pore diameter of synthesized zeolitic materials are in the range of 8-13Å [11], which is still within the microporous range.

In 1992, researchers [8,9] in Mobil used a new concept in the synthesis of porous material, which led to the first synthesis of well-defined mesoporous structures. They used surfactant molecule assembly, which was novel, as framework template instead of a single, solvated, organic molecule or metal ion (so called molecular templating) as the ones used for the synthesis of traditional zeolite. By using this supramolecular templating methodology, a family of mesoporous materials (called MCM) with well defined structures and adjustable pore size in the range of 16~100Å have been synthesized. In their procedure, 200g of a solution containing 26% of hexadecyltrimethylammonium ion, as $C_{16}H_{33}(CH_3)_3N^+$-OH/Cl (~30% hydroxide), were firstly mixed with 2g of Catapal Aluminum, 100g of TMA silicate solution (10% SiO_2, ratio of TMA/SiO_2 = 1), and 25g of precipitated silica (HiSil). The mixture was then put into a static autoclave at 150°C for 48 hours. After cooling to room

temperature, the solid product was retrieved by filtration, washed with water and dried in air at ambient temperature. The product then was subsequently calcined at 540°C for 1 hour in flowing nitrogen then 6 hours in flowing air. These materials had regular hexagonal arrays of uniform sized channels. The XRD patterns showed four peaks at low angle region that indexed on a hexagonal unit cell with a parameter of 4.5nm. The BET surface area for these materials was over 1000 m^2/g and the average pore diameter was about 4.0nm. There were several factors affecting the properties and structure pattern of the final product. Different synthetic conditions resulted in different structures such as hexagonal, cubic or lamellar phase. Changing the carbon chain length of the surfactant template, or adding swelling agent to the system, could alter the pore size of the MCM materials.

The supramolecular templating technique is based on the ability of surfactant molecules to form spherical or cylindrical micelles or even higher order phases in aqueous or nonaqueous solution. Surfactants are large organic molecules with a hydrophilic head and a long hydrophobic alkyl chain with variable carbon chain length. In order to reach the minimum energy configuration [12,13], these molecules aggregate their hydrophobic tails together and expose their hydrophilic heads to the aqueous solution. There is a dynamic equilibrium between the formed micelles and soluble surfactant molecules. The packing of surfactant molecules in solution is determined by several factors: the coulombic interactions between charged head groups, the tendency of alkyl chains to minimize their contact with water and maximize their organic interactions, and the solvation energies. A local effective surfactant packing parameter [12-14], g, which accounts for the first two interactions, is used to describe amphiphilic liquid crystal phases. It is defined as $g = V/a_o l$, where V is the total volume of the surfactant chains plus any co-solvent organic molecules between the chains, a_o

is the effective head group area on the surface of the surfactant micelle, and l is the kinetic surfactant tail length or the curvature elastic energy. If the value of g increases, phase transitions are expected in the order from cubic to hexagonal and finally to lamellar phase when g reaches 1.

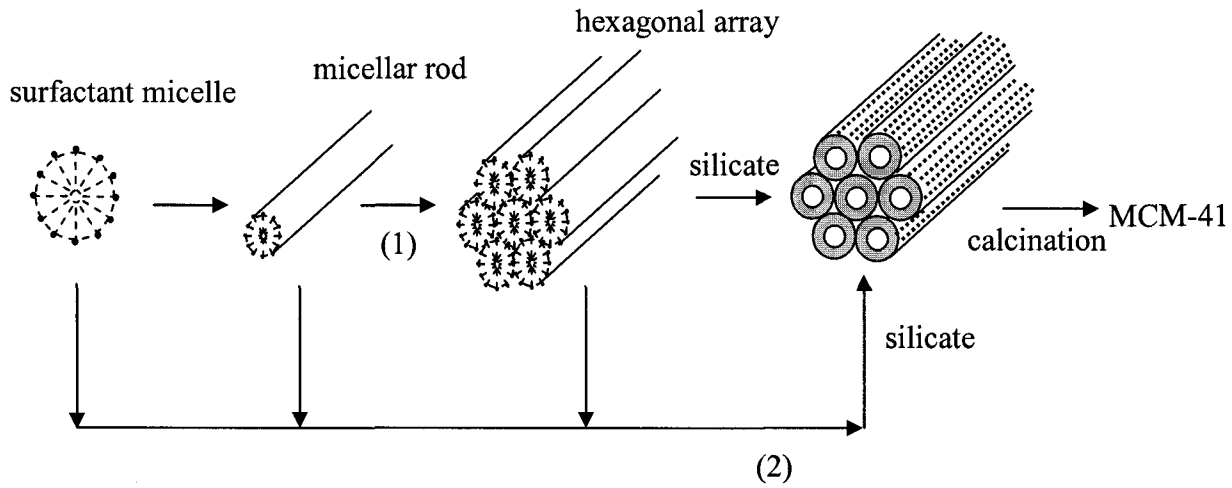

Figure 1-2. LCT mechanisms for the formation of MCM-41 [8].

The researchers in Mobil proposed two synthesis mechanisms [8,9] for the formation of the MCM materials. As shown in Figure 1-2, in the first mechanism, the surfactant hexagonal liquid crystal phase forms and directs the growth of the inorganic materials. The amine surfactant micelles aggregate into hexagonal arrays of rods. Silicate or aluminate anions present in the reaction mixture interact with the surfactant cationic head groups. Condensation of the silicate species on the outer surface of the formed surfactant rods leads to the formation of an inorganic polymer that mimics the original surfactant micelle shape. The surfactant removal process either by calcination or by solvent extraction leaves inorganic hollow cylinders with a hexagonal arrangement. However, Cheng et al. [15] found that the

hexagonal liquid crystal phase in the CTAB-water system at 25°C does not form unless the concentration of CTAB exceeds 40%. At low concentrations, only micelles exist in solution. In the second formation mechanism, the presence of silicate species in the reaction mixture induces the hexagonal ordering of surfactant micelles, which finally are the template for the mesoporous silica.

The invention of supramolecular templating technique stimulated the interest of synthesizing the mesoporous molecular sieves of a great array of metal oxides. Researchers used different methodologies of templating and structure-directing agents to modify the composition, pore structure and other properties of the products. The S^+I^- route originated by Beck and Kresge has been extended to S^-I^+, $S^+X^-I^+$ and $S^-M^+I^-$ synthesis routes [16]. In the S^-I^+ route, the products are synthesized by making use of the electrostatic force between a negatively charged surfactant (carboxylic acid, alkyl phosphates, etc.) and positively charged inorganic precursor. In the $S^+X^-I^+$ ($S^-M^+I^-$) route, the linkage of the template and the inorganic compound is mediated by a counterion such as Cl^-, Br^- (Na^+, K^+ in the $S^-M^+I^-$ route).

Hou et al. [16] conducted the first synthesis of mesoporous material in an acidic condition (pH < 2). The surfactants used were typically alkyltrimethylammonium ions, but species such as alkyldimethylamine, zwitterionic, and diametric quaternary ammonium ions were also found to be equally effective templates. It was speculated that the interactions between the cationic inorganic species and cationic organic species were mediated by the existence of halide ions in solution. The authors proposed a cooperative templating model to explain the formation of their materials. It consists of three steps that are not necessarily sequential. Firstly small silica oligomers compete for the cationic head groups of the

surfactant. The type of silica species present in the reaction mixture depends on the pH value of solution. At high pH, large silicate oligomers are completely ionized and are thus expected to bind to charged surfactant molecules. In contrast to the formation mechanism proposed by Chen et al. [17], this synthesis mechanism does not require the existence of rodlike surfactant micelles. The interface is quickly populated by tightly held silicate oligomers that act as multidentate ligands for the surfactant head groups. The second step is the silicate polymerization within the silicate-surfactant micelle interface. As the polymerization proceeds, the charge density within the inorganic wall decreases, and then may drive the rearrangement of the organic molecules, leading eventually to a phase transformation. In the early stage of the reaction, the presence of highly charged silica oligomer favors small surfactant head groups and a surfactant surface with a minimal curvature.

Tanev and Pinnavaia [18] demonstrated that neutral primary amine surfactant could also act as templates to direct the formation of mesoporous materials. In a typical synthesis, the silica source tetraethoxysilane (TEOS) was added to a solution of dodecylamine (DDA) in a mixture of ethanol and water. Then the resulted gellike mixture was allowed to age for 18 hours. This neutral templating route produced mesoporous silicas (denoted as HMS) with thicker pore walls, small scattering domain size. HMS materials had larger pore sizes compared to that of the MCM-41 materials, indicating that the surfactant owned a different conformation in the reaction. The authors proposed a neutral templating mechanism for the formation of their materials. Hydrolysis of silicate alkoxide in an aqueous solution of neutral amine surfactant yields a neutral inorganic precursor, which then binds to the outer surface of surfactant micelles through hydrogen bonding. This starts the formation of rodlike surfactant micelles. Further hydrolysis and condensation of the silanol groups produces the final short-

range order of hexagonal arrangement of inorganic species. Since most metals form alkoxide or neutral complexes suitable for hydrolysis and assembly as inorganic precursor, it is possible to synthesize mesostructures that are difficult to achieve by electrostatic templating methods. Furthermore, in this method, the template could be removed by solely solvent extraction since the hydrogen-bonding force is much weaker than the electrostatic force. This provided an environmentally benign and economically efficient method for the synthesis of mesoporous molecular sieves of metal oxides.

1.3. Synthesis of mesoporous aluminas

Many of the mesoporous metal oxides have been used successfully as catalysts, with the silicates and aluminosilicates receiving the most attention. For example, the silicates were used in oxidation, dehydroxylation and polymerization reactions [7]. At the same time, mesoporous materials offer great opportunities for other applications such as in separation, optoelectronics and selective adsorption. While there has been a lot of attention on the synthesis and application of silica-based mesoporous materials, there is a vacancy in the research of their alumina analogues. As mentioned before, alumina has many catalytic and noncatalytic applications in industry due to its unique surface chemistry and superb physical properties. Traditionally activated alumina is prepared by a precipitation method [19]. Its surface area is about 200 m^2/g, with textural porosity and a wide pore size distribution. It is of great interest to exploit the synthesis method of pure mesoporous aluminas with controllable pore size and narrow pore size distribution.

Huo et al. [16] tried the synthesis of mesoporous alumina materials by an electrostatic counterion-mediated method (the $S^-M^+I^-$ route). With $C_{15}H_{25}OPO_3H_2$ as the template and

$Al(NO)_3$ as the aluminum source, two lamellar mesophases: $[C_{15}H_{25}OPO_3]\cdot Al(OH)\cdot H_2O$ and $[C_{15}H_{25}OPO_3NaH]\cdot Al(OH)_3\cdot 7.5H_2O$ were synthesized under different pH conditions. The structure of the materials was investigated by ^{27}Al NMR. Both materials showed resonance signals with chemical shifts between 5 and –20 ppm relatively to $Al(NO)_3$ in aqueous solution indicating that all of the Aluminum atoms were octahedrally coordinated. Unfortunately, the as-synthesized products were not stable and collapsed upon surfactant removal during calcination process.

Yada et al. [20] synthesized mesoporous alumina by using a homogeneous precipitation method. With sodium dodecyl sulfate (SDS) as the template and aluminum nitrate monohydroxide as the aluminum source, a mesoporous alumina having hexagonally ordered structure was synthesized. The key for the synthesis was the use of urea as a pH modifier to generally change the acidity of the reaction mixture and hence, control the hydrolysis reaction rate. The mesostructure could not be maintained under a further surfactant removal by either thermal treatment or solvent extraction using ethanol or acetone. When the solid was aged in its mother solution for several days, however, the resulted material was reported to be more thermal resistant under a high temperature of 600°C.

Vaudry et al. [21] described a method of synthesizing pure alumina with mesoporosity and a narrow pore size distribution. Aluminum alkoxide was hydrolyzed by controlled amounts of water in low-molecular-weight alcoholic solvents. Carboxylic acids were used to obtain a self-assembled template phase on which the alumina condensed. The XRD patterns showed that, other than the intense peak at high d-spacing, four broad low-intensity peaks assignable to pseudoboehmite structure were found indicating the crystallinity of the material. The mesophases could be obtained over a variety of reaction conditions using

this aluminum alkoxide–alcohol-carboxylic acid system. The aging and hydrolysis reaction time seemed to have little effect on the formation of the material. Upon calcination, the mesoporous structure was maintained. Although they changed the alkyl chain length of the surfactant, the pore size couldn't be altered and was always centered at about 20Å, indicating that there was a different pore-size-controlling mechanism involved compared to that of the MCM materials.

Bagshaw et al. [22] reported a method to synthesize mesoporous alumina material by neutral templating. A copolymer consisting of a tri-block of polyethylene oxide (PEO) and polypropylene oxide (PPO) was used as a structure-directing agent. Aluminum alkoxide was hydrolyzed and condensed on the outer surface of surfactant micelle arrays due to the existence of a hydrogen bonding force between the organic and inorganic species. The BET results showed uniform pore size for the material, but no discernible long-range order was observed from its XRD patterns leading to the postulation of a "wormlike" pore motif. The material had surface areas in the range of 400-600 m^2/g and pore sizes in the range of 24-46Å. The authors claimed that this material did not have good thermal stability and subsequent work [23] has focused on the improvement of its thermal stability by incorporating rare earth elements into the framework of the mesoporous alumina molecular sieves.

Cabrera et al. [24,25] proposed a novel method to prepare mesoporous alumina material in which a "hydrolysis-retarding agent" was used. Instead of changing the alkyl chain length or adding auxiliary chemicals to control the pore size of mesoporous material, in their method, the pore size was controlled by carefully changing the ratio of water to "hydrolysis-retarding agent" such as triethanolamine (TEA). When aluminum alkoxide was

added to a mixture of water and triethanolamine, the corresponding atrane complex formed through transesterification of aluminum alkoxide. Since the resulting network of final product material is controlled by the aggregates in the precursor solution, the addition of hydrolysis-retarding reagent could change the hydrolysis rate by reducing the aluminum alkoxide species in solution. The authors claimed that the material had a wormlike pore structure and a highly interconnected pore system, and the pore size of the material could be mediated by a simple method. Their materials, however, had relatively poor textural properties with an irregular, sponge-like packing motif and wide pore size distribution.

Liu et al. [26] reported the synthesis of mesoporous alumina by hydrolyzing aluminum alkoxide in a solution of tartaric acid. The novelty of this method was the approach of changing the pore size. In the synthesis, the concentration of structure-directing agent (dibenzoyl-L-tartaric acid, DBTA) was used to tailor pore size of the materials. In a typical synthesis, 1g of aluminum alkoxide was hydrolyzed in 3.8g of water following by stirring for 30 minutes. Then the mixture was heated to 80-90°C for 30 minutes with stirring. 0.2g of HNO_3 was added to the mixture after it was cooled down to room temperature. The solution was mixed with DBTA solution in ethanol with stirring. Gelation occurred during drying process that was carried on at ambient temperature for a week. The XRD patterns of their materials showed a broad peak at low angle region. The intensity of this peak became stronger and the corresponding d-spacing increased toward to a high position. The wide angle XRD scans for the as-synthesized materials revealed the existence of a boehmite crystalline structure. The surface area of the materials was in the range of 386-425 m^2/g with pore volume around 0.5 cm^3/g. However, the pore size of this material could be altered only in a very small range of 33-42Å.

Ji et al. [27] synthesized high-surface-area aluminas by using aluminum tri-*sec*-butoxide-2,4-pentanedione-2-propanol-nitric acid precursors. The precursor solutions were prepared by dissolving aluminum tri-*sec*-butoxide (ASB) into *i*-PrOH together with acacH under magnetic stirring. Hydrolysis then started by adding HNO_3 solution or deionized water dropwisely to the solution. The resulting mixtures were then covered and agitated strongly until gelation occurred. An aging process was conducted at ambient temperature for 10 days. The crystallinity of the materials under different reaction conditions was investigated. It was found that the amorphous gels converted to γ-Al_2O_3 at 400-800°C and later to α-Al_2O_3 at 1000-1050°C. There were two successive surface area declines during the thermal treatment corresponding to the phase transformations. Mesoporous alumina could be obtained by calcining the starting xerogel.

Yao et al. [28] reported a novel sol-gel method for preparing alumina sol at room temperature with the assistance of ultrasound. Mesoporous alumina with narrow pore size distribution could be obtained by calcining the alumina sol at 550°C without adding any templates or other organic additives. XRD patterns of the alumina sol showed that the dominant phase of the material was pseudoboehmite, also known as gelatinous boehmite. Based on the existence of type IV adsorption/desorption isotherm plot and pore size distribution of the material, the authors claimed that mesoporous alumina was obtained by heating microporous alumina sols under certain temperatures. They speculated that the mesopores in the sample came from the packing of spherical γ-Al_2O_3 particle. Since the sizes of these spherical particles were uniform, mesopores that were basically interstitial voids between the nanoparticles had a narrow size distribution.

Recently, Hick and Pinnavaia [29] synthesized mesoporous boemite (AlOOH) using a nanoparticle assembly method. In a typical synthesis, aluminum tri-*sec*-butoxide was hydrolyzed by a solution of desired surfactant (for example, an amine surfactant) in a mixture of ethanol and deionized water at ambient temperature under vigorous stirring. The reaction mixture was allowed to age for 20 hours in a shaker bath either at ambient temperature or at 45°C. The fresh sample was retrieved by filtration, washed by water and ethanol. Low angle XRD patterns showed a characteristic peak between 1 and 3 degree of 2θ that could be assigned to a short-range ordering. During the aging process, there was a phase transformation from amorphous state to boehmite crystalline structure as detected by wide angle XRD for the samples having different reaction times. The authors speculated that mesoporosity of the material was created by the interstitial voids between boehmite nanapaticles whose size and intergrowth could be mediated by the surfactant. So basically there was no templating process involved in the formation of the mesoporous boehmite materials.

Although much effort has been devoted to developing synthetic routes for mesoporous alumina materials, the diversity and irreproducibility of the reported results suggest that there is significant progress required to obtain real control of a synthetic procedure for mesoporous alumina with tunable pore size, good thermal and chemical stability, and narrow pore size distribution.

1.4. Thermal stability of mesoporous alumina

Thermal stability is a critical property for mesoporous alumina material both in their preparation and applications. Some researchers have synthesized mesoporous aluminas

[16,20], but the materials could not withstand high temperature during the calcination process. Thermal stability of mesoporous alumina during calcination has also been investigated by Bagshaw and Pinnavaia [22], Vaudry et al. [21] and Cabrera et al. [24], the mesostructure of their materials could be maintained after the template removal by calcination. In addition to the thermal stability during calcination, the structural stability upon elevated heating (especially of interest is the temperature range of 500-800°C) is important when the materials are to be applied in catalysis. However, no reports related to this subject were found so far.

During thermal treatment, different aluminum hydroxides yield different thermal evolution routes. For example, gibbsite is dehydroxlated to transitional alumina (η-form) at about 300°C, while dehydroxylation of boehmite or pseudoboehmite to transitional alumina (γ-form) requires about 475°C [6]. In a typical sol-gel process [30], aluminum hydroxide derived from the hydrolysis of aluminum alkoxide gives bayerite or gibbsite structures when the reaction temperature is below 80°C and otherwise boehmite structure. The process for these aluminum hydroxide precursors to transform to transitional alumina coincides with structural as well as aluminum coordination changes in the alumina. The interrelationship between structural stability during elevated temperature treatment and the coordination states of aluminum has not reported for mesoporous alumina material.

1.5. Morphology control of mesoporous materials

Other than framework mesoporosity, which have been investigated extensively in numerous of reports, there exist textural mesoporosity and macroporosity that can also be very important in the utilization of porous materials. Textural mesoporosity is essentially the

porosity arising from noncrystalline intraaggregate voids and spaces formed by interparticle contact. Using fundamental particles as building blocks, morphologies of mesoporous materials at higher level of length scale could be constructed. Since the resulting materials have more than one level of well-defined structures, they can be called "hierarchically ordered materials". In the application of mesoporous materials, it would be useful to produce particles that have well-defined structure at the length of macroscale. For example, macroporosity upon the mesopores in the catalyst could facilitate diffusion of molecules into or out of the mesopores in which the reaction occurs.

The macroscale (0.1-10μm) morphology control of mesoporous silica material has received a great deal of attention recently. Schacht et al. [31] reported that macroscale morphology control could be achieved by using the oil-water (e.g. *n*-hexane-water system) interface in emulsified mixtures. Hollow mesoporous silica spheres with diameters of 1 to 100μm were synthesized by this method. The proposed mechanism speculated that the template for macrostructure was the emulsified oil-droplet, while nanometer-scale self-organized surfactant assembly controlled the mesostructures. In an acidic environment, tetraethoxysilane (TEOS) was dissolved in the oil droplets, hydrolyzed at the oil-water interface and then formed macrostructures, which reflected the size and shape of the oil droplets at a larger length scale.

Pauly et al. [32] investigated the importance of surfactant emulsions in controlling the mesopores of hierarchically ordered material where co-solvents were applied. The polarity of the solvent was correlated directly with the volume ratio of water to organic phase and the intensity of emulsion. When there was no emulsion in solution, the synthesized products were micrometer-sized monolithic particles. However, if the synthesis conditions were

changed such that a surfactant emulsion formed, the resulting mesoporous silica particles contained textural mesoporosity of about 50nm in size. The authors speculated that the fundamental particles, which were about 200nm in size, aggregated during the synthesis. Since the interstices of the fundamental particles were randomly distributed, the resulting macropores did not have well-defined structure although they could be measured from adsorption/desorption isotherm plot for the resulted material.

Lin et al. [33] reported a method to achieve "tubules in tubules " hierarchically ordered structures for the mesoporous silica material. The final products were small hollow tubules with 0.3 to 3μm in diameter. The walls of these tubules were mesoporous, and had the same well-defined structure as that of the MCM-41 material. Initially the solution was basic and the silicate-surfactant system was close to the lamellar-hexagonal phase boundary. A subsequent acidification step led to the condensation of silicate and a charge imbalance on the organic-inorganic interface, which favored the curvature of the interface along the transrod direction. The overall effect of neutralization was to bend the formed membrane completely into tubules with uniform size. The authors pointed out that two experimental factors were crucial to the formation of the hollow microtubules: the ratio of surfactant to water in the reaction mixture and the delayed slow neutralization process.

Other researchers [34,35,36] have reported their work on the macroscale morphological control of silica-based mesoporous materials. Particle morphologies with sphere, fiber or rod-like shape have been realized. Compared to particle morphology control of mesoporous silica material, however, less attention has been received by the fabrication of hierarchical structure of alumina material. Part of the reason is due to a high reactivity and

elusive chemical properties of aluminum alkoxide, which is usually a precursor of final mesoporous alumina material.

Luo et al. [37] reported the synthesis of nanometer-sized mesoporous alumina spheres. These spheres, with an average diameter of about 400nm, were produced by hydrolyzing aluminum tri-*sec*-butoxide by a surfactant solution in a mixture of water and acetonitrile. The whole process was catalyzed by aqueous ammonia or hydrochloride. Low angle XRD and BET data validated the mesoporosity of the resulted material. After calcination at 550°C in flowing air, morphology of the alumina spheres could be maintained but with a slight contraction in size. ^{27}Al NMR spectra showed that most of aluminum species for as-synthesized mesoporous alumina spheres were in octahedrally coordinated environment, however, both octahedral and tetrahedral aluminum were observed after calcination at 550°C showing a structure rearrangement occurred during the calcinations process. Unfortunately, the authors did not give any explanation on the formation mechanism for this hierarchically structured alumina.

It has been of more interest to synthesize hierarchically structured materials, however, the scarcity and diversity in methodologies and proposed mechanisms for the formation of those materials show that there is still a significant amount of work required to achieve a real control of macroscale morphology for mesoporous materials. To date, there have been only a few reports on the hierarchical morphology control for mesoporous alumina material. Reports on mesoporous alumina produced by supramolecular templating have focused on the mesoporous level such as pore size adjustment and other properties such as thermal stability. Most mesoporous aluminas produced by either nonionic or electrostatic templating methods typically yield macroscale particles of fairly random shape.

Reference

1. Anon., *Fed. Reg.* 57 (130) 1992.
2. Anon., *Catalysis looks to the future*, National Academy Press, Washington, DC, 1992.
3. D. E. W. Vaughan, *Industrial Uses of Zeolite Catalysts, Properties and Applications of Zeolites*, The Chemical Society, Burlington House, London, 1980.
4. J. Scherzer and A. Gruia, *Hydrocracking Science and Technology*, Marcel Dekker, Inc. New York, 1996.
5. G. Maczura, K. P. Goodboy, J. T. Koenig, *Aluminum oxide, Kirt Othmer Encyclopedia of Chemical Technology*, Vol.2, pp. 218-224, 3rd edition. Weily, New York, 1978.
6. Karl Wefers, Chanakya Misra, *oxide and hydroxide of Aluminum*. Alcoa Technical Paper No. 19, 1987.
7. R. K. Oberlander, in: B. E. Leach (Ed), *Applied Industrial Catalysis* Vol. 3, Academic Press, London, 1984, p63.
8. C.T. Kresge, M. E. Leonowicz, W. J. Roth, J. C. Vartuli, and J. S. Beck, *Nature* 359 (1992) 710.
9. J. S. Beck, J. C. Vartuli, W. J. Roth, M. E. Leonowicz, C.T. Kresge, K. D. Schmitt, C. T-W. Chu, D. H. Olson, E. W. Sheppard, S. B. McCullen, J. B. Higgins, and J. L. Schlenker, *J. Am. Chem. Soc.* 114 (1992) 10834.
10. IUPAC *Manul of Symbols and Terminology*, Appendix 2, Part 1, Colloid and Surface Chemistry, Pure Appl. Chem. 31 (1972) 578.
11. R. M. Dessau, J. L. Schlenker, J. B, Higgins, *Zeolites* 10 (1990) 522.
12. J. Israelachvili, *Colloids Surf. A: Physiocochem. Eng. Aspects* 91 (1994) 1.

13. H. T. Davis, *Colloids Surf. A: Physiocochem. Eng. Aspects* 91 (1994) 9.

14. J. N. Israelachvili, D. J. Mitchell, and B. W. Ninham, *Biochim. Biophys. Acta* 470 (1977) 185.

15. C, F. Cheng, H. He, W. Zhou, and J. Klinowski, *Chem. Phys. Lett.* 244 (1995) 117.

16. Q. Huo, D. I. Margolese, U. Ciesla, D. J. Demuth, P, Feng, T. E. Gier, P. Sieger, A, Firouzi, B. F. Chmelka, F. Schuth, and G. D. Stucky, *Chem. Mater.* (1994) 1176.

17. C-Y. Chen, S. L. Burkett, H-X. Li, and M. E. Davis, *Microporous Mater.* 2 (1993) 27.

18. T. P. Tanev, T. J. Pinnavaia, *Science* 267 (1995) 865.

19. R. K. Oberlander, in: B. E. Leach (Ed), *Applied Industrial Catalysis* Vol. 3, Academic Press, London, 1984, p80.

20. M. Yada, M. Machida, T. Kijima, *J. Chem. Soc.,Chem. Commun.* (1996) 769.

21. F. Vaudry, S. Khodabandeh, M. E. Davis, *Chem. Mater.* 8 (1996) 1451.

22. S. A. Bagshaw, T. J. Pinnavaia, *Angew. Chem. Int. Ed.* 35 (1996) 1102.

23. W. Zhang, T. J. Pinnavaia, *Chem. Conmun.* (1998) 1185.

24. S. Cabrera, J. E. Haskouri, J. Alamo, A. Beltrán, D. Beltrán, S. Mendioroz, M. D. Macros, P. Amorós, *Adv. Mater.* 5 (1999) 371.

25. S. Cabrera, J. E. Haskouri, C. Guilem, J. Latorre, A. Beltrán-porter, M. D. Marcos, and P. Amorós, *Solid State Sciences* 2 (2002) 405.

26. X. Liu, Y. Wei, D. Jin, W. Shih, *Mater. Lett.* 42 (2000) 143.

27. L. Ji, J. Lin, K. L. Tan, and H. C. Zeng, *Chem. Mater.* 12 (2000) 931.

28. N. Yao, J. Xiong, Y. Zhang, M. He, W. Yang, *Catalysis Today*, 68 (2001) 97.

29. R. W. Hicks, T. J. Pinnavaia, *Chem. Mater.* 15 (2003) 78.

30. B. Yadas, *J. Appl. Chem. Biotechnol.* 23 (1973) 803.

31. S. Schacht, Q. Huo, I. G. Voigt-Martin, G. D. Stucky, F. Schűth, *Science* 273 (1996) 768.

32. T. R. Pauly, Y. Liu, T. J. Pinnavaia, S. J. L. Billinge, T. P. Rieker, *J. Am. Chem. Soc.* 121 (1999) 8835.

33. H. Lin, C. Mou, *Science* 273 (1996) 765.

34. Q. Cai, Z. Luo, W. Pang, Y. Fan, X. Chen, F. Cui, *Chem. Mater.* 13 (2001) 258.

35. Q. Huo, J. Feng, F. Schűth, G. D. Stucky, *Chem. Mater.* 9 (1997) 14.

36. Q. Huo, D. Zhao, J. Feng, K. Weston, S. K. Buratto, G. D. Stucky, S. Schacht, F. Schűth, *Adv. Mater.* 9 (1997) 974.

37. Q. Luo, Z. Xue, D. Zhao, in *Studies in Surface Science and Catalysis* (Edt. A. Sayari e al.) Vol. 129, P37.

Chapter 2. Characterization of Mesoporous Alumina Molecular Sieves Synthesized by Nonionic Templating

2.1. Introduction

Aluminas are extensively used in catalyst, catalyst support, and adsorption applications [1], thus control of their surface area and pore size distributions has received a great deal of attention. The advent of the supramolecular templating method [2,3] for synthesizing mesoporous molecular sieves from metal oxides holds promise for producing high surface area aluminas with narrow pore size distributions in the mesoporous range. Unfortunately, the synthesis of such materials has proven to be more problematic than their silica-based analogues. Nonetheless, a wide-range of synthesis procedures [4-10] has now been reported for templating mesoporous aluminas including both nonionic and electrostatic assembly mechanisms. Of particular importance is the thermal stability of the resulting materials. Previous reports have generally discussed thermal stability with respect to the template removal process. However, the ability to maintain the surface area and pore structure upon prolonged heating is of critical importance for the catalytic applications.

Thermal stability of standard alumina supports has been examined relative to the phase of aluminum hydroxide precursor and the particle size. For example, the thermal evolution of an alumina initially synthesized as gibbsite differs from one with a boehmite precursor. Gibbsite will dehydroxylate to transitional alumina (η-form) at about 300°C, while dehydroxylation of boehmite to transitional alumina (γ-form) requires about 475°C [11]. This thermal stability behavior has been studied as well for sol-gel derived aluminas [12]. Sol-gel

derived aluminum hydroxides synthesized below 80°C gave gibbsite or bayerite structures with dehydroxylation to transitional alumina occurring at 320°C, as shown by TGA experiments. Synthesis above 80°C resulted in the boehmite structure with subsequent dehydroxylation to transitional alumina at 500°C. The transformation to transitional alumina, which is an important form for catalytic and adsorption processes, coincides with structural as well as aluminum coordination changes in the alumina.

The interrelationship between structural stability and coordination of aluminum has not been established for mesoporous alumina molecular sieves. In this work we examine and characterize the thermal stability of mesoporous aluminas synthesized using the nonionic templating method of Bagshaw and Pinnavaia [5]. The focus of the thermal stability is the prolonged heating at temperatures that would be required in many catalytic applications. The effect of synthesis temperature on the mesoporous alumina properties is also presented. Changes in aluminum coordination in the materials were monitored using the high resolution multiple quantum magic angle spinning (MQMAS) NMR method [13], which also allows for quantification of aluminum in each coordination state.

2.2. Experimental

2.2.1. Synthesis

The reagents used were aluminum tri-*sec*-butoxide (Aldrich), reagent-grade *sec*-butanol (Fisher Scientific), and Pluronic L64 (BASF). Pluronic L64 is a polyethylene oxide/ polypropylene oxide tri-block copolymer ($[PEO]_{13}[PPO]_{30}[PEO]_{13}$) commonly used in surfactant applications. The synthesis procedure used was the nonionic templating method described by Bagshaw and Pinnavaia [5]. A mixture of deionized water and *sec*-butanol was

slowly added to a solution of aluminum tri-*sec*-butoxide and Pluronic L64 in *sec*-butanol (the overall reaction stoichiometry was 0.1: 1.0: 2.0 for surfactant: Al: water). The resulting gel-like mixture was held at the desired synthesis temperature for 16 hours. The powder was removed by centrifugation, washed by ethanol and subsequently dried in air for a day and at 100°C for 6 hours. A standard initial calcination was performed at 500°C for 4 hours in flowing air (ambient air with a low flow rate). The resulting powder was split into four samples and received a final 2 hour calcination at 500, 600, 700, and 800°C, respectively. Long-term stability of the aluminas was investigated by extended calcination at 650°C. For all calcinations, a temperature ramp rate of 5° C/min from room temperature to the desired temperature was used. The nomenclature used for the samples is SB-X-T where X represents the synthesis temperatures with 0, 1, 2, and 3 corresponding to 25, 50, 70 and 90°C, respectively, and T is the final calcination temperature.

2.2.2. Characterization

Powder X-ray diffraction (XRD) patterns were acquired by a X_1 advanced diffraction system (Scintag, Inc.) using a CuK_α radiation source (λ = 0.154nm). Low angle diffraction with a 2θ range of 0.5-10° was used to investigate the long-range order and wide angle scans were performed at a 2θ range of 5-85° to validate the amorphous state of the alumina. Surface area (SA) and median pore diameter (MPD) were measured using a Micromeritics ASAP 2000, with SA determined by the Brunauer-Emmett-Teller (BET) method and pore volume (PV) and pore size distribution by the Barrett-Joyner-Helenda (BJH) method. Sample preparation included degassing at 90°C for 1 hour and then at 150°C for 4 hours. TGA and

DTG curves were recorded using a Perkin Elmer TGA7 thermogravimetric analyzer with a temperature ramp rate of 5°C/min.

The NMR spectra were recorded on a Chemagnetics Infinity 400 spectrometer using a 3.2-mm MAS probe and a sample rotation rate of 20 kHz. The MQMAS experiments used the z-filter scheme [14] with the RF fields of ~200 kHz and 17 kHz during the nonselective and selective pulses, respectively. The ^{27}Al spectra reported in this work use the δ scale, with positive values downfield, and are referenced to aluminum nitrate aqueous solution.

2.3. Results and discussion

Shown in Table 2-1 are the surface area (SA), median pore diameter (MPD), and pore volume (PV) of aluminas synthesized at 25°C and calcined over the range of calcination conditions. The nitrogen adsorption/desorption isotherm plots were of the Type H1 [15] reported previously for templated mesoporous aluminas [5-9]. SB-0 was synthesized under conditions like those described by Bagshaw and Pinnavaia [5] for MSU-3. While the surface area was similar for these two materials, the median pore diameter and pore volume of SB-0 were considerably higher than the 2.4 nm and 0.21 cc/g, respectively, reported for MSU-3. Low angle XRD patterns for SB-0 in both the as-synthesized and initial calcined forms are shown in Figure 2.1. The peaks characteristic of templated mesoporous aluminas having "wormlike" pores are evident at 2θ between 1-3° [5,7,8,10]. The intensity of this peak increased for the calcined sample, which is consistent with the removal of the template. Wide angle XRD gave no discernable structure indicating that the alumina in the mesoporous powders was amorphous.

The calcination results for the SB-0 series showed that the initial treatment at 500°C was not adequate to stabilize the surface area of the mesoporous alumina. The additional 2 hour calcination at 500°C further reduced the surface area from 470 to 390 m^2/g. Increasing the final calcination time beyond 2 hours did not lead to a further decrease in surface area. In addition, the use of a higher final temperature only led to a small further decrease in surface area and no significant change in the median pore diameter or pore volume. Therefore, SB-0 does appear to be thermally stable as long as an overall calcination time of at least 6 hours at 500°C is employed.

The thermal stability of SB-0 was further probed by examining the stability of the physical properties during more extended heat treatment at 650°C. For this test, SB-0 was treated with an initial 4 hour calcination at 500°C. The SB-0 sample was then split into four portions, which were subsequently calcined for additional 2, 12, 22, and 32 hours. As can be seen in Figure 2-2, no significant change in the surface area or median pore diameter was observed during the extended heating. This result combined with the information given in Table 2-1 shows that a mesoporous alumina synthesized by the nonionic templating method is structurally stable for template removal and prolonged heating at elevated temperatures.

In aluminas produced by the sol-gel method, the synthesis temperature influenced the thermal stability of the resulting aluminas [12,16]. This difference in stability was due to the particular aluminum hydroxide phase formed during the synthesis. To examine whether a temperature effect exists in the templated aluminas, the set of experiments discussed above was replicated using higher synthesis temperatures. Shown in Table 2-2 is a comparison of aluminas synthesized at 25, 50, 70, and 90°C. The samples compared are those with an initial

4 hour calcination at 500°C and final 2 hours at the calcination temperature given in the table. As can be seen from the table, the synthesis temperature was not significantly correlated with the final surface area (replicate of syntheses gave a standard deviation of about 30 m^2/g). However, the PV of the resulting aluminas was found to decrease with increasing synthesis temperature. Shown in Figure 2-3 is the relationship between MPD and synthesis temperature at each calcination condition. Clearly, the synthesis temperature has a more significant impact on the MPD than do the calcination conditions in the range of 500-800°C. Shown in Figure 2-4 is a comparison of the pore size distribution for SB-0-600 and SB-3-600. Both aluminas have unimodal pore size distributions with the pores shifted to smaller diameters at higher synthesis temperature. Since the pore size distributions are similar for the aluminas, the medium pore diameter can be used to compare the geometric trends of the samples, where SA = 4PV/D. This relation appears to hold for the alumina physical property data given in Table 2-2 and Figure 2-3, indicating that the measured surface areas are consistent with the calculated geometrical surface areas for the samples.

It has been shown that Pluronic L64 micelles induced by water in xylene can form a structure in which water is present in the micellar core [17]. Pluronic L64 in water is also known to have a lower critical solution temperature, which leads to the formation of two immiscible phases at increasing temperatures [18]. Therefore, the decrease in MPD and PV with increasing synthesis temperature could be due to structural changes in the surfactant micelle. At lower synthesis temperatures the micelle may contain water in the core leading to a larger micelle. As the synthesis temperature is increased, the presence of water in the micelle core would be increasingly thermodynamically unfavorable leading to a reduction in the micelle diameter.

The XRD patterns for the samples synthesized at higher temperatures share the same patterns as those of SB-0 (shown in Figure 2-1). Therefore, the synthesis temperature does not appear to impact the distance between the pores or the long range order of the aluminas. As shown in Figure 2-2, SB-3 demonstrates similar stability to extended thermal treatment as was observed for SB-0.

The above results demonstrate that thermally stable templated mesoporous aluminas can be produced for a range of synthesis temperatures using the nonionic templating method. However, these results do not define the impact of synthesis temperature on the chemical state of the aluminum hydroxide precursor and the subsequent heat-treated alumina. For aluminas produced by standard precipitation or by the sol-gel process, the synthesis temperature affects the synthesized aluminum hydroxide precursor. In sol-gel studies, hydrolysis of aluminum alkoxides below 80°C yielded aluminum trihydroxides upon aging, whereas hydrolysis above 80°C yielded aluminum monohydroxides [12,16]. Similarly, it has been shown that the thermal treatment of these materials produces different transitional aluminas with different aluminum coordination content [19-21]. For example, dehydration of the aluminum trihydroxide, bayerite, commencing at 325°C led to η-Al_2O_3. The relative ratio of octahedrally to tetrahedrally coordinated aluminum in the η-Al_2O_3 was 1.9. In contrast, the aluminum monohydroxide, boehmite, dehydration began at 500°C with the resulting γ- Al_2O_3 having an octahedral to tetrahedral aluminum coordination ratio of 3. The connection between hydrolysis temperature and aluminum coordination and subsequent effect on thermal stability in the calcined mesoporous aluminas has not been previously examined.

Earlier studies used single quantum magic angle spinning (MAS) NMR to quantify the populations of the aluminum coordination sites in alumina. A disadvantage of this

method is the need to de-convolute the ^{27}Al MAS NMR spectra, which cannot be done in an unambiguous manner due to strong overlap of various resonances, especially when 4-, 5-, and 6-coordinated Al sites coexist in the sample. In this work, the measurement of the coordination of aluminum was performed using MQMAS NMR, which provides high resolution (isotropic) spectra of half-integer quadrupolar spins [13]. The technique averages out the second order quadrupolar broadening in these nuclei, while retaining the isotropic shifts (chemical and quadrupolar) that discriminate between chemically inequivalent sites.

However, the MQMAS efficiency depends on the magnitude of the quadrupole splitting, which, in turn, varies with the crystallite orientation in a powdered sample. This causes distortions in the anisotropic dimension of the spectrum. The relative intensities observed along the isotropic dimension are also skewed, as the same mechanism is responsible for uneven excitation of different sites in a sample. For spin-3/2 nuclei, several strategies have been proposed to remedy this problem, which involve numerical simulations of the MQMAS spectra [22-24], as well as excitation and conversion schemes that are less sensitive to the magnitude of the quadrupole splitting [25,26]. For ^{27}Al nuclei, which have a spin of 5/2, we used the strategy that allows for quantitative analysis of various sites via numerical renormalization of the MQMAS spectra. This requires propagating the spin density matrix under the effects of MAS and a non-commuting Hamiltonian that includes the quadrupolar and chemical shift interactions and appropriately accounts for the radio frequency pulses. The input parameters for the calculations are obtained by careful calibration of the RF fields used during the experiment and by on-line evaluation of the quadrupolar and chemical shifts corresponding to the centers of gravity of the MQMAS line shapes for different sites.

Figure 2-5 shows examples of MQMAS spectra for as-synthesized SB-0 and SB-0-600. The as-synthesized SB-0 consisted predominantly of octaherally coordinated Al with only a small amount of Al in tetrahedral coordination. Calcination led to a significant change in Al coordination as evidenced by SB-0-600 spectra. The resonances from 4-, 5- and 6-coordinated Al sites (Al^{IV}, Al^{V}, and Al^{VI}) overlap in the MAS (anisotropic) dimension (ν_2) where the (scaled) second order quadrupolar interaction is operable. In the isotropic dimension (ν_1), the resolution is governed by the distribution of chemical and quadrupolar shifts in the sample. However, the three sites become separated in the two-dimensional spectrum allowing for subsequent quantification.

Shown in Table 2-3 are the quantified populations of aluminum sites in the SB-X-T samples. As seen from the table, the synthesis temperature has no apparent affect on the aluminum coordination in the aluminas. The ratio of Al^{VI}/Al^{IV} sites was about 2.2 for most of the samples. Therefore, the mesoporous aluminas, which have amorphous alumina walls, have Al^{VI}/Al^{IV} ratios between that of the transitional alumina phases γ- Al_2O_3 and η-Al_2O_3. It is interesting to note that the SB-X-600 powders appear to have lower Al^{VI}/Al^{IV} ratios than the other samples perhaps indicating a slight structural rearrangement occurring during the calcination at 600°C. The most apparent trend from the data is the decrease in population of coordinatively unsaturated Al^{V} sites with increasing calcination temperature. These sites have been speculated to be a source of Lewis acidity in transitional aluminas [27, 28]. While being affected by calcination temperature, the population of the Al^{V} sites was not dependent on the synthesis temperature.

TGA experiments were used to examine the thermal evolution of the templated aluminas. Shown in Figure 2-6 are the TGA and DTG curves for SB-0 and SB-3 taken under

the flow of nitrogen. The curves for SB-1 and SB-2 (not shown) lay between those for SB-0 and SB-3. While the curves have similar shapes, the amount of weight loss is significantly higher for SB-0 than SB-3. The small weight loss at about 100°C can be attributed to removal of residual physisorbed water. No significant weight loss was observed above 500°C, so the weight loss occurring between 200 and 500°C in both samples must include template removal and dehydroxylation. Unfortunately, these experiments do not allow for resolution of the different weight loss phenomena.

Shown in Figure 2-7 are the TGA and DTG curves for SB-X taken using air flow instead of nitrogen. The use of air in the experiment provided better resolution of the weight loss events during the heat treatment. The DTG curves for SB-2 and SB-3 give three weight loss regions. Initiating at 100°C is a weight loss due to the desorption of physisorbed water. The large weight loss beginning at 190°C is the removal of the surfactant template and the final weight loss, with maximum rate at about 300°C, is due to the dehydroxylation of the alumina. The location of the template weight loss was verified by a TGA experiment in flowing air with only Pluronic 64L, which gave combustion of the surfactant between 190 and 230°C with a maximum rate at about 210°C.

The DTG curves for SB-0 and SB-1 have the same three weight loss regions occurring at similar temperatures as seen with SB-2 and SB-3, but they have an additional weight loss initiating at about 150°C. It is important to note the magnitude of the third weight loss in SB-0 is similar to that of the second peak in SB-3. Due to the location and magnitude of the weight loss, this third peak is again assigned to the removal of the surfactant template. The additional peak at 150°C may be attributed to the removal of water that was present

within the core of the surfactant micelle. As discussed above, the presence of water within the micelle core is known for this type of system in the absence of the inorganic species used in the current study. The lower critical solution temperature phenomena for Pluronic 64L in water would be consistent with why this water attributed peak is not observed for the higher synthesis temperature. Therefore, the TGA results appear to lend support to the proposed mechanism for the decreasing MPD and PV with increasing synthesis temperature.

The weight loss due to dehydroxylation of the aluminas occurs at the same temperature for each of the aluminas with a maximum rate at about 300°C. The overall weight losses during this period are about 14% for SB-0 and 15% for SB-3. If the as-synthesized materials were aluminum monohydroxide the dehydroxylation reaction would be given by:

$$2AlOOH \rightarrow Al_2O_3 + H_2O$$

The expected weight loss would be 15%. In contrast, formation of the aluminum trihydroxide would result in a weight loss of about 35% upon dehydroxylation to transitional alumina. The agreement between the observed weight loss and the stoichiometric value strongly supports the conclusion that all of the alumina powders produced in this work were in the aluminum monohydroxide form when synthesized. As such, the thermal evolution of the aluminum hydroxides to transitional aluminas is independent of synthesis temperature.

2.4. Conclusions

The physical structure of mesoporous aluminas synthesized using a nonionic templating method was found to be thermally stable not only to template removal, but also to

prolonged heating at elevated temperature. Therefore, these aluminas would be able to maintain their unique structural features in fairly demanding catalyst preparations and catalytic applications. Unlike sol-gel derived aluminas, the synthesis temperature used for the hydrolysis and condensation of the aluminum alkoxide did not affect the resulting thermal evolution from the aluminum hydroxide to transitional alumina and the subsequent thermal stability of the transitional alumina. This consistency of thermal behavior across the range of synthesis temperatures was confirmed by quantitative characterization of the aluminum coordination using MQMAS NMR. The only observed effect of synthesis temperature was the impact on median pore diameter and pore volume. This structural effect can be attributed to the thermal response of the surfactant/solvent system used in the synthesis.

References

1. R. K. Oberlander, in: B. E. Leach (Ed), *Applied Industrial Catalysis* Vol. 3, Academic Press, London, 1984, p63.
2. C.T. Kresge, M. E. Leonowicz, W. J. Roth, J. C. Vartuli, J. S. Beck, *Nature* 359 (1992) 710.
3. J. S. Beck, J. C. Vartuli, W. J. Roth, M. E. Leonowicz, C.T. Kresge, K. D. Schmitt, C. T-W. Chu, D. H. Olson, E. W. Sheppard, S. B. McCullen, J. B. Higgins, J. L. Schlenker, *J. Am. Chem. Soc.* 114 (1992) 10834.
4. T. P. Tanev, T. J. Pinnavaia, *Science* 267 (1995) 865.
5. S. A. Bagshaw, T. J. Pinnavaia, *Angew. Chem. Int. Ed.* 35 (1996) 1102.
6. W. Zhang, T. J. Pinnavaia, *Chem. Conmun.* (1998) 1185.
7. F. Vaudry, S. Khodabandeh, M. E. Davis, *Chem. Mater.* 8 (1996) 1451.
8. S. Cabrera, J. E. Haskouri, J. Alamo, A. Beltrán, D. Beltrán, S. Mendioroz, M. D. Macros, P. Amorós, *Adv. Mater.* 5 (1999) 371.
9. X. Liu, Y. Wei, D. Jin, W. Shih, *Mater. Lett.* 42 (2000) 143.
10. S. Valange, J.-L. Guth, F. Kolenda, S. Lacombe, Z. Gabelica, *Microporous Mesoporous Mater.* 35-36 (2000) 597.
11. Karl Wefers, Chanakya Misra, *Oxide and Hydroxide of Aluminum. Alcoa Technical Paper* No.19, 1987.
12. R. I. Zakharchenya, T. N. Vasilevskaya, *J. Mater. Sci.* 29 (1994) 2806.
13. L. Frydman, J. S. Harwood, *J. Am. Chem. Soc.* 117 (1995) 5367.
14. J.-P. Amoureux, C. Fernandez, S. Steuernagel, *J. Magn. Reson.* A123, (1996) 116.

15. K. S. W. Sing, D. H. Everett, R. A. W. Haul, L. Moscou, R. A. Pierotti, J. Rouquérol, T. Siemieniewaka, *Pure & Appl. Chem.* 57 (1985) 603.

16. B. Yoldas, *J. Appl. Chem. Biotechnol.* 23 (1973) 803.

17. B. Chu, *Langmuir* 11 (1995) 414.

18. Z. Zhou, B. Chu, *Macromolecules* 27 (1994) 2025.

19. C. S. John, N. C. M. Alma, G. R. Hays, *Applied Catalysis* 6 (1983) 341.

20. T. H. Walter, E. Oldfield, *J. Phys. Chem.* 93 (1989) 6744.

21. C. Pecharromán, I. Sobrados, J. E. Iglesias, T. González-Carreño, J. Sanz, *J. Phys. Chem. B* 103 (1999) 6160.

22. S. J. Hwang, C. Fernandez, J.-P. Amoureux, J. W. Han, J. Cho, S. W. Martin, M. Pruski, *J. Am. Chem. Soc.* 120 (1998) 7337.

23. L. Delevoye, Ph.D. Thesis, University of Lille, France, 1998.

24. T. Charpentier, Ph.D. Thesis, Université de Paris Sud, France, 1998.

25. G. Wu, D. Rovnyak, R. G. Griffin, *J. Am. Chem. Soc.* 118 (1996) 9326.

26. P. K. Madhu, A. Goldbourt, L. Frydman, S. Vega, *Chem. Phys. Lett.* 307 (1999) 41.

27. D. Coster, J. J. Fripiat, *Chem. Mater.* 5 (1993) 1204.

28. D. Coster, A. L. Blumenfeld, and J. J. Fripiat, *J. Phys. Chem.* 98 (1994) 6201.

Table 2-1. SB-0 physical properties upon calcinations.

Sample ID	Final Calcination Temp. (°C)	SA (m^2/g)	MPD (nm)	PV (cc/g)
SB-0	500 (initial)	470	8.7	1.1
SB-0-500	500	390	10	1.0
SB-0-600	600	400	9.7	1.0
SB-0-700	700	350	10	0.97
SB-0-800	800	300	11	0.89

Table 2-2. Effect of synthesis temperature on the SA and PV of the resulting aluminas.

Sample ID	Calcined at 500°C		Calcined at 600°C		Calcined at 700°C		Calcined at 800°C	
	SA (m^2/g)	PV (cc/g)	SA (m^2/g)	PV (cc/g)	SA (m^2/g)	PV (cc/g)	SA (m^2/g)	PV (cc/g)
SB-0	390	1.0	400	1.0	350	0.97	300	0.89
SB-1	320	0.65	390	0.82	360	0.79	310	0.65
SB-2	400	0.84	450	0.85	360	0.75	380	0.71
SB-3	370	0.63	400	0.63	330	0.52	350	0.53

Table 2-3. The population of aluminum coordination sites in the calcined aluminas.

Sample ID	Al^{VI} (%)	Al^{V} (%)	Al^{IV} (%)	Al^{VI}/Al^{IV}
SB-0-500	74	5.0	21	3.5
SB-0-600	66	8.0	26	2.5
SB-0-700	66	8.0	26	2.5
SB-0-800	71	4.0	25	2.8
SB-1-500	68	4.0	26	2.7
SB-1-600	64	2.5	34	1.9
SB-1-700	67	1.9	31	2.2
SB-1-800	68	0.83	32	2.1
SB-2-500	65	6.2	29	2.2
SB-2-600	61	4.1	35	1.7
SB-2-700	68	0.66	31	2.2
SB-2-800	65	1.9	32	2.0
SB-3-500	67	6.5	29	2.3
SB-3-600	60	3.3	36	1.7
SB-3-700	69	1.8	29	2.4
SB-3-800	67	1.4	31	2.1

Figure captions:

Figure 2-1. XRD patterns for SB-0 before and after initial calcination.

Figure 2-2. The effect of extended thermal treatment at 650°C for SB-0 and SB-3.

Figure 2-3. The relationship between synthesis temperature and MPD for SB-X.

Figure 2-4. Pore size distribution for SB-0-600 and SB-3-60.

Figure 2-5. ^{27}Al 3QMAS NMR spectra for mesoporous alumina, a) as-synthesized SB-0, and b) SB-0-600.

Figure 2-6. TGA and DTG curves for SB-0 and SB-3 under nitrogen.

Figure 2-7. TGA and DTG curves for SB-0 and SB-3 under air.

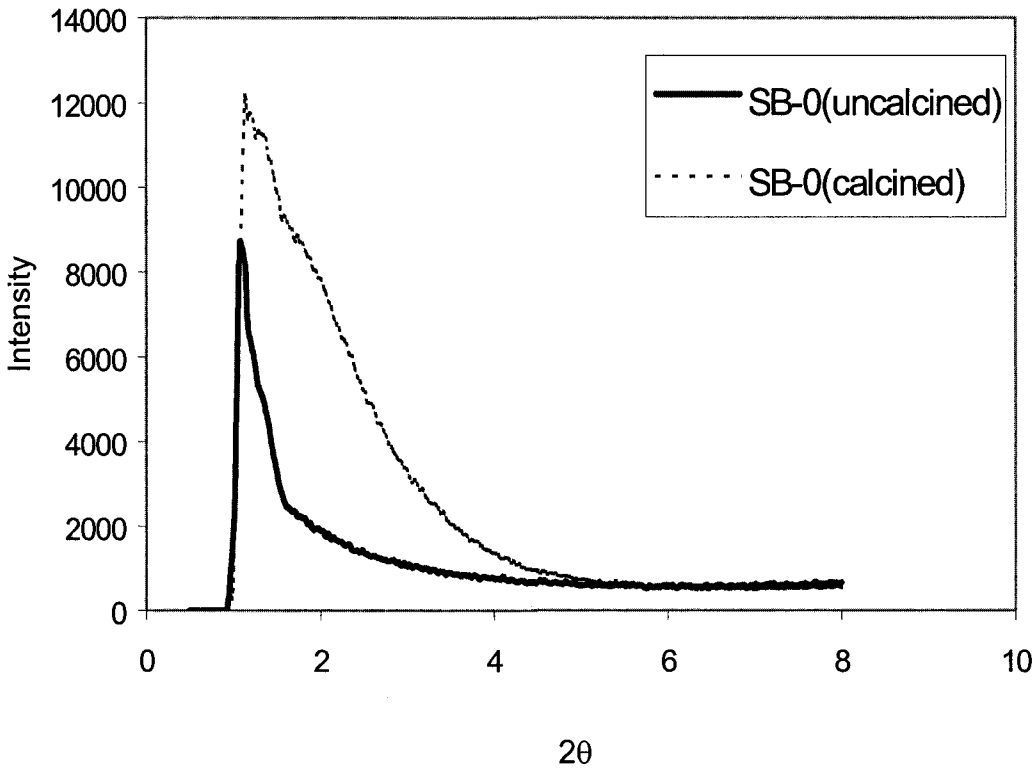
14000
12000
10000
8000
6000
4000
2000
0
Intensity
0
2
4
6
8
10
2θ
SB-0(uncalcined)
SB-0(calcined)

Figure. 2-1

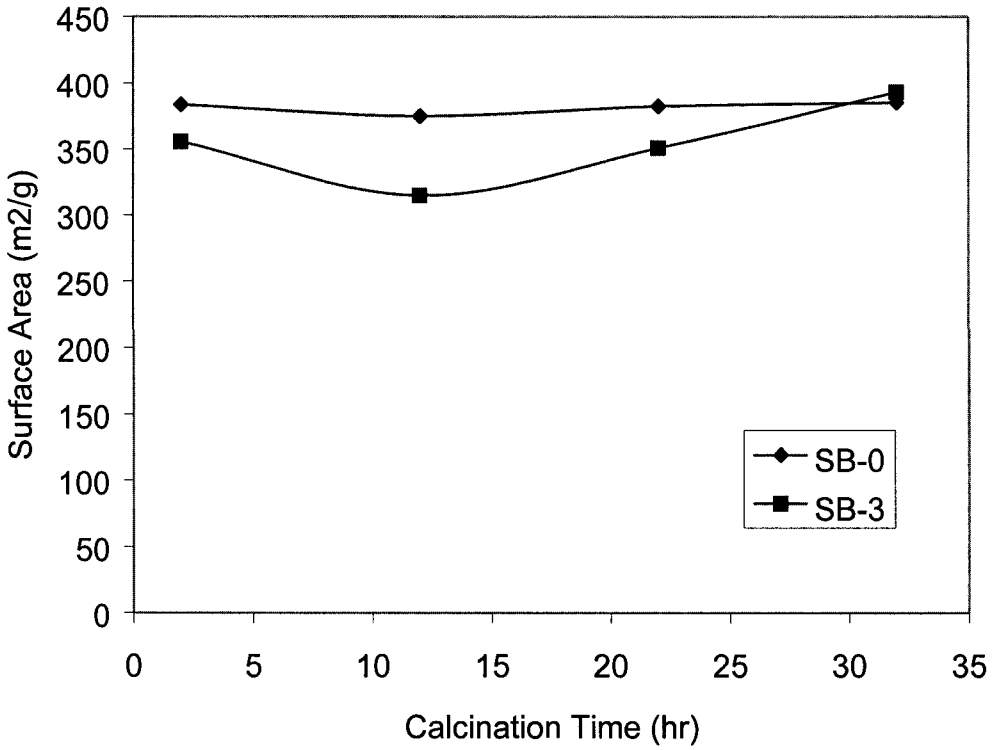
450
400
350
300
250
200
150
100
50
0
Surface Area (m2/g)
0
5
10
15
20
25
30
35
Calcination Time (hr)
SB-0
SB-3

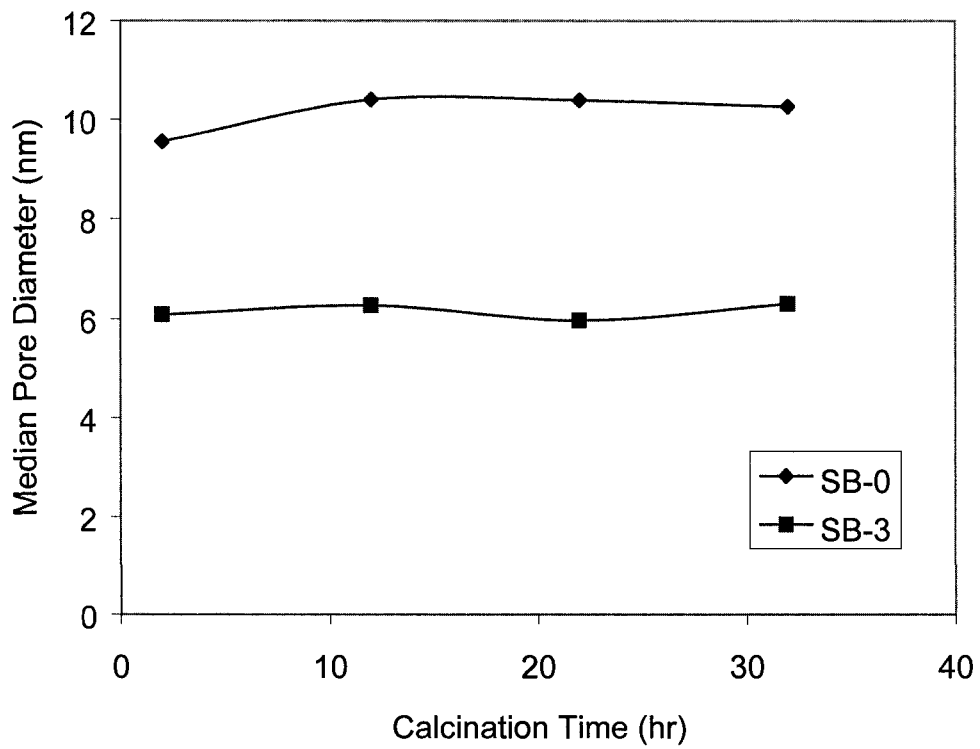
12
10
8
6
4
2
0
Median Pore Diameter (nm)
0
10
20
30
40
Calcination Time (hr)
SB-0
SB-3

Figure. 2-2

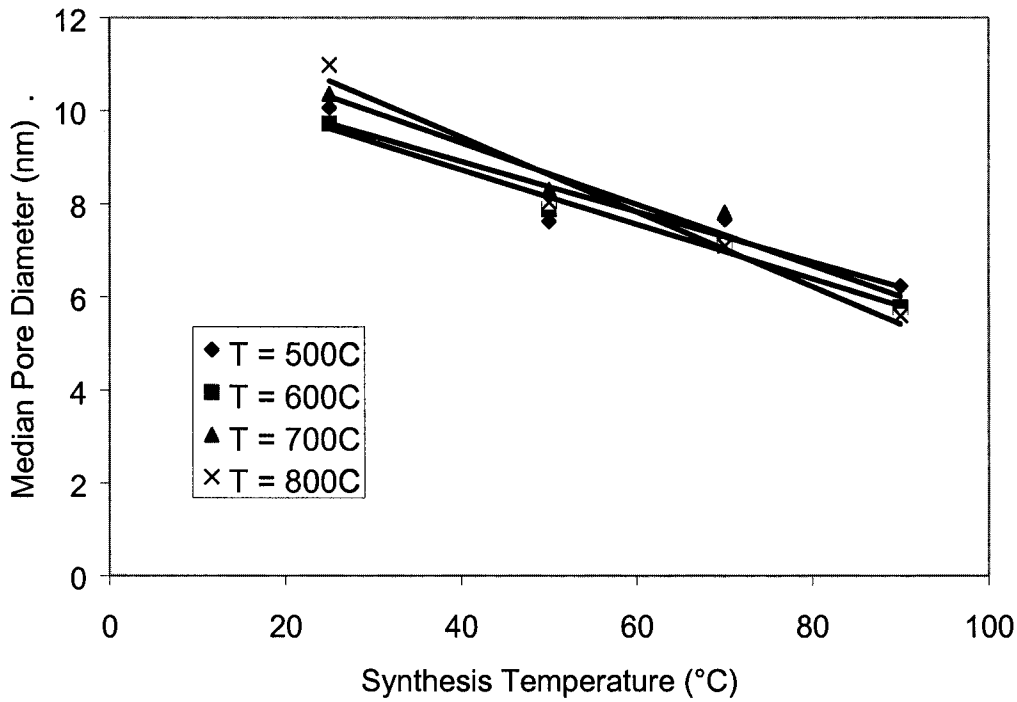
Median Pore Diameter (nm) .
12
10
8
6
4
2
0
0
20
40
60
80
100
Synthesis Temperature (°C)
T = 500C
T = 600C
T = 700C
T = 800C

Figure. 2-3

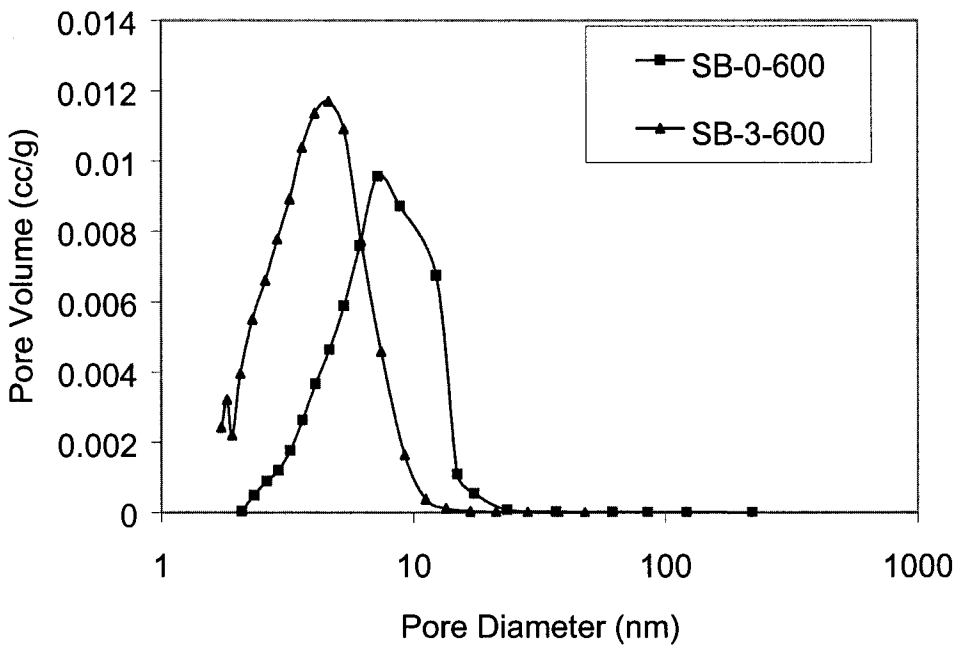
0.014
0.012
0.01
0.008
0.006
0.004
0.002
0
Pore Volume (cc/g)
1
10
100
1000
Pore Diameter (nm)
SB-0-600
SB-3-600

Figure. 2-4

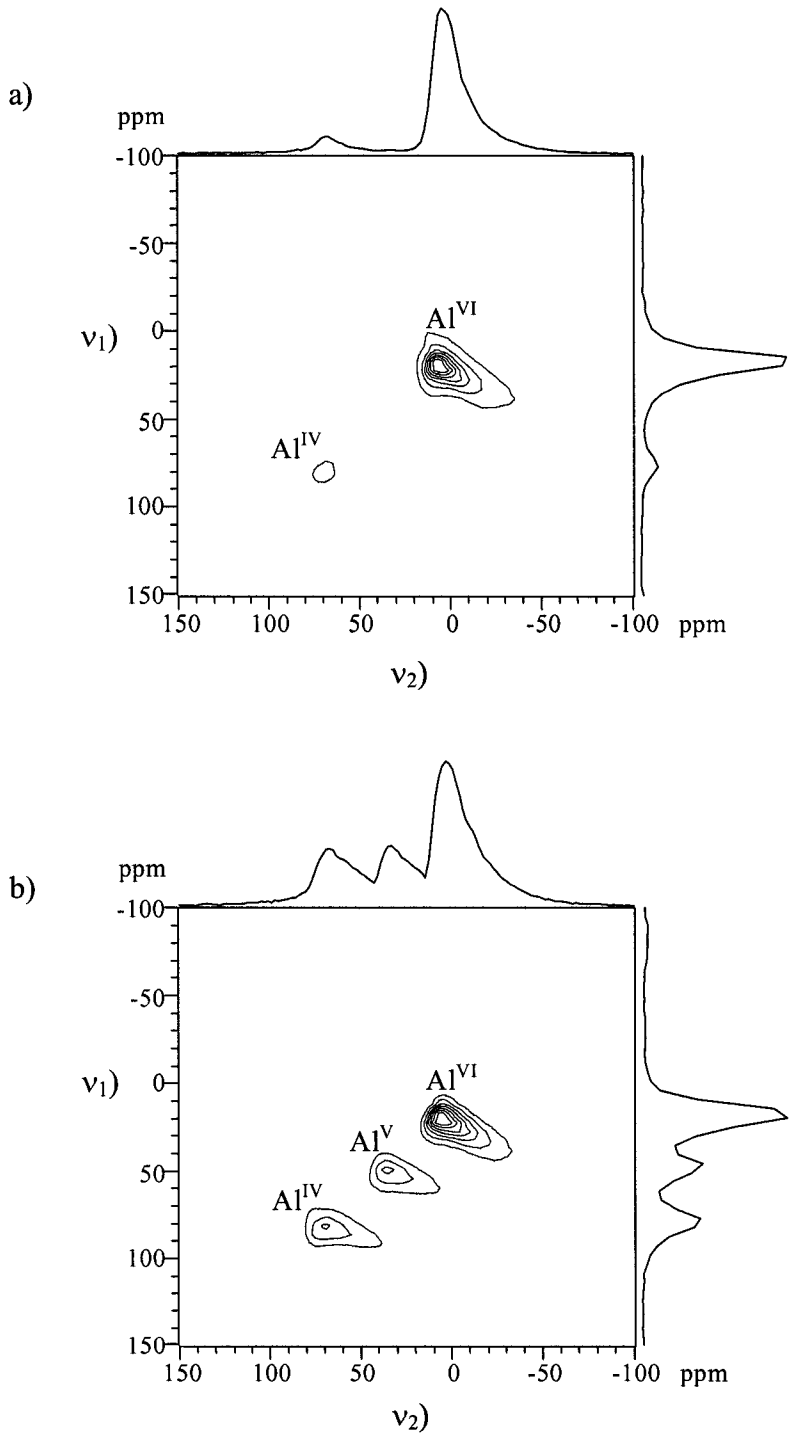
a)
ppm
-100
-50
0
50
100
150
ν_1)
Al^{VI}
Al^{IV}
150
100
50
0
-50
-100
ppm
ν_2)
b)
ppm
-100
-50
0
50
100
150
ν_1)
Al^{VI}
Al^{V}
Al^{IV}
150
100
50
0
-50
-100
ppm
ν_2)

Figure. 2-5

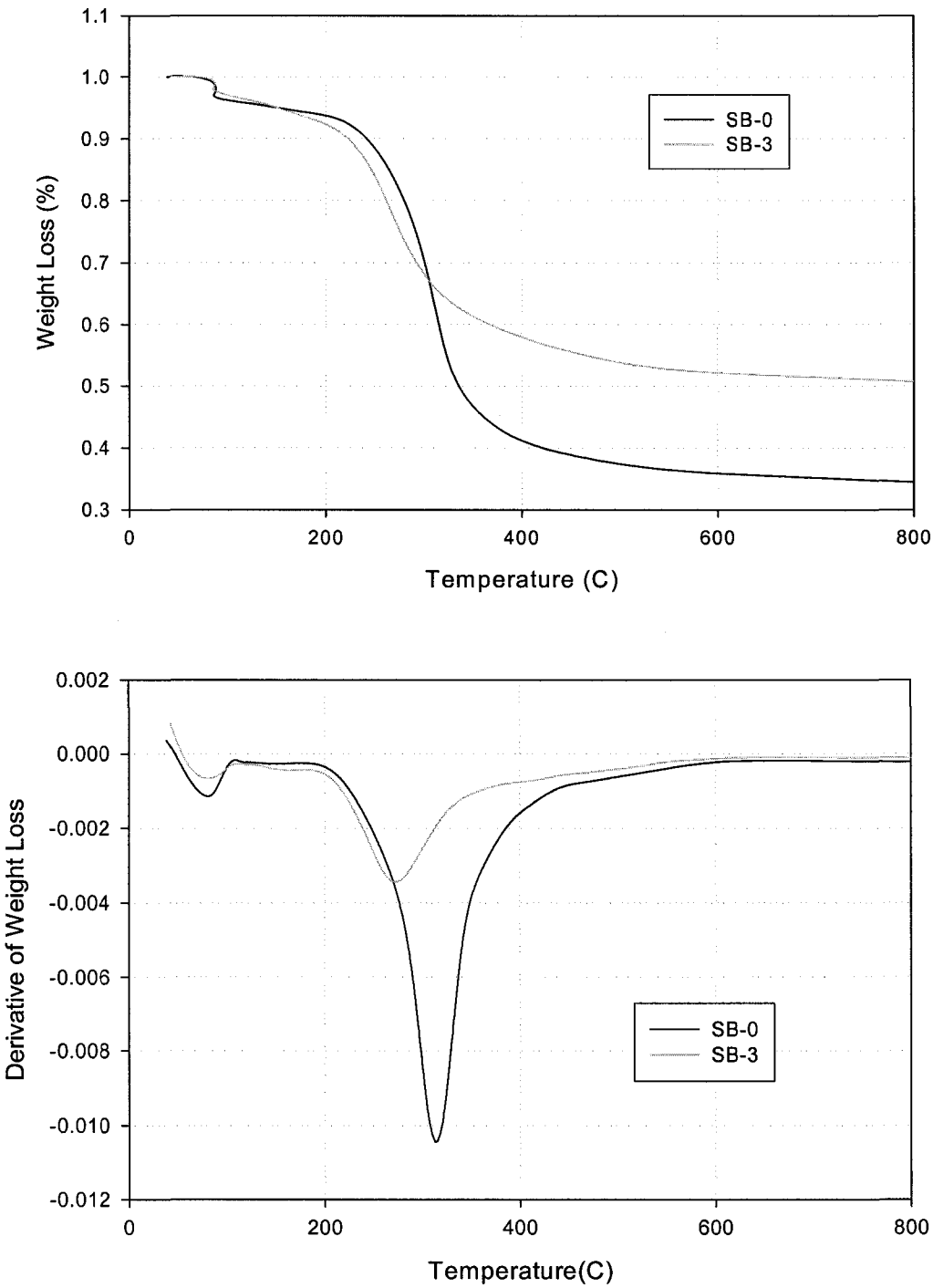
1.1
1.0
0.9
0.8
0.7
0.6
0.5
0.4
0.3
Weight Loss (%)
0
200
400
600
800
Temperature (C)
SB-0
SB-3
0.002
0.000
-0.002
-0.004
-0.006
-0.008
-0.010
-0.012
Derivative of Weight Loss
0
200
400
600
800
Temperature(C)
SB-0
SB-3

Figure. 2-6

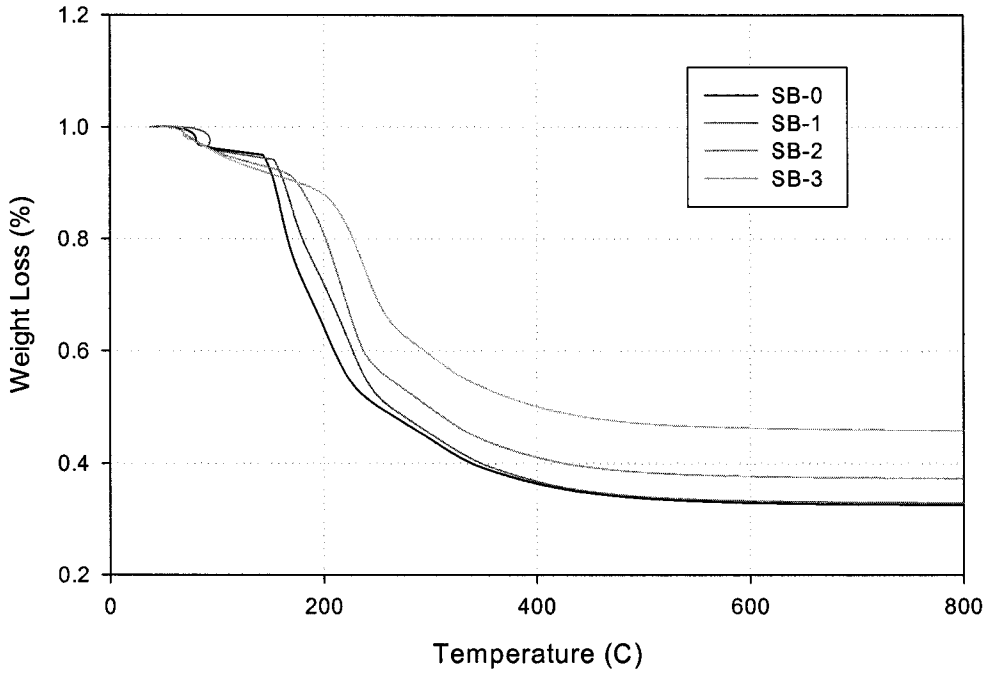
1.2
1.0
0.8
0.6
0.4
0.2
Weight Loss (%)
0
200
400
600
800
Temperature (C)
SB-0
SB-1
SB-2
SB-3

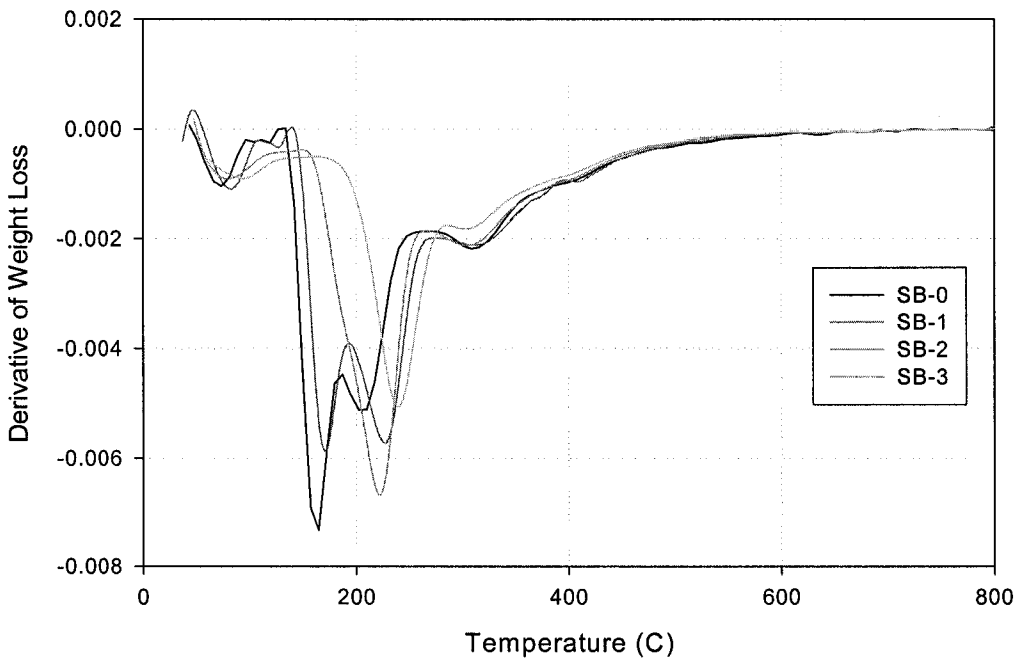
0.002
0.000
-0.002
-0.004
-0.006
-0.008
Derivative of Weight Loss
0
200
400
600
800
Temperature (C)
SB-0
SB-1
SB-2
SB-3

Figure. 2-7

Chapter 3. Surfactant-Assisted Synthesis of Alumina with Hierarchical Nanopores

3.1. Introduction

The advent of the supramolecular templating technique [1-2] has created the ability to synthesize an array of mesoporous metal oxide materials with potential application in areas that include catalysis, separations, chemical sensing, environmental remediation and optics [3]. Use of the mesoporous materials in these applications will require the ability to control their nanostructure. Systematic control of the diameter of the mesopores has been amply demonstrated, but control of pore length, which is manifest in the shape of the material particles, is less well developed. Also, studies on mesoporous particle morphology have primarily been limited to MCM-type silicas.

Several synthesis strategies have been reported for control of the particle morphology of mesoporous silicas. Macroscale particle morphologies including fibers, hollow spheres, hard spheres, and thin sheets were achieved using supramolecular assembly at the interface between oil-water mixtures [4-6]. This synthesis approach used the oil-water interface to control the macroscale morphology while concurrently exploiting nanoscale assembly of the mesopores thereby constructing structure at two length scales. Spherical particles, with diameters in the μm range, were generated by creating an emulsion of oil in water [4]. The use of emulsions was also reported as an approach to generate textural mesoporosity in mesoporous materials synthesized using nonionic templating [7,8]. Randomly distributed interstitial porosity was generated by the emulsion-induced aggregation of primary particles

synthesized in a water/co-solvent mixture. Aggregation of self-assembled silicate micelles has been proposed as the mechanism for the synthesis of spherical and oblate MCM-41 particles with characteristic sizes of 110nm and 1μm, respectively [9]. Hierarchically ordered "tubules-within-a-tubule" MCM-41 material was synthesized in which a hollow tubule of about 1μm in diameter was generated with coaxial mesopores in the wall [10]. The structure was proposed to be generated from a mixed lamellar-hexagonal silicate phase. Synthesis strategies that extend beyond standard surfactant templating have been demonstrated to create a wealth of hierarchically structured mesoporous silicas [11-13].

Despite their many potential applications, mesoporous aluminas have received considerably less attention than mesoporous silicas. Mesoporous alumina synthesis has been more problematic than that of mesoporous silica, although a variety of synthesis strategies have now been reported [14-18]. With the synthesis of mesoporous aluminas and validation of their structural stability during thermal treatment [19], their potential application in catalysis appears promising. However, control of pore length and, hence, intra-diffusive properties will be critical for the use of mesoporous aluminas. Unfortunately, mesoporous alumina produced by either nonionic or electrostatic templating methods has typically yielded macroscale particles of fairly random shape. In this paper, we report the first synthesis of mesoporous aluminas with hierarchically ordered pore structures.

3.2. Experimental

The base case synthesis procedure consisted of adding 1.2g cetyltrimethylammonium bromide (CTAB, Aldrich) to a mixture of 105ml deionized water and 45ml ethanol (200 proof, Fisher Scientific) under vigorous stirring at room temperature. Then, 2ml of

ammonium hydroxide was added under mixing and, finally, ~6g of aluminum tri-*sec*-butoxide. The resulting mixture was held at room temperature with stirring for 3 hours. The as-synthesized product was retrieved by centrifugation, washed with ethanol and subsequently dried in air for 12 hours. Calcination was performed at 500°C for 5.5 hours in flowing air following a temperature ramp of 2 °C/min from room temperature to 500°C. The effect of synthesis factors such as water/ethanol ratio, surfactant concentration ratio, reaction temperature, and mixing rate on the morphology of the resulting alumina particles was examined. The range of conditions used in the experiments is shown in Table 3-1. Syntheses were also performed with methanol, butanol, and acetone co-solvents. Several syntheses were performed in which silica alkoxides (TEOS and TMOS) were used in place of the aluminum alkoxide.

Powder x-ray diffraction (XRD) patterns were acquired by a X_1 advanced diffraction system (Scintag, Inc.) using a CuK_α radiation source (λ = 0.154nm). Low angle diffraction with a 2θ range of 0.5-10° was used to investigate the long-range order of the materials and wide angle scans were performed at a 2θ range of 5-85° to validate the amorphous state of the alumina. Surface area (SA) and median pore diameter (MPD) were measured using a Micromeritics ASAP 2000, with SA determined by the Brunauer-Emmett-Teller (BET) method and pore volume (PV) and pore size distribution by the Barrett-Joyner-Helenda (BJH) method. Sample preparation included degassing at 90°C for 1 hour and then at 150°C for 4 hours. SEM images were taken using a JSM-840 scanning microscope (JEOL Inc).

3.3. Results and discussion

Shown in Figure 3-1 is a SEM image of the alumina resulting from the base case synthesis. While the distribution of overall particle shapes was found to be random as observed in other mesoporous alumina syntheses, about 40% of the particles were found to contain regular arrays of macropores having diameters of about 300nm. Individual particles were found to either fully contain a regular array of macropores or no macropores at all. Macropores, when present, were always orthogonal to the face of the monolithic particles. The presence of the macropores resulting from the base case conditions was replicated in duplicate syntheses.

The adsorption/desorption isotherm for the base case synthesized alumina is given in Figure 3-2 (above). As can be seen from the data, the alumina was found from nitrogen adsorption/desorption to only contain mesopores since the macropores are too large to be measured using nitrogen adsorption/desorption. The SA of the alumina was 450 m^2/g with a MPD of 6.4nm and PV of 0.76 cm^3/g. Low angle XRD patterns of the sample gave a broad peak between 1 and 3° of 2θ, which is characteristic of a disordered mesostructure [14]. The existence of this disordered mesostructure is consistent with the hysteresis loop seen in the adsorption/desorption data and is indicative of interconnections between the mesopores.

The macroporous structure was found to form relatively rapidly after introduction of the aluminum tri-*sec*-butoxide to the synthesis mixture. Shown in Figure 3-1 (below) and Figure 3-2 (below) are the SEM image and the adsorption/desorption data for alumina produced under the base conditions when the reaction was terminated at 10 minutes instead of the standard 3 hours. The macropores are already present in a regular array through the

particles. From the side view of the monolithic particles, the extension of the parallel arrayed macropores completely through the particles can be clearly seen.

To determine the effect of synthesis conditions on the presence of macropores in the final alumina, a range of conditions were examined. Shown in Table 3-1 is a subset of the preparation condition parameter space that was explored. Sample 1 was prepared using the base case conditions. The factors that were varied were the water/ethanol ratio, surfactant concentration, reaction temperature, and mixing rate. The physical properties of the resulting aluminas are also given in Table 3-1, which includes BET characterization as well as the presence of macropores, their approximate diameter, and percentage of alumina particles found to contain macropores as determined by SEM.

Samples 2 and 3 examine the effect of the water/ethanol ratio on the synthesis. As shown in Figure 3-3 (below) and Figure 3-4 (below), ethanol rich mixtures completely suppressed the formation of a macroporous structure, but the resulting alumina had SA, MPD, and PV similar to that of the other aluminas. In contrast, the higher water/ethanol ratio still gave macropores, but the primary particles began to have an aggregated appearance with poorer definition for the macropores (Figure 3-3(above) and Figure 3-4 (above)). Synthesis with even higher water content resulted in aggregates possessing no macropores. Once again, the physical properties of Sample 2 as determined by BET characterization were similar to the other aluminas in the study.

The surfactant concentration used in the base case synthesis is above the critical micelle concentration for CTAB in a water/ethanol mixture [20]. The effect of halving and doubling the surfactant concentration is given by Samples 4 and 5. Even the lower surfactant

concentration used in Sample 4 is above the critical micelle concentration for the CTAB/water/ethanol system. Both Sample 4 and 5 were found to contain macropores.

Samples 6 and 7 examined the effect of synthesis temperature and pH, respectively. Syntheses were performed at 40 and 58°C with Sample 6 corresponding to the higher temperature. Macropores were not observed when the synthesis temperature was increased from room temperature to 40 or 58°C. Sample 7 resulted from substitution of hydrochloric acid for ammonium hydroxide in the base synthesis. This substitution, which lowered the synthesis pH from about 9 to 5, still resulted in the formation of alumina particles that contained macropores.

Under the base case synthesis conditions, addition of the CTAB to the water/ethanol mixture under strong stirring resulted in the formation of shear-induced emulsified droplets. Several studies have shown that hydrodynamic and emulsification effects can play a significant role in particle morphology of mesoporous materials [4,6-8]. The impact of stirring rate on macropore formation in the current system are given by comparison of Samples 1, 8 and 9. Sample 8 used a mixing rate of half that in the base synthesis. The SEM image and adsorption/desorption data for this sample are given in Figure 3-5 and Figure 3-6. Nearly all of the particles were found to contain macropores and the macropores appeared to be more pronounced at this lower stirring rate. In addition, the wall thickness between the macropores was significantly lower at these conditions. While the MPD of Sample 8 is similar to that of the other syntheses, the pore size distribution for the mesopores as shown in Figure 3-6 has two maximums at 3.5 and 8.0nm. For Sample 9, mixing of the CTAB/water/ethanol was stopped prior to the introduction of the aluminum tri-*sec*-butoxide.

The macropores were still found to be widely present in the alumina particles synthesized under the static conditions in which emulsified droplets did not exist.

While changing the water/ethanol ratio impacts the polarity of the synthesis mixture, this ratio likely impacts the aluminum alkoxide hydrolysis rate as well, so merely changing the ratio does not allow the decoupling of polarity and hydrolysis rate effects. To examine polarity effects, syntheses were performed at the base conditions with methanol and butanol substituted for ethanol, Samples 10 and 11, respectively. The physical properties of the resulting alumina powders are shown in Table 3-1. The use of methanol resulted in alumina particles with similar mesoporosity as with ethanol, but only a minor presence of macropores. Substitution of butanol for ethanol also yielded alumina particles with similar mesoporosity and macroporosity. Acetone has similar polarity to ethanol, which has been shown to yield similar ordered hexagonal regions in silica/surfactant mesophases [20]. Sample 12 is an alumina synthesized with an acetone co-solvent rather than ethanol. As can be seen from Table 3-1, the use the acetone aprotic co-solvent led to particles with similar mesoporous characteristics as the ethanol co-solvent case, and the sample particles showed the existence of a significant amount of macropores also.

To determine whether the macrostructure could be generalized to other metal oxides, syntheses were performed with TEOS or TMOS used in place of the aluminum alkoxide. All other conditions from the base synthesis case were the same. Shown in Figure 3-7 is the SEM image only for the TEOS-derived silica, since the use of TMOS gave the same result. As can be seen in the figure, the synthesis led to the formation of fairly uniform spherical particles with diameters of about 200nm and no macroporosity.

The striking feature of the aluminas synthesized in the present study is the presence of pores having two characteristic length scales of about 4 and 400nm, respectively. As seen in the SEM images, the larger pores exist in regular arrays whereas the mesopores would appear from the XRD and adsorption/desorption data to be disordered, which is the typical result for mesoporous aluminas [14-19]. The orientation of the mesopores relative to the macropores is not known definitively, but the data supports that the walls between the macropores must contain mesopores. This relationship between pores is validated by Sample 8 in which all of the particles contained macropores, so the only possible location of the mesopores was within the walls between the larger pores. Therefore, these aluminas would appear to have excellent potential for use in catalytic applications. The macropores will facilitate mass transfer to the high surface area contained within the mesopores. This transport enhancement is very important for applications of mesoporous materials in liquid phase reactions and when reacting substrates of sufficient size to exploit the potential for shape selectivity in the mesopores. The macropores should help to overcome the diffusive resistance that will be experienced in typical mesoporous alumina, which have monolithic particles.

The generation of hierarchical structure in mesoporous materials using an emulsified state during the synthesis has been reported [4-8]. In the current work, shear-induced emulsified droplets were observed in the water/ethanol/CTAB mixture at any of the mixing conditions employed. However, the macropores were found to exist in the final alumina powder even when the aluminum alkoxide was added under static conditions in which no emulsified droplets existed. Therefore, the formation of the macropores cannot be mechanistically related to the presence of an emulsified state.

The choice of co-solvent is not important to the formation of the macroporous structure. Use of the less polar butanol co-solvent or more polar methanol co-solvent did not change the macropore formation or macropore population significantly. The similar phenomenological behavior resulting from the substitution of acetone for ethanol is in accordance with the behavior of CTAB micelles in water/co-solvent systems, where the use of ethanol or acetone as the co-solvent resulted in similar surfactant micelle formation behavior [20]. It seems that different co-solvents have a similar function in structural organization of the material. The formation of the macropores cannot be simply qualitatively related to the polarity of the co-solvent as has been suggested for the introduction of textural mesoporosity [7].

From the current parametric study, it is clear that the hierarchically structured material could be obtained over a broad range of reaction conditions. We propose that the macropores result from an interaction between surfactant precursor solution and kinetics of the alumina hydrolysis and condensation reaction. Except in Sample 8 in which nearly all of the alumina particles contain macropores, all of the other samples that contain macroporous particles also have particles without macropores. This reflects an unbalanced structure evolution for the aluminum precursors. The sample shown in Figure 3-1 (below), which terminated the synthesis step after 10 minutes, shows that the macroporous structure is formed rapidly after the addition of the alumina precursor. This quick structure formation indicates that the process can likely be attributed to a kinetics controlled one.

In this work, all syntheses were conducted in an uncontrolled hydrodynamic environment. It was found that the formation of macroporous materials were sensitive to the hydrodynamic forces exerted on the reaction. With other reaction variable fixed, a change in

stirring rate could result in different particle morphologies. The sample synthesized with butanol co-solvent, for example, showed different particle morphologies with and without macropores under various hydrodynamic conditions. The samples that compare hydrodynamic effects (Sample 1, 8 and 9) also show that the population of particles having macropores varied with stirring rate. It seems that the intensity of a hydrodynamic field in which the reaction is conducted is crucial for the formation of the hierarchically structured material. More work is needed to reveal the relationship between the shear force and the macropore formation.

3.4. Conclusions

The phenomenological appearance of hierarchical nanopores from the surfactant-assisted synthesis of aluminas has been demonstrated in the current work for a range of synthesis conditions. Within the set of synthesis conditions, the mesopores have relatively consistent structure. However, the mechanism for the formation of the material is still unclear. Elucidating this mechanism is not only important for understanding the formation of the hierarchical alumina structures shown here, but has potential implication in the hierarchical structures observed in biomineralization.

References

1. C.T. Kresge, M. E. Leonowicz, W. J. Roth, J. C. Vartuli, and J. S. Beck, *Nature* 359 (1992) 710.
2. J. S. Beck, J. C. Vartuli, W. J. Roth, M. E. Leonowicz, C.T. Kresge, K. D. Schmitt, C. T-W. Chu, D. H. Olson, E. W. Sheppard, S. B. McCullen, J. B. Higgins, and J. L. Schlenker, *J. Am. Chem. Soc.* 114 (1992) 10834.
3. A. Stein, B. J. Melde, R. C. Schroden, *Adv. Mater.* 12 (2000) 1403.
4. S. Schacht, Q. Huo, I. G. Voigt-Martin, G. D. Stucky, F. Schűth, *Science* 273 (1996) 768.
5. Q. Huo, J. Feng, F. Schűth, G. D. Stucky, *Chem. Mater.* 9 (1997) 14.
6. Q. Huo, D. Zhao, J. Feng, K. Weston, S. K. Buratto, G. D. Stucky, S. Schacht, F. Schűth, *Adv. Mater.*9 (1997) 974.
7. W. Zhang, T. R. Pauly, T. J. Pinnavaia, *Chem. Mater.* 9 (1997) 2491.
8. T. R. Pauly, Y. Liu, T. J. Pinnavaia, S. J. L. Billinge, T. P. Rieker, *J. Am. Chem. Soc.* 121 (1999) 8835.
9. Q. Cai, Z. Luo, W. Pang, Y. Fan, X. Chen, F. Cui, *Chem. Mater.* 13 (2001) 258.
10. H. Lin, C. Mou, *Science* 273 (1996) 765.
11. H. Yang, C. T. Kresge, G. A. Ozin, *Adv. Mater.* 10 (1998) 883.
12. G. A. Ozin, *Can. J. Chem.* 77 (1999) 2001.
13. G. A. Ozin, *Chem. Commun.* 6 (2000) 419.
14. S. A. Bagshaw, T. J. Pinnavaia, *Angew. Chem. Int. Ed.* 35 (1996) 1102.
15. F. Vaudry, S. Khodabandeh, M. E. Davis, *Chem. Mater.* 8 (1996) 1451.

16. S. Cabrera, J. E. Haskouri, J. Alamo, A. Beltrán, D. Beltrán, S. Mendioroz, M. D. Macros, P. Amorós, *Adv. Mater.* 5 (1999) 371.

17. S. Valange, J.-L. Guth, F. Kolenda, S. Lacombe, Z. Gabelica, *Micropor. Mesopor. Mater.* 35-36 (2000) 597.

18. X. Liu, Y. Wei, D. Jin, W. Shih, *Mater. Lett.* 42 (2000) 143.

19. W. Deng, P. Bodart, M. Pruski, B. H. Shanks, *Micropor. Mesopor. Mater.* 52 (2002) 169.

20. M. T. Anderson, J. E. Martin, J. G. Odinek, P. Newcomer, *Chem. Mater.* 10 (1998) 311.

Table 3-1. Preparation conditions and characterization results for selected sample set.

Sample ID	Water (ml)	Co-solvent (ml)	CTAB (g)	Alum. (g)	Temp. (°C)	Stirring Rate	SA (m^2/g)	MPD (nm)	PV (cc/g)	Macro-pore	Macropore Diameter (nm)	Occurrence (%)
1	105	45	1.2	6.24	25	Fast	450	6.4	0.76	Y	300	40
2	135	15	1.2	5.65	25	Fast	300	3.7	0.28	Y	400	60
3	15	135	1.2	5.92	25	Fast	390	5.1	0.53	N	N/A	0
4	105	45	0.6	6.2	25	Fast	370	4.1	0.40	Y	400	50
5	105	45	3.0	6.28	25	Fast	460	4.7	0.56	Y	400	70
6	105	45	1.2	6.04	58	Fast	470	3.9	0.47	N	N/A	0
7	105	45	1.2	5.70	25	Fast	290	4.8	0.37	Y	450	60
8	105	45	1.2	6.24	25	Slow	470	4.7	0.58	Y	300	>90
9	105	45	1.2	5.80	25	No	390	4.6	0.47	Y	250	30
10[a]	105	45	1.2	5.70	25	Fast	430	3.9	0.44	Y	350	25
11[a]	105	45	1.2	6.07	25	Fast	420	4.3	0.46	Y	400	50
12[a]	105	45	1.2	5.72	25	Fast	350	4.2	0.38	Y	400	70

[a] In these syntheses, methanol, butanol and acetone were used as the co-solvent, respectively.

Figure Captions:

Figure 3-1. SEM images for Sample 1 (above) and short time synthesized alumina (below).

Figure 3-2. Adsorption/desorption isotherm plots for Sample 1 (above) and short time synthesized sample (below).

Figure 3-3. SEM images for Sample 2 (above, 1μm scale bar), and Sample 3 (below, 1μm scale bar).

Figure 3-4. Adsorption/desorption isotherm plots for Sample 2 (above) and Sample 3(below).

Figure 3-5. SEM image (1μm scale bar) for the sample synthesized at low stirring rate.

Figure 3-6. Adsorption/desorption isotherm plot and BJH pore size distribution for the sample synthesized at low stirring rate.

Figure 3-7. SEM image (200nm scale bar) for the TEOS-derived silica material.

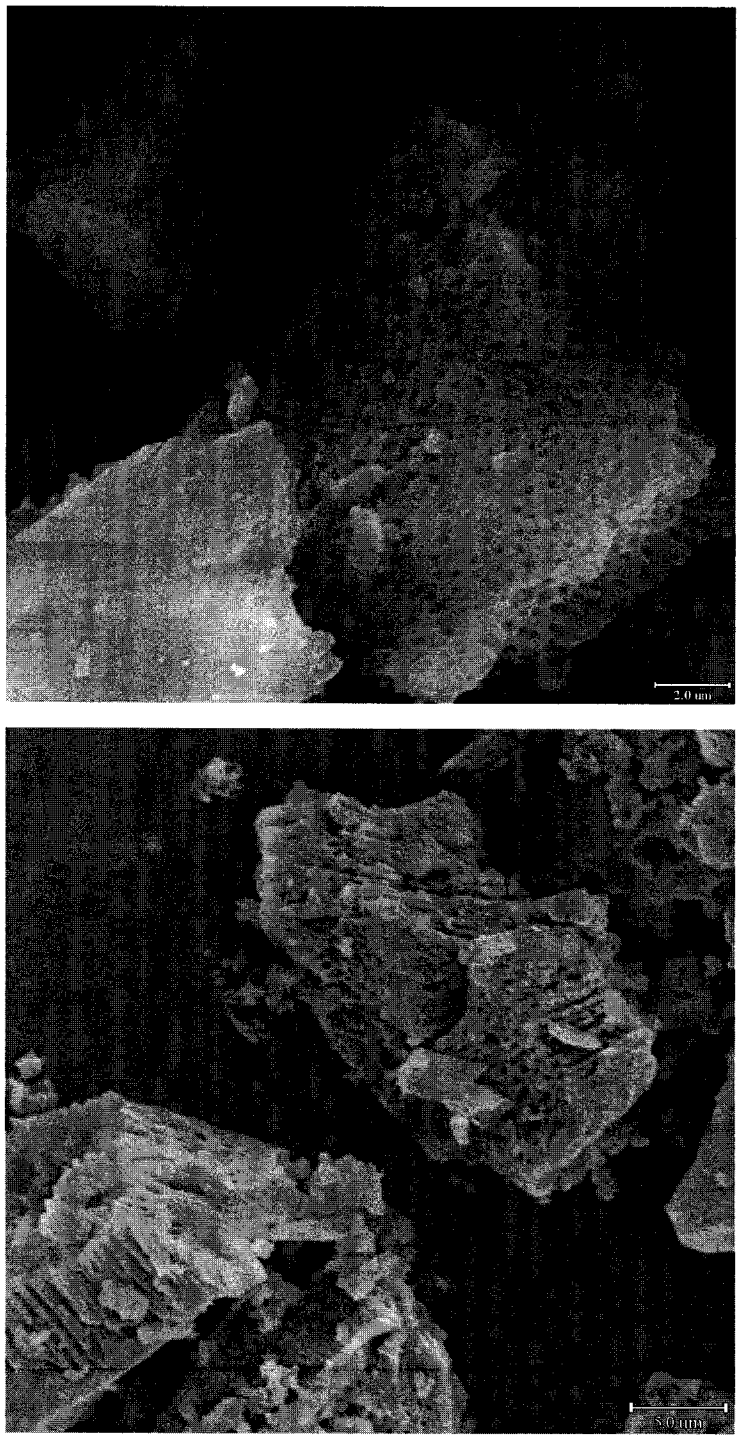

Figure. 3-1

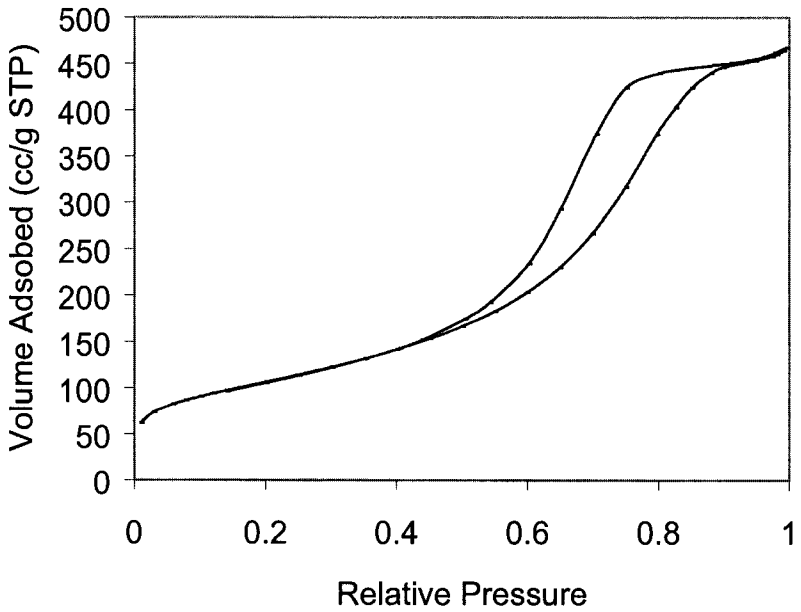
Volume Adsobed (cc/g STP)
500
450
400
350
300
250
200
150
100
50
0
0
0.2
0.4
0.6
0.8
1
Relative Pressure

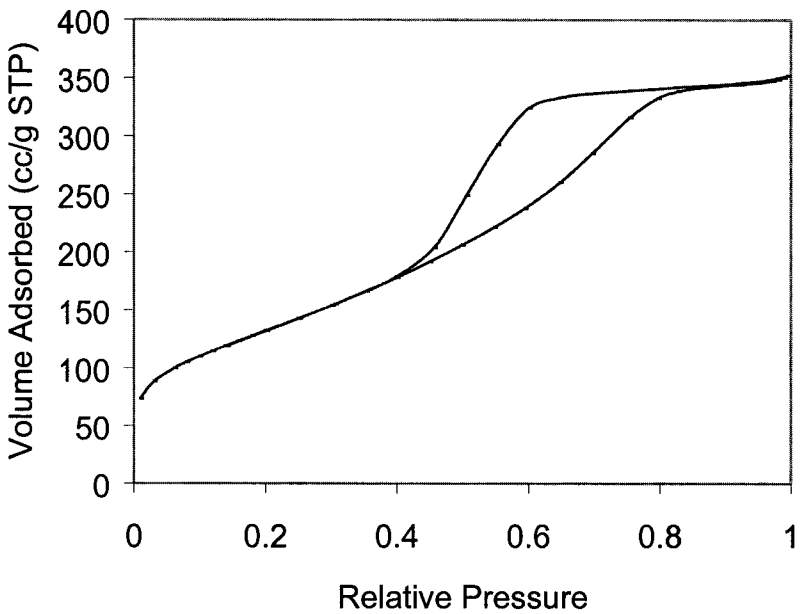
Volume Adsorbed (cc/g STP)
400
350
300
250
200
150
100
50
0
0
0.2
0.4
0.6
0.8
1
Relative Pressure

Figure. 3-2

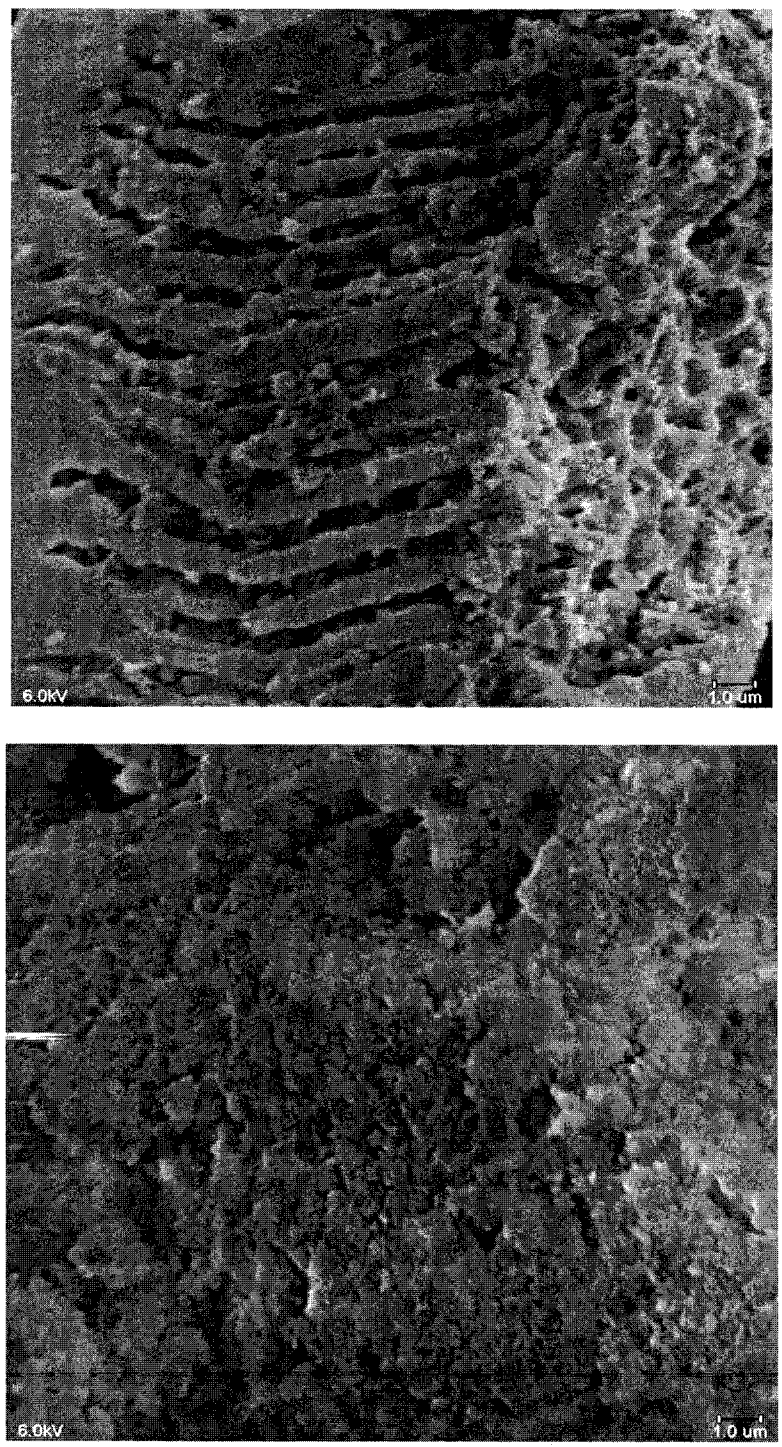

Figure. 3-3

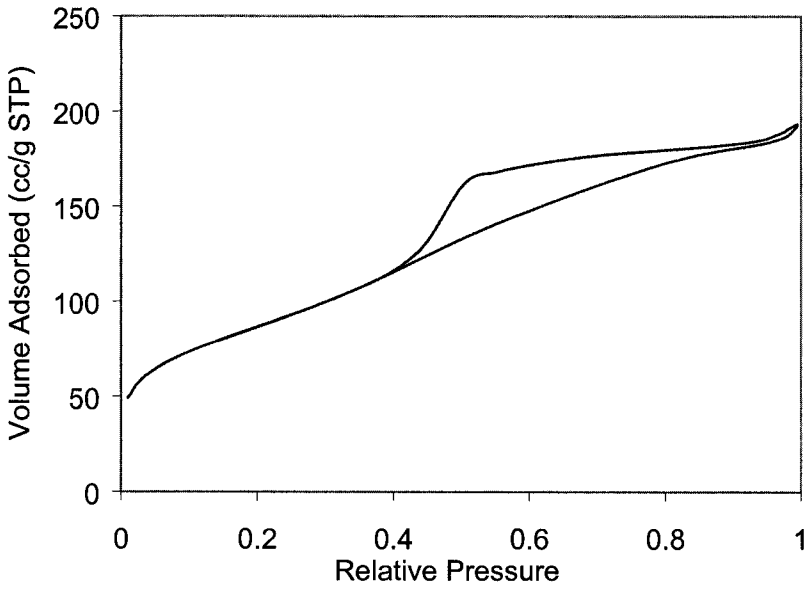
250
200
150
100
50
0
Volume Adsorbed (cc/g STP)
0
0.2
0.4
0.6
0.8
1
Relative Pressure

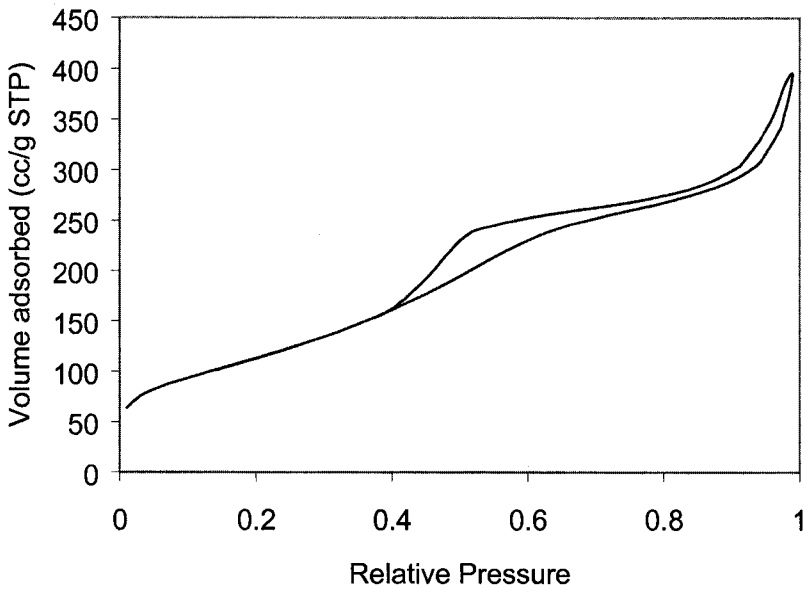
450
400
350
300
250
200
150
100
50
0
Volume adsorbed (cc/g STP)
0
0.2
0.4
0.6
0.8
1
Relative Pressure

Figure. 3-4

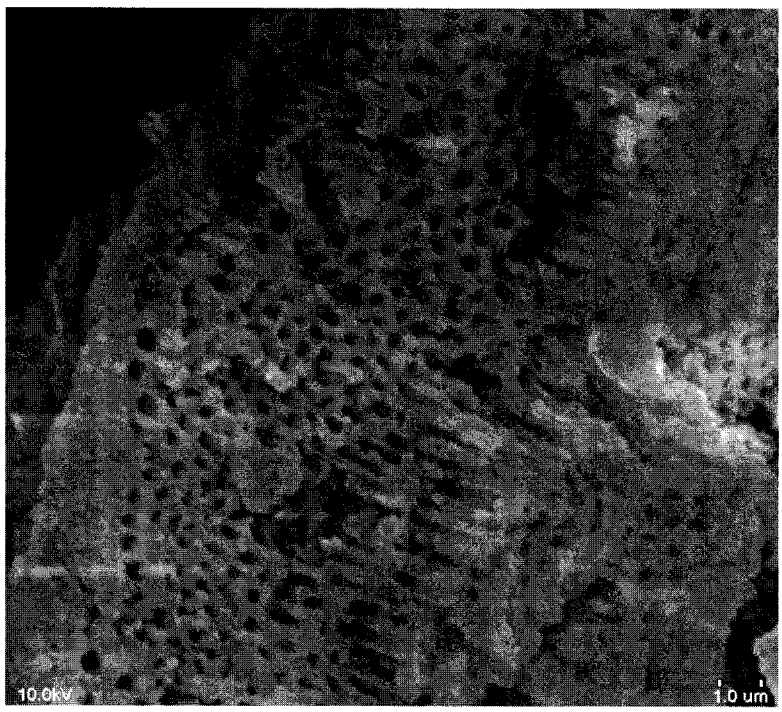

Figure. 3-5

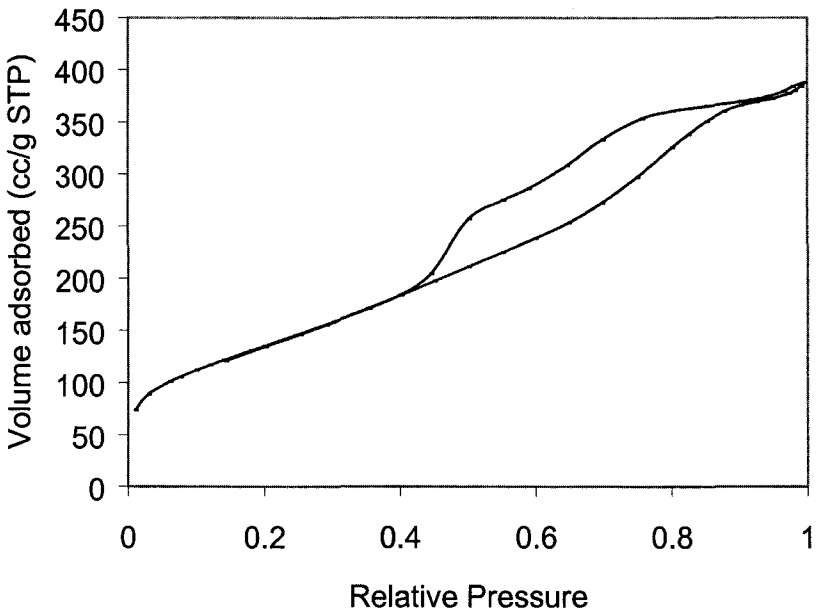
Volume adsorbed (cc/g STP)
450
400
350
300
250
200
150
100
50
0
0
0.2
0.4
0.6
0.8
1
Relative Pressure

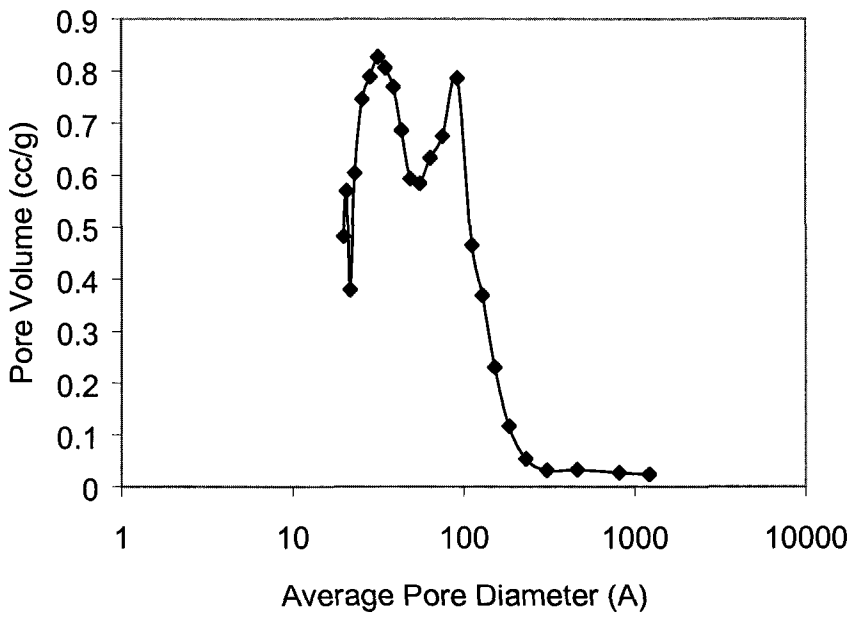
Pore Volume (cc/g)
0.9
0.8
0.7
0.6
0.5
0.4
0.3
0.2
0.1
0
1
10
100
1000
10000
Average Pore Diameter (A)

Figure. 3-6

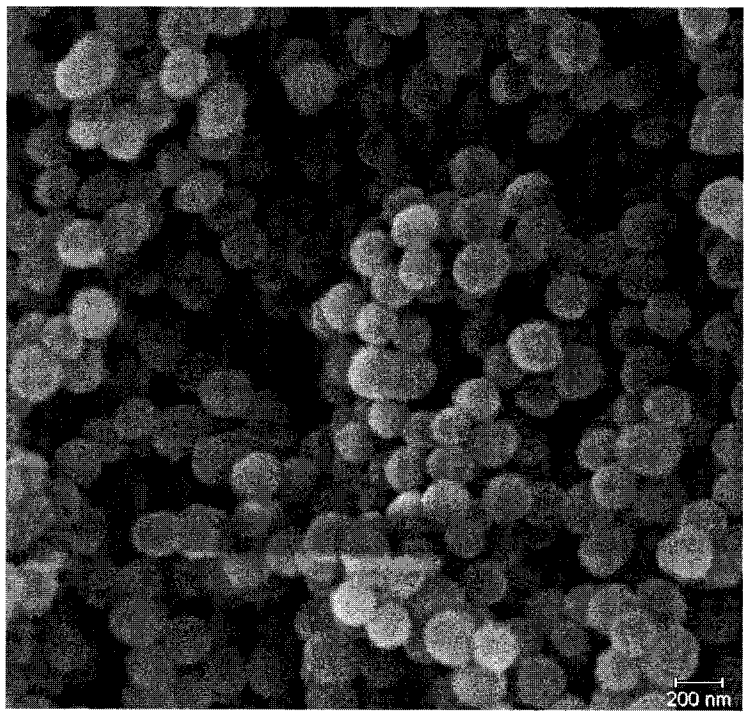

Figure. 3-7

Chapter 4. Synthesis of Hierarchically Structured Aluminas under Controlled Hydrodynamic Conditions

4.1. Introduction

Transitional aluminas, which are derived from aluminum hydroxide and oxyhydroxide by thermal treatment [1], have been extensively used for many decades in industry as catalyst supports [2], adsorption media and catalysts in processes such as petroleum refining [3], hydrodesulfurization [4], and the Claus reaction as well as automotive emission control [5,6]. The discovery of the supramolecular templating technique [7,8] made possible the synthesis of alumina with unique and promising textural properties relative to traditional alumina, which has the potential to further extend its industrial applications. While their synthesis has proven more problematic than their silica analogs, a number of synthesis mesostructured alumina strategies using either ionic or nonionic templating methods have been reported in which the pore diameter can be tuned to a desired dimension [9-14].

While pore diameter is an important property dictating the mass transfer characteristics of mesoporous alumina, the pore length also plays an important role in mass transfer. The pore length in these materials is largely determined by the morphology of the mesoporous particle. As such, morphology control of mesoporous materials has received increasing attention. A number of studies have demonstrated synthesis methods for mesoporous silica with morphology control resulting in structures that include particle shapes ranging from spheres to needles to nanotubes [15-21]. Relative to the morphology control

achieved with mesoporous silica materials only a few alumina analogs have been reported [22].

We recently reported the "one-pot" synthesis of a novel macropore/mesopore hierarchically structured alumina in which the alumina particles had parallel arrays of macropores interconnected with mesopores [23]. These materials are interesting for their potential use in catalysis and adsorption applications due to the enhanced access to the mesopores as provided by the regularly arrayed macropores. Subsequent to our report several groups have reported similar structures for other metal oxides. Su and co-workers have reported the surfactant-mediated and surfactant-free synthesis of hierarchically structured metal oxides such as zirconia, alumina and aluminosilicate [24-29]. Mann and co-workers have demonstrated the template-free synthesis of ordered macroporous titania [30].

In our initial report a preliminary study of the synthesis parameter space was explored. The hierarchical structures were found to form quite rapidly making direct observation of the synthesis progression difficult [23]. Importantly, it was found that the hydrodynamic environment present during the synthesis had a significant effect on the formation of the unique particle morphology. To provide a well-controlled hydrodynamic environment, a cone/plate apparatus [31-33] designed and adopted as the synthesis reactor in the current work. Under these carefully controlled hydrodynamic conditions, a systematic study examining the effect of synthesis conditions on the formation of the hierarchical alumina structure was performed. The results from the parametric synthesis study were then used to discuss possible mechanisms for the formation of the hierarchical structure.

4.2. Experimental

Aluminum *sec*-butoxide (97%) and amine surfactants (dodecyl-, cetyl-, and octadecyl-trimethylamonium bromide) were used as purchased from Aldrich (USA). Also used in the study was a nonionic polyethylene oxide/polypropylene oxide tri-block copolymer surfactant (Pluronic L64, BASF, USA), ethanol (100%, Fisher Scientific, USA) and deionized water.

All syntheses were conducted in a cone/plate apparatus (CPA) as shown in Figure 4-1, which consisted of a small angle (around 5°) rotating cone within a cylindrical vessel. The apparatus, which is equivalent in structure to a cone/plate viscometer, allowed the synthesis to be conducted in a well-controlled and uniform shear field. The ratio of the centrifugal to viscous force acting on the fluid in the CPA can be characterized using a dimensionless parameter R, which is a Reynolds number [31],

$$R = r^2\omega\alpha^2/12\nu$$

where r is the radial distance from the cone center to the inlet of a unidirectional valve at the bottom of the vessel, ω the angular velocity of the cone, α the cone angle in radians and, ν the kinematic viscosity of the fluid.

A typical synthesis was performed by first introducing the surfactant, water and ethanol mixture into the CPA where it was mixed under stirring conditions for 10 minute. Then, the aluminum tri-*sec*-butoxide was directly introduced into the system by injection at a rate of about 1ml/min through a unidirectional valve of 1/16 in. diameter installed on the bottom of the vessel. The mixture was aged under a constant cone velocity for 60 minutes. The sample was retrieved by filtration and washed by water and ethanol thoroughly and dried

in air at ambient temperature for about 12 hours. The samples were calcined for 5 hours in flowing air at 500°C using a temperature ramp rate of 2°C/min from room temperature to that temperature. The synthesis factors evaluated in the parametric study were cone velocity, surfactant choice, water/ethanol ratio, as well as co-solvent selection. Shown in Table 4-1 is a representative set of the range of parameters used for the study.

Powder X-ray diffraction (XRD) patterns were acquired by an X_1 advanced diffraction system (Scintag, Inc.) using a CuK_α radiation source (λ = 0.154 nm). Low angle X-ray diffraction with a 2θ range of 0.5-10° was used to investigate the mesoporosity of the materials and wide angle scans were performed within a 2θ range of 5-85° to determine the crystallinity of the materials. The surface area (SA) and pore size distribution were measured using a Micromeritics ASAP 2000. The SA was determined using the Brunauer-Emmett-Teller (BET) method and the Barrett-Joyner-Helenda (BJH) method was used to determine pore volume (PV) and pore size distribution. Sample preparation included degassing at 90°C for 1 hour followed by 200°C for at least 4 hours. SEM images were taken using a JSM-840 scanning microscope (JEOL Inc.) with gold coating sample preparation. For the transmisson electron microscopy (TEM) studies, thin sections of samples (60-80nm) embedded in epoxy resin were obtained using ultramicrotomy. The resulting sample was examined with a Philips model CM-30 TEM operated at 300KV. TGA and DTG curves were recorded using a Perkin Elmer TGA7 thermogravimetric analyzer with a 10°C/min temperature ramp rate and a purging gas of air.

4.3 Results

Shown in Table 4-1 are the parametric synthesis conditions for a representative set of aluminas synthesized for the study. The table also provides the textural properties measured for the resulting materials using BET characterization and SEM observation. For a given synthesis that resulted in particles with macropores, the macropores were sometimes only found in a portion of the sample particles. The column labeled "Occurrence" denotes the percentage of the total alumina particles that were found to contain macropores as determined by SEM. Although the macropore diameter varied under different synthesis conditions in an interval between 500nm and 1500nm, it was found to have a relatively narrow size distribution for a specific sample. Shown in Figure 4-2 is a representative SEM image for Sample 4 and the resulting macropore size distribution obtained from analysis of the image. For this sample, a median macropore diameter (MMPD) of about 1000nm was determined. The MMPD for the materials containing macropores are also included in Table 4-1.

Low angle XRD patterns for all samples gave a broad peak between 2θ of 1 and 3° indicating the existence of a mesostructure. The intensity of this peak was found to increase following calcination of the samples. A TEM image for a sample prepared under Sample 2 conditions is given in Figure 4-3a). An irregular mesopore motif can be seen in the walls of the material between the macropores, which are about 1000 nm in size. Shown in Figure 4-3b) are wide angle XRD patterns for representative materials synthesized under Sample 2 conditions at two different aging times. The Sample 2, which was aged for 60 minutes, had discrete peaks that could be assigned to the boehmite structure [34]. In contrast, the sample

that was only aged for 10 minutes did not display significant boehmite structure as measured by XRD. The XRD result for the typical synthesis was inconsistent with surfactant-templated mesoporous aluminas that are amorphous, but was consistent with mesoporous materials resulting from the assembly of nanoparticles. The presence of the boehmite structure, which was seen across the entire set of hierarchical materials, in conjunction with the TEM suggested that the macropores in the material were interconnected with networks of mesopores created by interstitial voids between crystalline boehmite nanoparticles.

Samples 1-5 were synthesized under the base water/ethanol/surfactant concentrations used in the previous study [23]. However, the mixing conditions used in each synthesis were varied. For Samples 1-4, the cone speed was increased from 100 to 750 rpm corresponding to R-values of 8.8 to 66. Whereas, for Sample 5 the aluminum alkoxide was first mixed with the *sec*-butanol, which insured complete dissolution of the aluminum alkoxide, and then the mixture was introduced to the CPA. Shown in Figure 4-4 are representative SEM images for Samples 1, 3, 4, and 5. As seen previously, the hydrodynamic conditions had a strong effect on particle morphologies. For Samples 1-3 regular parallel arrays of macropores having relatively uniform size were seen quite clearly in nearly every alumina particle. The macropores were orthogonal to the face of the particles and were found to either pass completely through the particle or to be closed off at one side after passing through most of the particle. Increasing the strength of the shear force that was manifest in higher R-values resulted in suppression of the macroporous structure. The R-value of 66 used in Sample 4 gave only a limited number of particles (25%) having any macropores and those macropores that were present were significantly more irregular than in Samples 1-3. No macropores were observed when R-values of greater than 100 were used. In addition to ultimately causing

complete suppression of the macropores, increasing the shear force appeared to cause the MMPD to increase. When the aluminum alkoxide was introduced in a dispersed state as in Sample 5 rather than directly as droplets, no macropores were observed in the resulting alumina particles. Therefore, the introduction of an aluminum alkoxide droplet into the synthesis mixture was clearly required for the formation of macropores.

The N_2 adsorption-desorption isotherm plots and pore size distribution (PSD) curves for the aluminas synthesized under different mixing conditions are shown in Figure 4-5. Each of the materials had a type IV isotherm with a fairly broad H2 hysteresis loop between relative pressures 0.4 and 0.8 indicating a distribution of pores in the mesoporous range [35]. The broad hysteresis loop suggests that these mesopores are not cylindrical but exist as a network of pores containing "inkbottle" pores [35]. The PV and median pore diameter (MPD) of Samples 1-4 were effectively independent of the mixing conditions. In contrast, Sample 5, which had the aluminum alkoxide was first dissolved in *sec*-butanol, gave lower values for the PV and MPD.

To examine the role of the surfactant on the formation of the hierarchical structures, syntheses were performed with other surfactants. Samples 6-8 were synthesized under varying mixing conditions using the nonionic Pluronic L64 surfactant rather than the ionic cetyltrimethylammonium bromide (CTAB) surfactant. The textural properties for these samples are given in Table 4-1 and the SEM images for Sample 6 and 7 are given in Figure 4-6a) and 4-6b), respectively. As can be seen from the micrographs, the macroscopic particle morphologies for these samples were similar to that of the base case. For all three samples nearly all of the particles contained macroporous structure. As with the previous set, increasing the shear rates such that the R-value increased above about 100 eliminated the

formation of macropores in the particles. An upward trend in MMPD again was found to correspond with increasing R-values.

While the macroporous structure was similar for materials synthesized with either CTAB or Pluronic L64 under comparable mixing conditions, the mesoporous structure was influenced by the choice of surfactant. The samples synthesized in the presence of Pluronic L64 had lower PV and MPD than those in which CTAB was used. The difference in PV and MPD was also manifest in the pore size distribution as can be seen from comparing the pore size distributions in Figure 4-7 and Figure 4-5. The materials made in the presence of Pluronic L64 had significantly broader pore size distributions and sharper decreases on the desorption branch indicating an "inkbottle" pore structure. Despite the difference in mesoporous structure, both the Pluronic L64 and CTAB-based samples were found from wide angle XRD to contain boehmite.

Syntheses were also performed with ionic surfactants having longer carbon chain length. Samples 9 and 10 correspond to materials made in the presence of dodecyltrimethylammonium and octadecyltrimethylamonium bromide, respectively, at R-values of about 10. In these samples nearly all of the particles contained macropores. The textural properties determined from BET analysis were similar to those of the materials made in the presence of CTAB. From the alternative surfactant work, the response of the mesopore structure to the choice of surfactant was not correlated as would be expected if the mesopores were being created by a templating-type interaction, but was consistent with the results reported for nanoparticle assembly in aluminas [32].

The role of the co-solvent in the formation of the hierarchical structure was examined by varying the ethanol/water ratio as well as substituting other solvents for the ethanol. All of

the samples were synthesized at R-values of about 10. Samples 1 and 11-13 provided a comparison of the effect of the ethanol/water ratio. Representative SEM images for this set of samples are shown in Figure 4-8. Two notable regions can be seen in the micrographs of the samples. The macropores can be seen on one face of the particle and the other face of the particle contained no macropores. As reported in the macroporous titania system [28], many of the macroporous alumina particles in the current work appeared to have macropores that did not extend completely through the particle. However, there were also other particles in which the macropores did transverse the entire particle. As a qualitative observation from the ethanol/water ratio samples, the thickness of the macropore-free portion of the particle appeared to increase with the increasing of ethanol/water volumetric ratio. Increasing the ethanol/water ratio from 0.25 to 0.67 maintained the macropores in most of the particles, but a further increase to 1.5 (Sample 12) diminished the particles containing macropores to 25%. The formation of macropores was completely suppressed when an ethanol/water ratio of 4 was used. With the exception of the PV for Sample 11, the characteristic textural properties as determined from N_2 adsorption/desorption for the ethanol/water ratio samples were similar.

Surface areas of higher ethanol/water ratio samples are not very different from that of the base case synthesized samples, however, PV and pore structure of these samples vary significantly as can be seen in Table 4-1. Unlike isotherms shown previously, the ethanol-rich samples had N_2 adsorption-desorption isotherms with distinctly different shape. Each isotherm had two hysteresis loops: one between relative pressure of 0.4 and 0.85 and another in the higher relative pressure region. The first hysteresis loop, which is in type H2, can be

attributed to similar mesporous structure in the other samples and the second could be assigned to the existence of textural mesoporosity in the material [34].

In previous initial screening work, *sec*-butanol and acetone were used to investigate the co-solvent effect on the formation of hierarchically structured aluminas [23]. Since the heterogeneous mixing conditions used in that synthesis were effectively in the transition region to shear rates above those able to sustain formation of macropores, the effect of using *sec*-butanol and acetone as the co-solvents on the formation of macropores was reexamined under control mixing at low R-values. These materials correspond to Sample 14 and 15 for *sec*-butanol and acetone, respectively. As can be seen from Table 4-1, these materials had macropores and textural properties that were the same as when ethanol was used as the co-solvent. Therefore, when the synthesis of the hierarchical alumina was performed within a controlled mixing regime, the choice of co-solvent had no effect on the morphologies of the resulting powders.

Since macropore formation appeared to be independent of the surfactant or co-solvent used, syntheses were performed in the absence of either a surfactant or co-solvent. The textural properties of these materials (Samples 16-19), which were made under varying mixing conditions are given in Table 4-1. The presence of regular arrays of macropores can be clearly seen in representative SEM images for Samples 16 and 17 as seen in Figure 4-6a) and 4-6b). As with the surfactant-containing synthesis, the formation of macropores was suppressed in the surfactant-free synthesis when mixing conditions were increased to R-values of above 100. Due to the lower viscosity of the synthesis mixture, lower cone speeds were required when a surfactant was not used. The consistent R-value required for macropore formation indicated that the Reynolds number parameter could be used to define the

hydrodynamic conditions that would yield a hierarchically structured material. The trend of increasing MMPD with increasing R-value was seen in Samples 16-18 as it was in surfactant-mediated syntheses at varying mixing conditions.

While the textural properties of the samples synthesized without surfactant or co-solvent were similar to those measured for the base case materials, the PVs for Samples 16-18 were somewhat lower than for Samples 1-4. Shown in Figure 4-9 are the N_2 adsorption-desorption isotherm plots and PSD curves for Samples 16-19. The pore size distributions for these samples were similar to those for the base case materials. Upon comparing all of the samples, the co-solvent appeared to have no impact on the structure of the mesopores. However, the choice of surfactant (ionic or nonionic) as well as the use of a surfactant was found to have some effect on defining the size and morphology of the resulting mesoporous structure.

Samples synthesized with and without the use of a surfactant were tested in the TGA following the 12 hour drying period. Similarly shaped TGA curves were observed for both types of samples with significant weight losses only in the 70 to 120°C region, which could be attributed to the loss of physisorbed water, and the 300 to 500°C region, which was due to dehydroxylation. If the surfactant was present after the water and ethanol washing procedure, it would cause a weight loss centered at about 300°C [36]. The lack of a significant weight loss at that temperature, indicated that no significant surfactant was left after the washing procedure, which is inconsistent with the ionic surfactant serving a templating role. The high water loss levels observed, particularly for Samples 1 and 6, were consistent with "inkbottle" type restricted pores that would retain water even after ethanol washing.

4.4. Discussion

The experimental results demonstrated that aluminas with pores at two distinct length scales could be produced from a defined range of synthesis conditions. Additionally, the set of conditions used in the study would strongly suggest that the formation of these two different characteristic pore morphologies were decoupled since they could be individually manipulated by the choice of synthesis condition. For example, the macropore formation was strongly influenced by changes in the hydrodynamic environment for a given synthesis composition, but the mesoporous structure was unaffected. Whereas, the choice of surfactant or the use of no surfactant affected the mesoporous structure while not affecting the macroporous structure at a fixed R-value. Therefore, it is possible to discuss the formation mechanisms for the two types of pores serially.

The formation mechanism for the mesoscale structure in the aluminas reported here would appear to be similar to that proposed by Hicks and Pinnavaia, where the mesopores correspond to the interstitial voids between boehmite nanoparticles [34]. As with the N_2 adsorption-desorption isotherms for their materials, broad hystersis loops were observed in the mesopore size range indicating a network of interconnected pores that are not cylindrical, but have restrictions leading to "inkbottle" shaped pores. The presence of boehmite particles was clearly evident by the XRD patterns, which became more pronounced with increased aging time.

Previous work with the synthesis of mesostructured aluminas, demonstrated that the choice of mediating surfactant influenced the resulting mesostructure with ionic and nonionic surfactants yielding different nanoparticle aggregation [34,37]. Unlike in the templating

mechanism, change in the chain length of the ionic amine surfactant used in the synthesis was reported to have no impact on the resulting mesopore structure. As demonstrated by Samples 1, 9 and 10 that were synthesized with different carbon chain length ionic surfactants, this same invariance was observed in these materials. The change to a nonionic surfactant or the elimination of a surfactant entirely from the synthesis did lead to changes in the mesoporous structure further demonstrating that the surfactant did influence the aggregation of the boehmite nanoparticles.

While the mesoporous structure formation mechanism in the materials appeared to be consistent with previous reports, the macropore formation mechanism has not been previously resolved. The current set of parametric syntheses under well-defined hydrodynamic conditions demonstrates synthesis conditions necessary for the macroporous structure to form. Critically important is the presence of an alkoxide droplet in the synthesis solution. As demonstrated in Sample 5, the pre-dispersal of the alkoxide in anhydrous alcohol completely suppressed macropore formation. In addition, high Reynolds number (R-value), which would cause more rapid break-up of the alkoxide droplets, also suppressed macropore formation. The need for an intact alkoxide droplet is also consistent with the rapid formation of the macroporous structure, which would not occur with a slower assembly process such as that seen with templated mesoporous silicas.

The surfactant did not appear to play any direct role in the macroporous structure as demonstrated by generation of macropores even in the absence of any surfactant. Indirectly, the surfactant influenced the macropores by changing the hydrodynamic environment. Due to the increased solution viscosity upon inclusion of the surfactant, a larger range of mixing speeds could be employed that would still stay within the envelope of Reynolds numbers

required for macropore formation. As such, a synthesis being performed in the presence of a surfactant in a standard flask with heterogeneity of mixing conditions would be more likely to form macropores than without the surfactant since the range of Reynolds numbers being accessed would be attenuated. The lack of direct surfactant role in the synthesis of the macroporous structure was consistent with that reported by Mann and co-workers [30] and Su et al. [28,29].

Due to the rapid formation of the macropores, the porous structure can be attributed to a kinetically accessed framework rather than an equilibrated structure. Therefore, the rates of hydrolysis of the aluminum alkoxide and condensation of the aluminate are critically important. The results in the current work and previous studies clearly demonstrate that the hydrolysis rate must be within a specific range to form the macropores. A commonality between our alumina macroporous structures and those reported for titania and zirconia was that highly reactive alkoxide precursors were required. When the hydrolysis rate was slowed by dilution with the alcohol co-solvent, the macropores did not form. As shown in our prior paper, increasing the hydrolysis rate by increasing the synthesis temperature also suppressed macropore formation [23].

From the results, the overall formation of the hierarchical structures appears to occur via hydrolysis and condensation on the external surface of the alkoxide droplets. Once the alumina particles reach a certain size range, they detach from the droplet surface thereby exposing a "fresh" alkoxide surface to begin the process again. The use of an alkoxide that readily hydrolyzes insures that the hydrolysis will occur more rapidly at the surface than dissolution of the alkoxide into the solvent.

The clear requirement for the presence of an alkoxide droplet does not, however, explain the formation of the macropore structure and the rapid rate of macropore structure formation makes direct observation of the formation mechanism difficult. Precedent does exist for the formation of regularly arrayed macroporous metal oxides. The synthesis of hexagonal arrayed macroporous alumina by aluminum anodization has been the subject of extensive studies [38-40]. The striking similarity in organization and length scale of the anodization-derived materials and our materials suggests that some analogies might exist in the formation mechanisms of the materials.

The anodic oxidation of aluminum occurs by placing a voltage on an aluminum substrate to create a current density that drives oxidation of the surface aluminum. During the anodization process three distinct regions exist: the aluminum substrate, the aluminum oxide surface layer, and the acidic electrolyte solution. Growth of the oxide layer is coupled with some dissolution of Al^{3+} into solution. The generation of regularly arrayed porous alumina from the anodic oxidation of aluminum has two important steps, initiation of the hexagonal pattern of the pores on the surface of the aluminum and the propagation of the pores through the aluminum substrate.

Significant debate still exists about the mechanism of the pore initiation with attention largely centered upon the nanoscale morphology of the original aluminum substrate. During initiation of the oxidation, an oxide film forms across the entire surface. The film thickens since oxygen transport through the film and oxidation at the metal-film interface occurs more readily than dissolution of Al^{3+}. As the film reaches a thickness exceeding the height of initial features in the aluminum surface a regular scalloped pattern develops at the metal-film interface. At this point, a higher local conduction resistance occurs at the ridges of the scallop

relative to the valleys. The higher current density in the valleys causes locally enhanced rates of oxidation and dissolution [41,42]. The electrochemical enhancement of the oxidation and Al^{3+} dissolution rates in the hemispherical-shaped valleys that are established in the initiation step leads to propagation of the base of the pore through the aluminum. As the pore propagates the current density at the base of the pore greatly exceeds that through the wall leading to the second stage of macropore formation, which is the growth of the pore.

In principle, the hydrolysis and dissolution occurring at the surface of the aluminum alkoxide droplet is analogous to the oxidation and dissolution occurring at the aluminum substrate surface. While the applied voltage provides the driving force for the oxidation reaction, the hydrolysis reaction has a sufficient chemical driving force to proceed rapidly. If a scalloped-type pattern was established at the droplet surface, enhanced rates of hydrolysis and solubilization would be expected in the valleys where the alkoxide/solvent interaface was most exposed. Once the pores initiated they would propagate towards the alkoxide preferentially to causing any change in the pore walls. After the condensed macroporous alumina particle reached a sufficient size it would then break off from the alkoxide droplet.

This proposed macropore development mechanism leaves several unanswered questions. As with the anodization process, the cause of the initiation of the macropore array is unclear. Secondly, as reported in the titania work by Mann and co-workers [30], many of the macroporous alumina particles contained macropores that did not transverse the entire particle as seen clearly in Figures 4-8 a) and b).

The macropore-free shell on one side of the particle coupled with the curvature of the particle led Mann and co-workers to propose a formation mechanism that involved initial formation of a mesoporous semi-permeable membrane on the outside of the alkoxide droplet.

They propose the formation of this membrane restricts the hydrolysis/condensation domain such that the reaction subsequently moves inward. The formation of the macropore channels are attributed to microphase-separated regions of metal oxide and solvent established by flow of the solvent across the membrane to the alkoxide interface. This proposed formation mechanism for the macroporous titania material would appear to be consistent with many of the observations for the hierarchically-structured aluminas. Once the macropore channels were formed they would preferentially propagate toward the alkoxide since it would provide the least resistant path for the water to react at the solution/alkoxide interface. The driving force for the flow would be the gradient in water concentration caused by hydrolysis.

As with the annodization process, initiation of the regularly-arrayed macroporous pattern is more difficult to discern. Hexagonal arrayed structures are energetically favored, which may be the cause of the resulting macropore pattern as proposed within the microphase-separated region. However, as shown in Table 4-1 an increase in solvent Reynolds number led to a systematic increase in the MMPD. If the macropore formation was initiated after a permeable shell was formed on the alkoxide droplet, the hydrodynamic conditions in the solvent would not be expected to influence the microphase segregation on the other side of the permeable shell. Although the presence of the non-macroporous region was seen on many particles containing macropores, some of the particles had macropores that completely transversed the particle as seen in Figure 4-6d).

Seminal to the proposed formation mechanism is the diffusion of water across the membrane and through the liquid channel to the alkoxide surface. Due to the high hydrolysis rate of the aluminum alkoxide, the water concentration at the interface should be extremely small leading to a large water concentration gradient from the free solvent to droplet surface.

However, this diffusion would need to occur against counterdiffusion of butanol formed in the hydrolysis reaction. It is not clear that the diffusion of water against the counterdiffusional flow of butanol and the resistance of the permeable shell would be sufficiently rapid. Therefore, the proposed mechanism does explain many of the observation, but still appears to leave several outstanding questions.

4.5 Conclusions

Hierarchically structured aluminas with bimodal pore distribution on the meso- and macro-scale were synthesized within a well-characterized parameter space. The parametric synthesis study demonstrated that the pore structure at the two length scales could be independently modified. The use of a surfactant was found to influence the mesoscale structure, but not the macroscale structure as long as the synthesis was performed at the same hydrodynamic conditions. The formation of the macroporous structure was found to depend strongly on the hydrodynamic conditions in the synthesis mixture as well as the presence of an aluminum alkoxide droplet in the synthesis mixture. A previously proposed formation mechanism described many, but not all of the features seen in the synthesis study suggesting that the precise mechanism underlying these hierarchical aluminas remains elusive.

References

1. K. Wefers, C. Misra, *Oxide and Hydroxide of Aluminum.* Alcoa Technical Paper No.**19**, 1987.
2. P. Braunstrin, H. P. Kormann, W. Meyer-Zaika, R. Pugin, G. Schmid, *Chem. Eur. J.* 6 (2000) 4637.
3. C. Mirsa, *American Chemical Society monograph, Vol. 184: Industrial alumina chemicals*; American Chemical Society: Washington, DC, 1986.
4. R. K. Oberlander, in: B. E. Leach, (Ed), *Applied Industrial Catalysis Vol. 3*, Academic Press, London, 1984.
5. K. C. Tylor, *Catal. Rev.-Sci. Eng.* 35 (1993) 457.
6. D. N. Belton, K. C. Tylor, *Cur. Opin. Solid State Mater. Sci.* 4 (1999) 97.
7. C. T. Kresge, M. E. Leonowicz, W. J. Roth, J. C. Vartuli, J. S. Beck, *Nature* 359 (1992) 710.
8. J. S. Beck, J. C. Vartuli, W. J. Roth, M. E. Leonowicz; C. T. Kresge, K. D. Schmitt, C. T-W. Chu, D. H. Olson, E. W. Sheppard, S. B. McCullen, J. B. Higgins, J. L. Schlenker, *J. Am. Chem. Soc.* 114 (1992) 10834.
9. T. P. Tanev, T. J. Pinnavaia, *Science* 267 (1995) 865.
10. S. A. Bagshaw, T. J. Pinnavaia, *Angew. Chem. Int. Ed. Engl.* 35 (1996) 1102.
11. F. Vaudry, S. Khodabandeh, M. E. Davis, *Chem. Mater.* 8 (1996) 1451.
12. S. Cabrera, J. E. Haskouri, J. Alamo, A. Beltrán, D. Beltrán, S. Mendioroz, M. D. Macros, P. Amorós, *Adv. Mater.* 5 (1999) 371.
13. X. Liu, Y. Wei, D. Jin, D. Shih, *Mater. Lett.* 42 (2000) 143.

14. S. Valange, J.-L. Guth, F. Kolenda, S. Lacombe, Z. Gabelica, *Microporous Mesoporous Mater.* 35-36 (2000) 597.

15. S. Schacht, Q. Huo, I. G. Voigt-Martin, G. D. Stucky, F. Schűth, *Science* 273 (1996) 768.

16. Q. Huo, J. Feng, F. Schűth, G. D. Stucky, *Chem. Mater.* 9 (1997) 14.

17. Q. Huo, D. Zhao, J. Feng, K. Weston, S. K. Buratto, G. D. Stucky, S. F. Schűth, *Adv. Mater.* 9 (1997) 974.

18. W. Zhang, T. R. Pauly, T. J. Pinnavaia, *Chem. Mater.* 9 (1997) 2491.

19. T. R. Pauly, Y. Liu, T. J. Pinnavaia, S. J. L. Billinge, T. P. Rieker, *J. Am. Chem. Soc.* 121 (1999) 8835.

20. Q. Cai, Z. Luo, Z. Pang, Y. Fan, X. Chen, F. Cui, *Chem. Mater.* 13 (2001) 258.

21. H. Lin, C. Mou, *Science* 273 (1996) 765.

22. Q. Luo, L. Li, Z. Xue, D. Zhao, in: Sayari. Et al. (Editors), *Studies in Surface Science and Catalysis, Vol.129.* **2000**, Elsevier Science, P37.

23. W. Deng, M. W. Toepke, B. H. Shanks, *Adv. Funct. Mater.* 13 (2003) 61.

24. Z. Yuan, A. Vantomme, A. Leonard, B. Su, *Chem. Commun.* (2003) 1559.

25. Z. Yuan, T. Ren, B. Su,. *Adv. Mater.* 15 (2003) 1462.

26. J. Blin, A. Leonard, Z. Yuan, L. Gigot, A. Vantomme, A. K. Cheetham, B. Su, *Angew. Chem. Int. Ed.* 42 (2003) 2872.

27. T. Ren, Z. Yuan, B. Su, *Langmuir* 20 (2004) 1531

28. Z. Y. Yuan, T. Z. Ren, A. Vantomme, B. Su, *Chem. Mater.* 16 (2004) 5096.

29. A. Leonard, B. Su, *Chem. Commun.* (2004) 1674.

30. A. Collins, D. Carriazo, S. A. Davis, S. Mann, *Chem. Comm.* (2004) 568.

31. H. P. Sdougos, S. R. Bussolari, C. F. Dewey, *J. Fluid Mech.* 138 (1984) 379.

32. S. Einav, C. F. Dewey, Hartenbaum, *H. Experiments in Fluids*, 16 (1994) 196.

33. Y. Grad, S. Einav, *Experiments in Fluids*, 28 (2000) 336.

34. R. H. Hicks, T. J. Pinnavaia, *Chem. Mater.* 15 (2003) 78.

35. J. C. Groen, J. Perez-Ramirez, *Appl. Catal. A: Gen.* 268 (2004) 121.

36. W. Deng, P. Bodart, M. Pruski, B. H. Shanks, *Microporous Mesoporous Mater.* 52 (2002) 169.

37. Z. Zhang, R. W. Hicks,T. R. Pauly, T J. Pinnavaia, *J. Am. Chem. Soc.* 124 (2002) 1592.

38. G. E. Thompson, G. C. Woo, *Anodic Films on Aluminum*, in: J. C. Scully, (Editor), *Aqueous Processes and Passive Films, Academic*, London 1983.

39. H. Masuda, K. Fukuda, *Science* 268 (1995) 1466.

40. O. Jessensky, F. Müller, U. Gösele, *Appl. Phys. Lett.* 72 (1998) 1173.

41. H. Wu, X. Zhang, K. R. J. Hebert, *Electrochem. Soc.* 147 (2000) 2126.

42. S. K. Thamida, H.-C. Chang, *Chaos* 12 (2002) 240.

Table 4-1. Preparation conditions and characterization results for a set of syntheses.

ID	Co-S/S (V/V)	$C_{Surfactant}$	Cone Speed	R	Occurrence	MMPD	SA	PV	MPD
		mM	rpm		%	nm	m^2/g	cm^3/g	A
1	0.25	0.022	100	8.8	90	500	430	0.56	50
2	0.25	0.022	200	18	90	650	410	0.5	47
3	0.25	0.022	500	44	95	850	370	0.51	53
4	0.25	0.022	750	66	25	1000	380	0.52	52
5	0.25	0.022	100	8.8	0	N/A	340	0.36	40
6	0.25	0.014	100	7.9	90	600	440	0.44	38
7	0.25	0.014	500	39	90	850	420	0.41	38
8	0.25	0.014	1000	79	90	1000	370	0.42	44
9	0.25	0.022	100	11	95	550	400	0.46	44
10	0.25	0.022	100	10	85	750	360	0.4	42
11	0.67	0.022	100	7.4	75	1000	470	0.91	75
12	1.5	0.022	100	6.9	25	600	420	0.56	51
13	4	0.022	100	7.7	0	N/A	440	0.56	48
14	0.25	0.022	100	10	85	1000	470	0.49	39
15	0.25	0.022	100	14	90	700	420	0.51	46
16	0	0	100	17	90	750	460	0.49	40
17	0	0	200	34	90	850	480	0.46	37
18	0	0	500	86	90	1200	390	0.43	41
19	0	0	750	130	0	N/A	310	0.32	41

Figure captions:

Figure 4-1. Schematic of the cone/plate apparatus.

Figure 4-2. Representative SEM image from Sample 4 and its macropore size distribution.

Figure 4-3. a) TEM image for Sample 2 (~700 nm macropores); b) wide angle XRD scans for Sample 2 with 60 minute aging (above) and 10 minute aging (below).

Figure 4-4. SEM images (5μm scale bar): a) Sample 1, b) Sample 3, c) Sample 4, and d) sample 5.

Figure 4-5. N_2 adsorption-desorption isotherm plots and pore size distribution curves.

Figure 4-6. SEM images (5μm scale bar) for the Pluronic L64 samples: a) Sample 6, b) Sample 7, and for the aluminum alkoxide/water only samples: c) Sample 16, d) Sample 17.

Figure 4-7. N_2 adsorption-desorption isotherm plots and pore size distribution curves for the Pluronic L64 samples.

Figure 4-8. SEM images (5μm scale bar for a and b, 2 μm scale bar for c and d) for ethanol/water ratio samples: a) Sample 1, b) Sample 11, c) Sample 12, and d) Sample 13.

Figure 4-9. N_2 adsorption-desorption isotherm plots and pore size distribution curves for the aluminum alkoxide/water only samples.

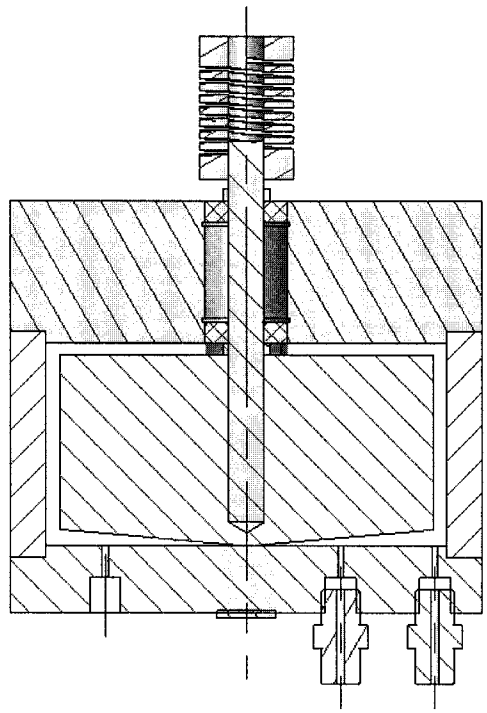

Figure. 4-1

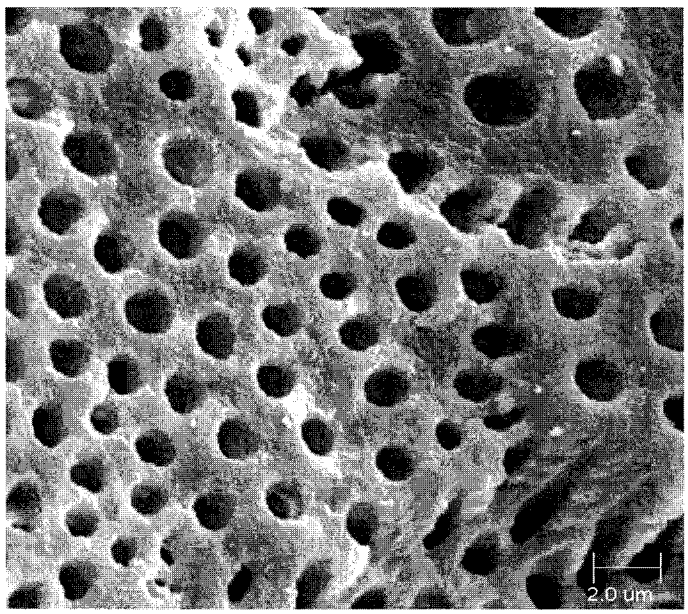
2.0 um

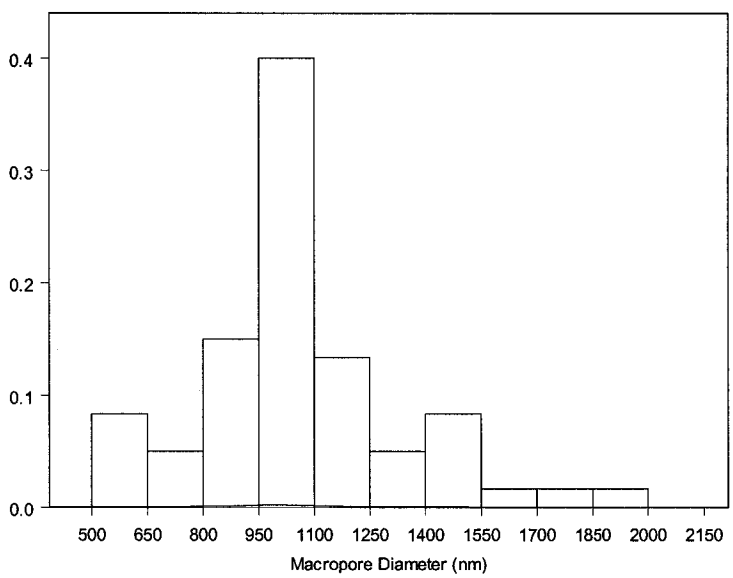
0.4
0.3
0.2
0.1
0.0
500
650
800
950
1100
1250
1400
1550
1700
1850
2000
2150
Macropore Diameter (nm)

Figure. 4-2

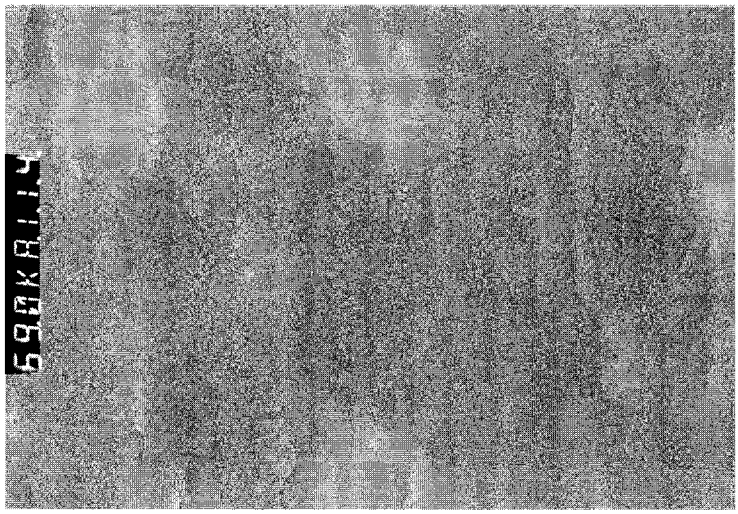

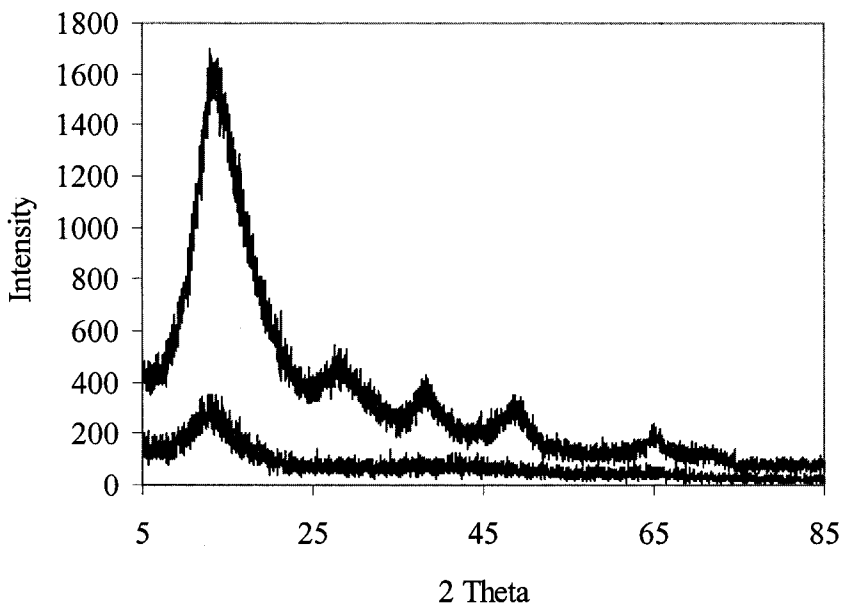
1800
1600
1400
1200
1000
800
600
400
200
0
Intensity
5
25
45
65
85
2 Theta

Figure. 4-3

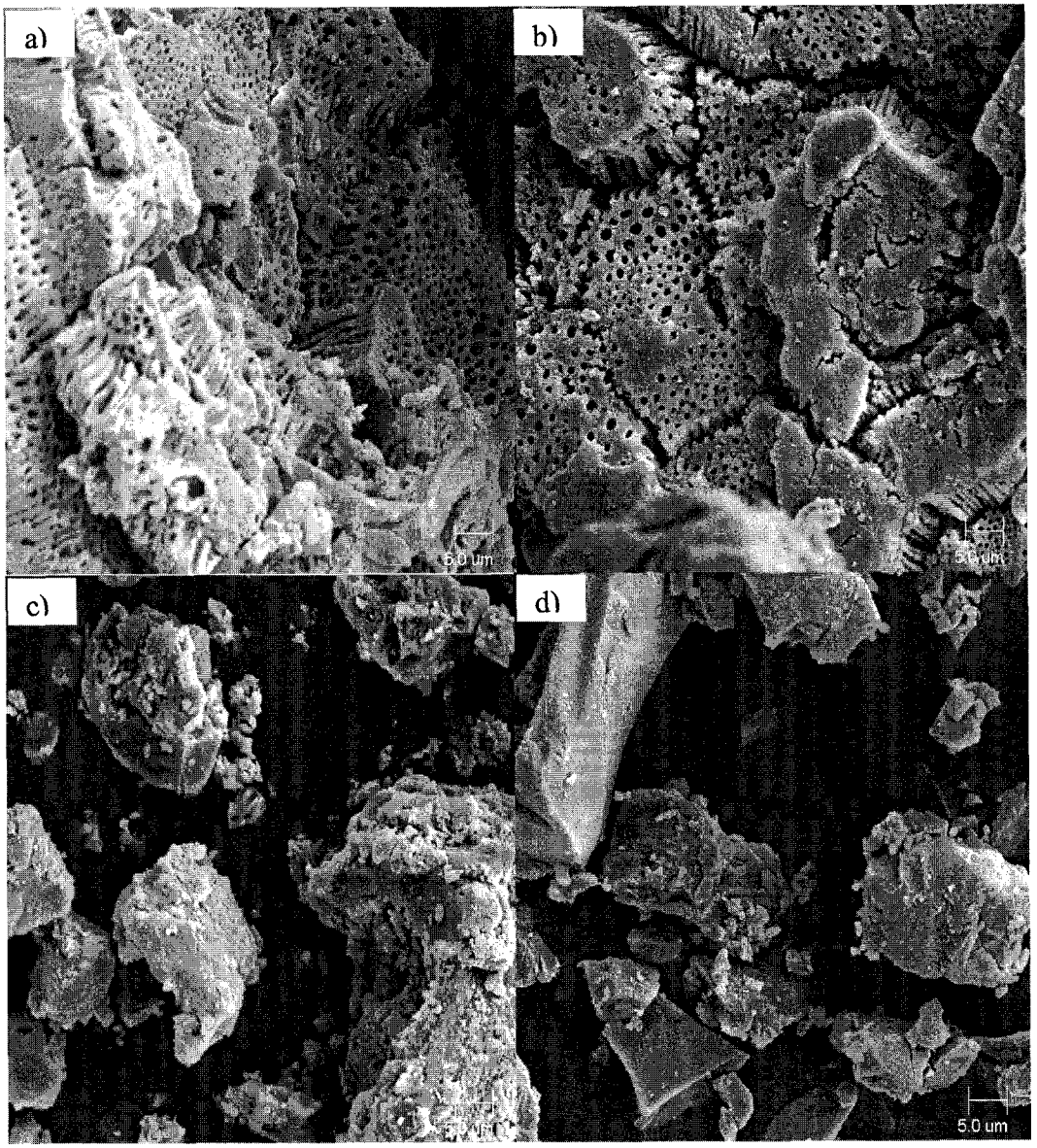

Figure. 4-4

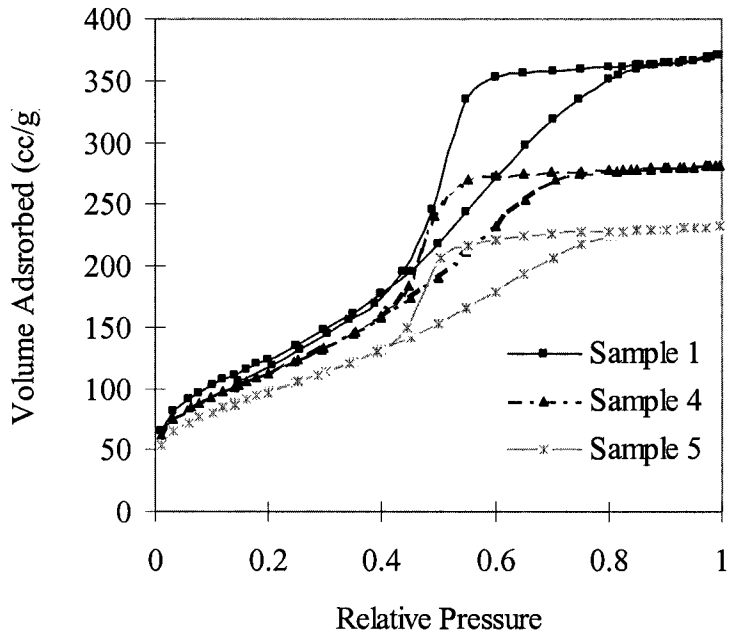
400
350
300
250
200
150
100
50
0
Volume Adsrorbed (cc/g
0
0.2
0.4
0.6
0.8
1
Relative Pressure
Sample 1
Sample 4
Sample 5

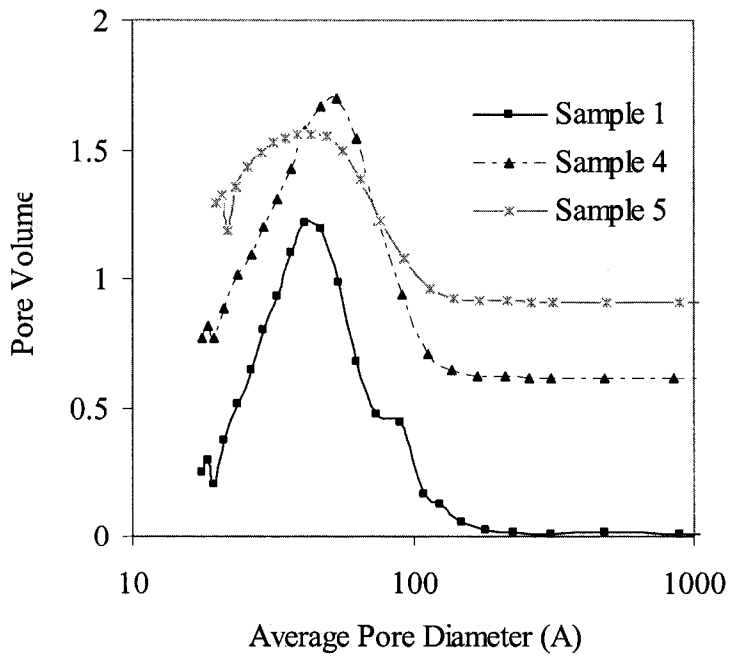
2
1.5
1
0.5
0
Pore Volume
10
100
1000
Average Pore Diameter (A)
Sample 1
Sample 4
Sample 5

Figure. 4-5

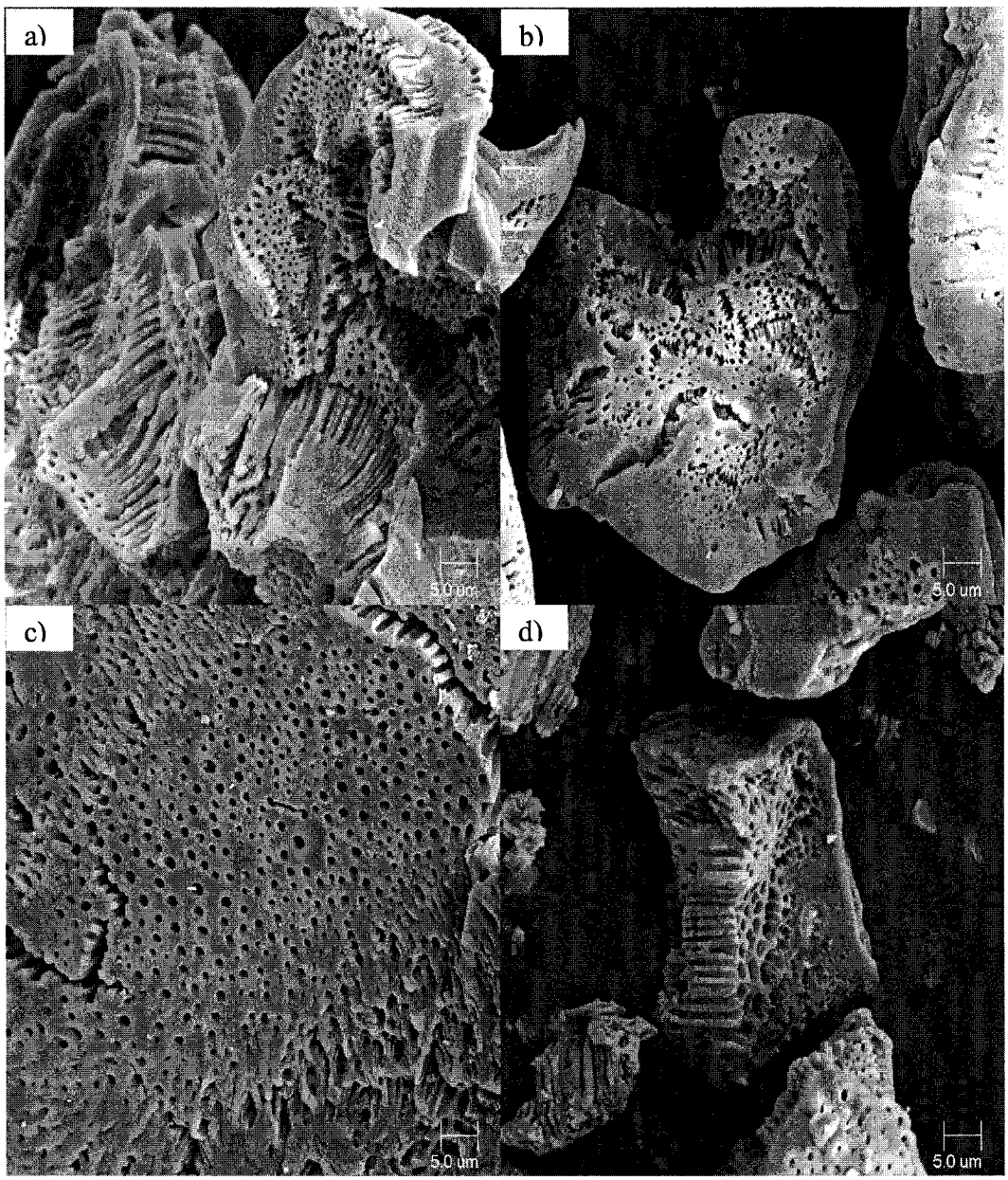

Figure. 4-6

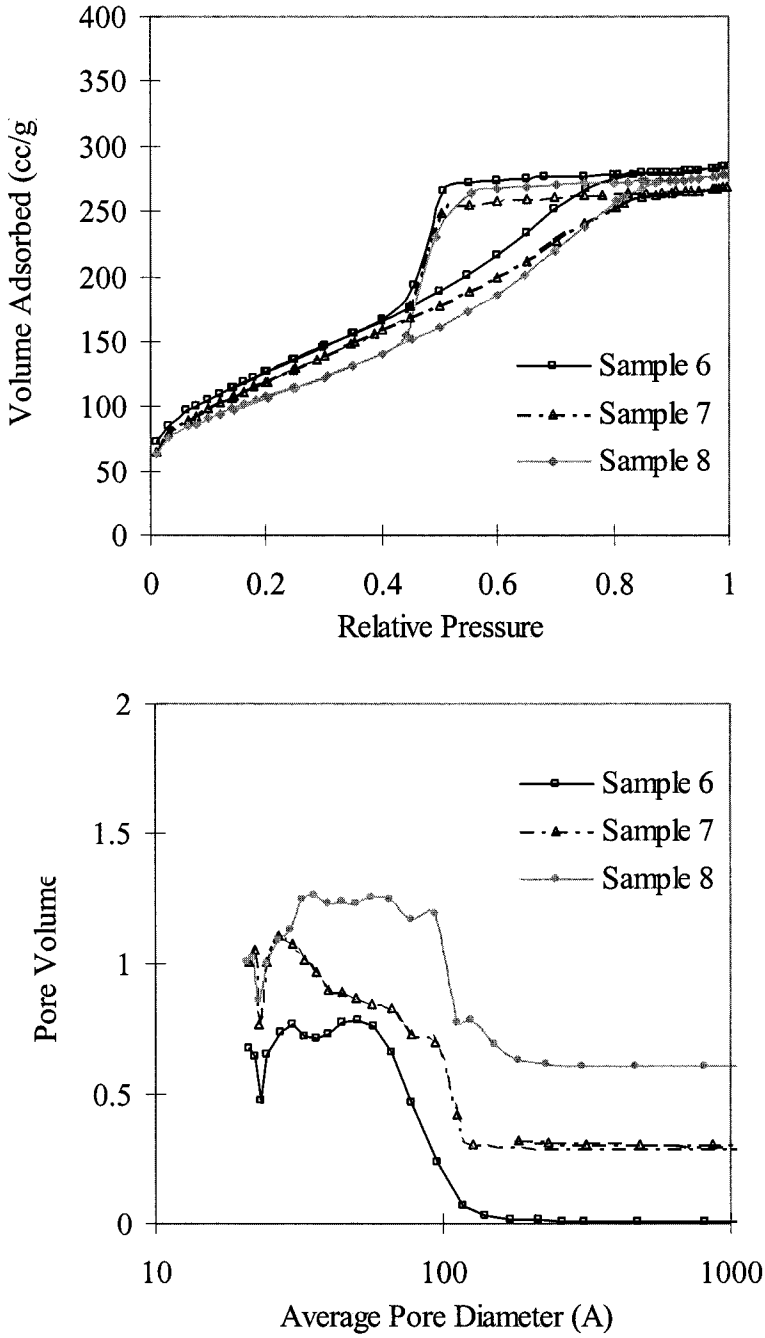
Volume Adsorbed (cc/g
400
350
300
250
200
150
100
50
0
0
0.2
0.4
0.6
0.8
1
Relative Pressure
Sample 6
Sample 7
Sample 8
Pore Volume
2
1.5
1
0.5
0
10
100
1000
Average Pore Diameter (A)
Sample 6
Sample 7
Sample 8

Figure. 4-7

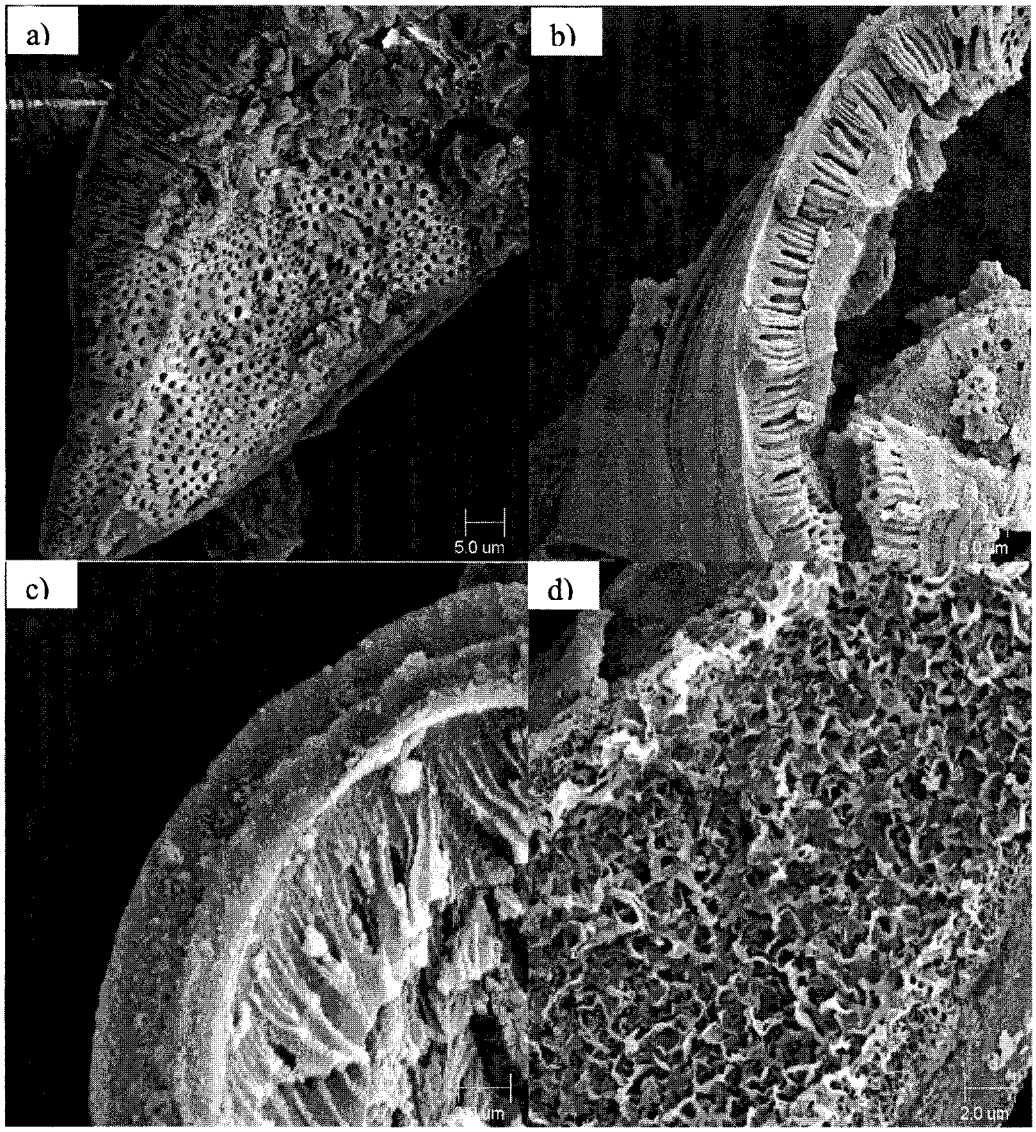

Figure. 4-8

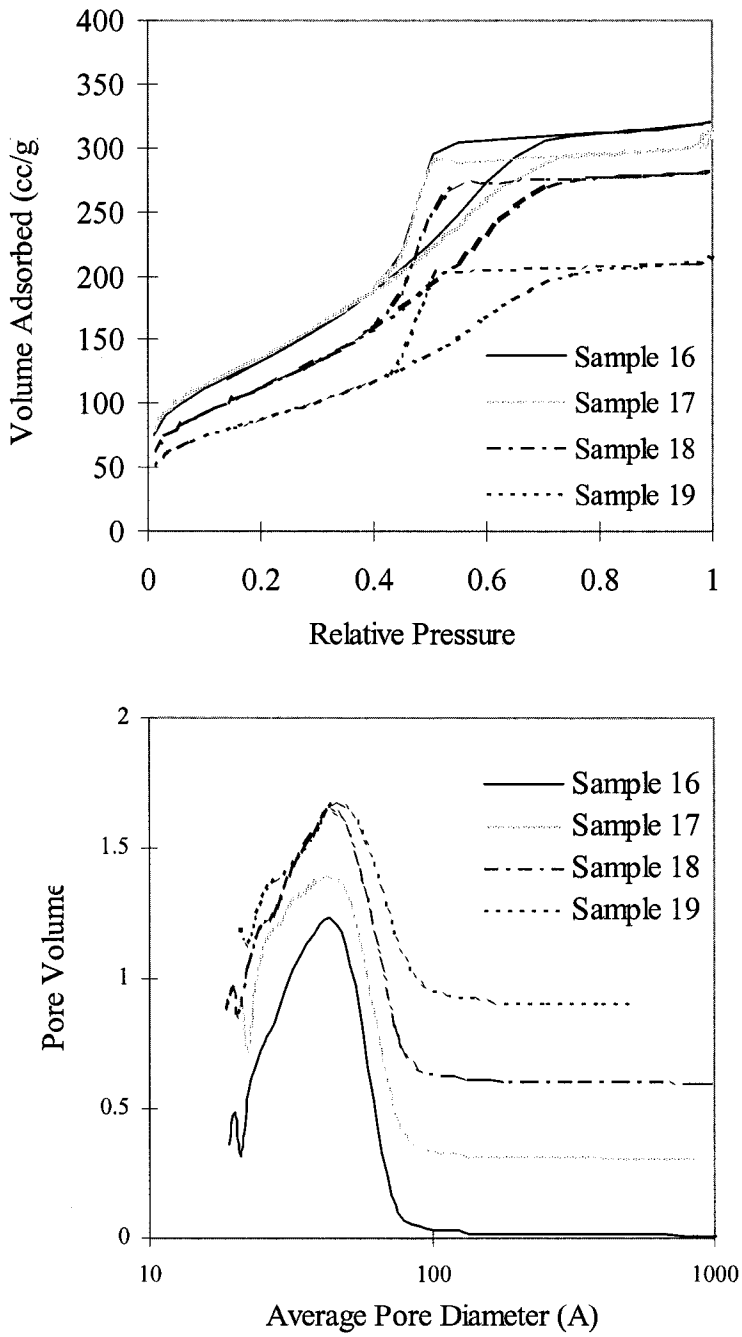
Volume Adsorbed (cc/g
400
350
300
250
200
150
100
50
0
0
0.2
0.4
0.6
0.8
1
Relative Pressure
Sample 16
Sample 17
Sample 18
Sample 19
Pore Volume
2
1.5
1
0.5
0
10
100
1000
Average Pore Diameter (A)
Sample 16
Sample 17
Sample 18
Sample 19

Figure. 4-9

Chapter 5. Synthesis of Higher Order Hierarchically Structured Aluminas

5.1. Introduction

The research on mesoporous material started by Mobil researchers [1,2] provides new chances to improve the poor textural properties of traditional alumina [3] and hence design a new generation of alumina materials that can satisfy its industrial needs as a ideal catalyst, catalyst carrier or adsorption medium [4]. Recently fabrication of hierarchical structure has received an increasing attention [5,6]. Controlling particle morphology of mesoporous material is not only essential for improving its properties, for example, catalytic performance: the existence of certain morphology could affect the mass transfer of guest molecules into the catalytic surface, it also provides insights into understanding similar processes that are observed in nature. We firstly reported [7] the synthesis of a hierarchically structured alumina. This mesoporous material that features the existence of regular arrays of macropores with several hundreds nanometers in diameter could be synthesized within a fairly broad parametric space. Following our results, Su et al. subsequently reported similar structures for zirconia [8] and later for aluminosilicate [9]. Here we report the first synthesis of a higher order hierarchically structured alumina. Several factors affecting its formation are investigated and a possible formation mechanism for the materials is proposed.

5.2. Experimental

All syntheses were conducted in a cone/plate apparatus, which can provide a constant shear force field to the reaction system. A base case synthesis is described as below:

aluminium tri-*sec*-butoxide was hydrolysed in a solution of surfactant (CTAB or Pluronic L64) in a mixture of water and ethanol. After 60 minute aging the fresh sample was retrieved by filtration and washed by water and ethanol. Calcinations were taken under 500°C for 5 hours in airflow. Several factors such as ethanol/water volumetric ratio, the choice of surfactant and co-solvent as well as hydrodynamic field strength were investigated.

5.3. Results and discussion

Shown in Figure 5-1 are SEM images for the hierarchically nanostructured materials. From Figure 5-1a and Figure 5-1b, hollow alumina tube with size of 50-100 micrometers can be seen clearly and moreover, the wall of these tubes consists of clusters of macropores with 1-1.5 micrometer in diameter. These macropores are not interconnected and on the radical direction of the alumina tube. Noticed that the macropores open only on the inner surface of the tube and the later has a fairly smooth outer surface. TEM image for the material shows a wormlike mesopore motif, which is typical for mesoporous alumina. This assertion is also supported by low angle XRD and BET characterizations. Wide angle XRD scan (Figure 5-2) for this material shows a pattern that can be assigned to boehmite crystalline structure of alumina [10]. This result is in accordance with that of mesoporous alumina synthesized by hydrolysing aluminium alkoxide in an aqueous medium [11]. The material, which has well defined structures at three length scales of tens of micrometers, micrometers and nanometers, respectively, could be obtained without the assistance of surfactant and co-solvent, indicating that they are not essential in the formation of this hierarchically structured material.

Figure 5-3 shows a N_2 adsorption-desorption isotherm plot and a pore size distribution (PSD) curve for the material. The isotherm, which is in type IV, has a H2 type

hysteresis loop manifesting the mesoporosity of the material [12]. A narrow PSD centred at around 5nm is observed for the material. It has specific surface areas ranging from 400-500 m^2/g, higher than that of activated alumina produced by a traditional sol-gel method [13]. Amine surfactants with different carbon chain length were used in the synthesis of this material. There is no apparent correlation between carbon chain length of the surfactant molecule and median pore diameter of the resulted material indicating that probably a templating process is not involved in the formation of mesostructures.

A nanoparticle assembly mechanism [14] might operate in the formation of mesostructure of the material. The introduced aluminium alkoxide hydrolyses very quickly due to its high reactivity and the existence of excess amount of water. The hydrolysis product undergoes a structural rearrangement to form boehmite nanoparticles. This process, taking hours to finish, has been detected by XRD for a similar reaction system [14]. Since surfactant could mediate the size and aggregation of nanoparticles during the aging process, the SA and PV of the material, which largely originate from the interstitial voids of nanoparticles [15], were affected by the existence of surfactant or by the choice of surfactant species. While surfactant plays a role in mediating mesoporosity of the material, it is not necessary for the formation of macropores or higher order hierarchically structured alumina. Particles having this morphology could be found in a sample synthesized by hydrolysing aluminium alkoxide solely by water. This fact, showing that macropores and higher order hierarchical structure originate from a cooperative interaction of aluminium alkoxide and water, has not been reported before.

In this work, the aluminium alkoxide was added to the reaction medium as droplets. The initial hydrolysis and following aging processes were conducted under moderate

hydrodynamic field strength in order to keep the integrity of the droplet. Here we propose a formation mechanism, which is similar to a mechanism of macropore formation during aluminum anodization [16,17] for the higher order hierarchically structured alumina material. As explained in Figure-4, basically there are three steps in the whole formation process: macropore initialization, macropore propagation and bending of alumina/ aluminium alkoxide composite.

Soon after aluminium alkoxide droplets are introduced into the reaction mixture, the hydrolysis reaction takes place on the outer surface of a droplet and a thin layer of alumina (aluminium hydroxide), which will inhibit the further solubilization of aluminium alkoxide, forms. There might exist diffusions through this layer that, combined with a moderate hydrodynamic agitation, could destroy the still relatively soft alumina layer and results in dissolution of alumina species to the solution after the layer reaches certain thickness. This initial dissolution creates a surface heterogeneity that triggers the pore initialization process. Conceptually this process results in a distribution of cavities with uniform size and these cavities are hexagonally arranged on the alumina surface and have a hemisphere bottom since this arrangement is energetically favoured. At this point, a scalloped-shape pattern form is established as shown in Figure 5-4. The following unidirectional dissolution propagate the bottom of the cavities toward to the inner part of the droplet through competing processes of hydrolysis of aluminium alkoxide and dissolution of alumina at aluminium alkoxide/alumina and alumina/solution interface, respectively.

The macropore propagation accompanying by the dissolution of alumina causes shrinkage of the porous alumina layer while the original aluminium alkoxide maintains its shape. A force imbalance hence is created due to different contractions of these two species.

A small piece of alumina/aluminium alkoxide composite will be peeled off from the droplet as a result of bending toward the alumina side caused by an intensified force imbalance. The new exposed aluminium alkoxide below the alumna layer undergoes a quick hydrolysis, however, macropore initialization and propagation on this side could not be developed further because of the lacking of aluminium alkoxide - alumina from both sides meets together. The detached alumina/aluminium composite with parallel macropores on continues to bend and finally forms the alumina tube with tens of micrometers in diameter. It should be emphasized that structure organization at different length scales for the material occurs simultaneously except that macrostructure formation is much faster than the evolution of boehmite nanoparticles from hydrolysis products. Only very limited amount of sample particles shows this higher order structure, others have macropore-containing plate, half-curved plate indicating that the whole system is a highly kinetics controlled one.

5.4. Conclusions

In this work, a higher order hierarchically structured alumina has been synthesized for the first time. A possible formation mechanism that elucidates the formation of this structure is given. Synthesis of this material is providing new chances not only in designing new materials for industrial applications but also in gaining insights into understanding the formation of hierarchical structures frequently observed in nature.

References

1. J. S. Beck, J. C. Vartuli, W. J. Roth, M. E. Leonowicz, C. T. Kresge, K. D. Schmitt, C. T.-W. Chu, D. H. Olson, E. W. Sheppard, S. B. McCullen, J. B. Higgins, J. L. Schlenker, *Journal of the American Chemical Society*, 114 (1992) 10834.
2. C. T. Kresge, M. E. Leonowicz, W. J. Roth, J. C. Vartuli, J. S. Beck, *Nature*, 359 (1992) 710.
3. C. Mirsa, American chemical society monograph, **184**: *Industrial alumina chemicals;* American chemical society: Washington, DC, 1986.
4. R. K.Oberlander, in: B. E. Leach, (Ed), *Applied Industrial Catalysis* **3**, Academic Press, London, 1984.
5. S. Schacht; Q. Huo, I. G. Voigt-Martin, G. D. Stucky, S.F.Schűth, *Science* 1996, *273*, 768; Q. Huo, D. Zhao, J. Feng, K. Weston, S. K. K. Buratto, G. D. Stucky, S. F. Schűth, *Adv. Mater.* 9 (1997) 974.
6. Q. Cai, Z. Luo, Z. Pang, Y. Fan, X. Chen and F. Cui, *Chem. Mater.* 2001, **13**, 258; H. Lin, C. Mou, *Science* 273 (1996) 765.
7. W. Deng, M.W. Toepke, B. H. Shanks, *Adv. Funct. Mater.*13 (2003) 61.
8. Z. Yuan, A. Vantomme, A. Leonard, B. Su, *Chem. Commun.* (2003) 1559.
9. A. Leonard, J. Blin, B.Su, *Chem. Commun.* (2003).
10. Z. Zhang, T. J. Pinnavaia, *Journal of the American Chemical Society*, 124 (2002) 12294.
11. X. Liu, Y. Wei, D. Jin, D. Shih, *Mater. Lett.* 42 (2000) 143.
12. K. S. W. Sing, D. H. Everett, R. A. Haul, L. Moscou, R. A. Pierotti, J. Rouquerol, T. Siemieniewska, *Pure & Appl. Chem.* 57 (1985) 603.

13. B. E. Yoldas, *Journal of Applied Chemistry & Biotechnology*, 23 (1973) 803.

14. R. H. Hicks, T. J. Pinnavaia, *Chem. Mater.* 15 (2003) 78.

15. N. Yao, G. Xiong, Y. Zhang, M. He, W. Yang, *Catalysis Today* 68 (2001) 97.

16. H. Wu, X. Zhang, K. R. Hebert, *Electrochem. Soc.* 147 (2000) 2126.

17. S. K. Thamida, H.-C. Chang, *Chaos* 12 (2002) 240.

Figure captions:

Figure 5-1. SEM images for a high order hierarchically structured alumina: a) hollow tube with macropores on the wall, and b) outer surface.

Figure 5-2. Wide angle XRD scan for the sample showing a boehmite structure.

Figure 5-3. N_2 adsorption-desorption isotherm and pore size distribution for the material.

Figure 5-4. A schematic explanation of the formation mechanism for the material.

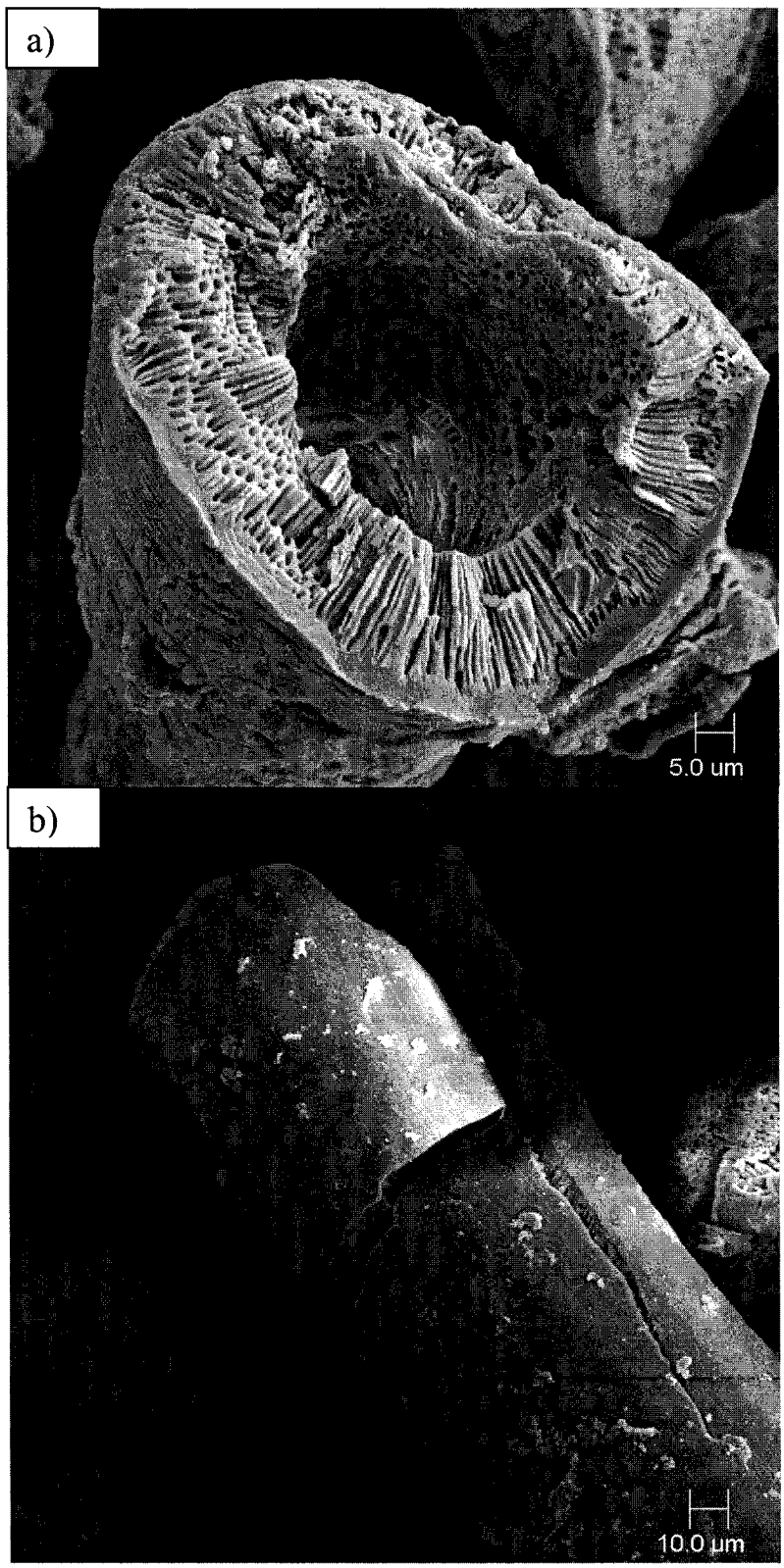

Figure. 5-1

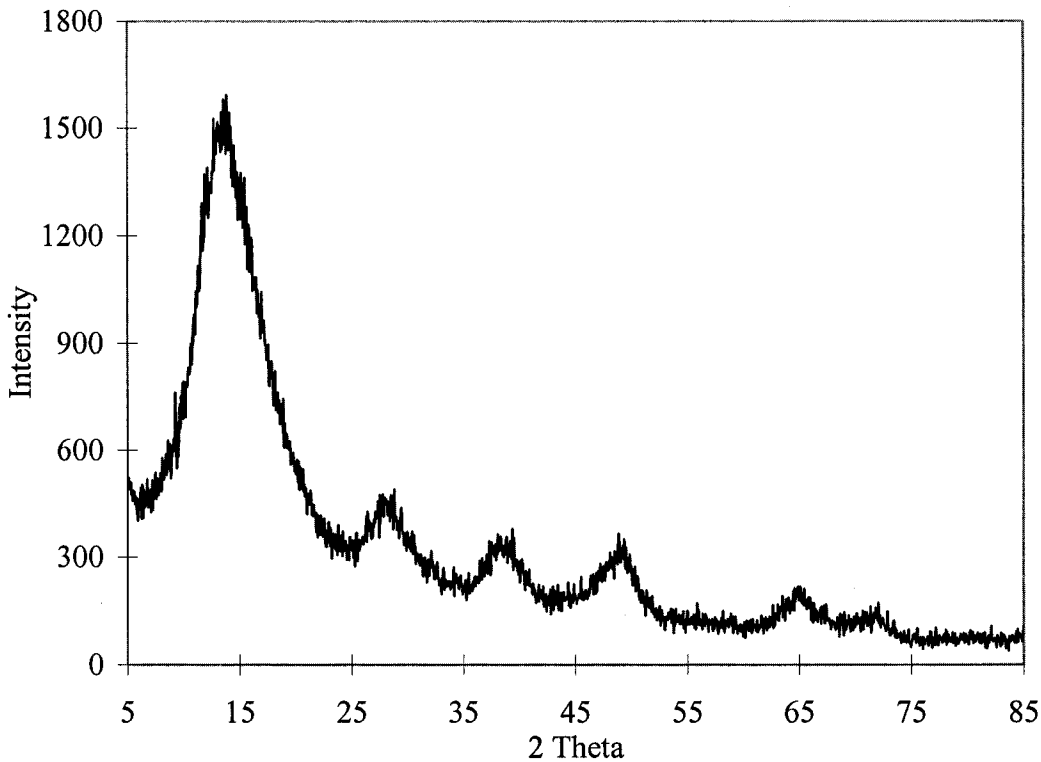
1800
1500
1200
900
600
300
0
Intensity
5
15
25
35
45
55
65
75
85
2 Theta

Figure. 5-2

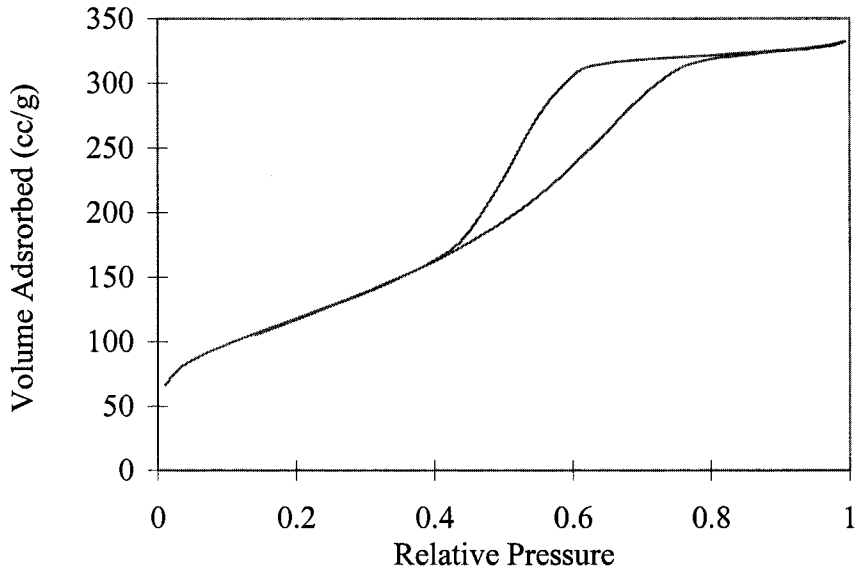
Volume Adsrorbed (cc/g)
350
300
250
200
150
100
50
0
0
0.2
0.4
0.6
0.8
1
Relative Pressure

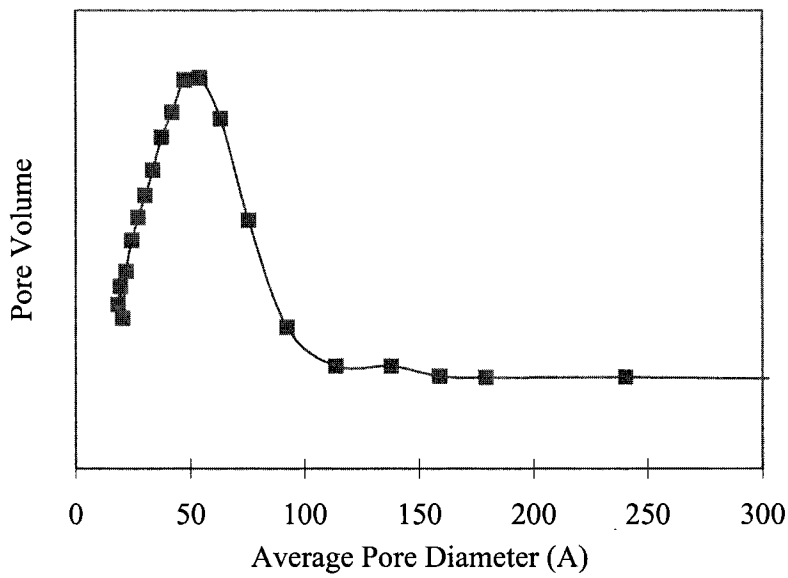
Pore Volume
0
50
100
150
200
250
300
Average Pore Diameter (A)

Figure. 5-3

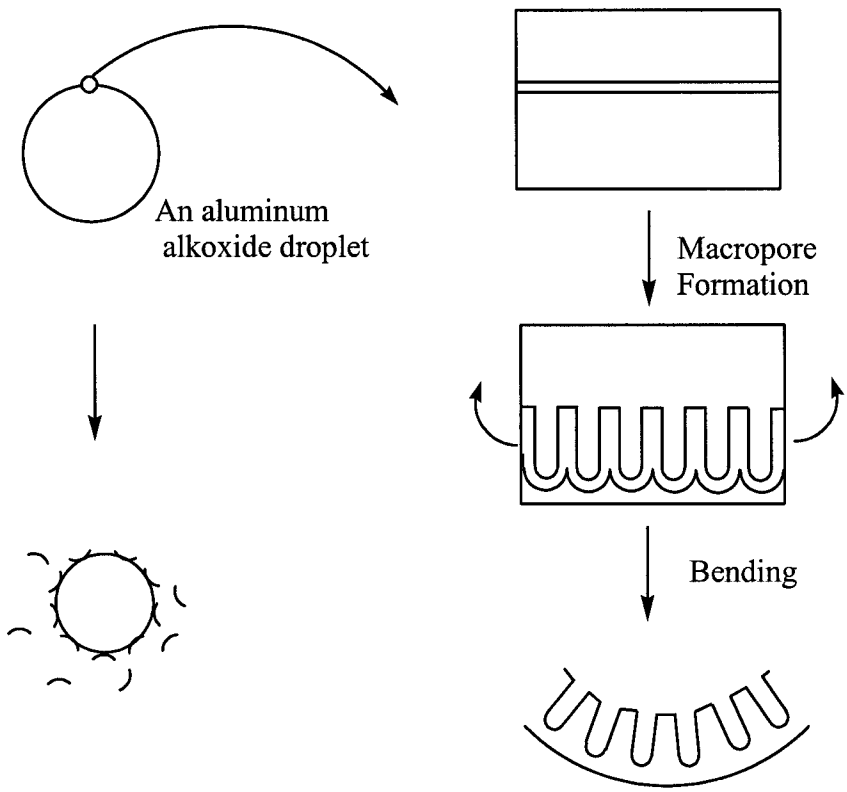
An aluminum
alkoxide droplet
Macropore
Formation
Bending

Figure. 5-4

Chapter 6. General Conclusions and Future Work

6.1. General conclusions

The focus of this work is the synthesis and characterization of mesoporous alumina materials that have desired properties and structures using different methodologies. In the work, mesoporous aluminas were produced by nonionic supramolecular templating and characterized to determine the stability of their physical structure during extended calcination at elevated temperatures. The effect of synthesis temperature on the physical structure of these materials and the resulting thermal evolution from synthesized aluminum hydroxide to transitional alumina was studied using thermogravimetric analysis. A high resolution multiple quantum magic angle spinning NMR spectroscopy method was used to determine quantitatively the evolution of the aluminum coordination during the thermal processing. The mesoporous alumina exhibited high stability upon prolonged heating, which is essential for their future applications in catalytic chemistry.

Using surfactant-mediated synthesis, aluminas with hierarchical nanopores were produced. The hierarchical structures are composed of 4 nm in diameter mesopores and macropores with diameters of about 300 nm. The structures were found to be stable to the thermal removal of the surfactant. Synthesis factors affecting the appearance of the hierarchically structured alumina material were discussed and a parameter space in which macropores could be obtained was determined.

Based on the results from a parameter study and the similarity of the process to the macropore formation on anodized aluminum surface, a mechanism in which an interaction of

water and aluminum alkoxide droplet played a important role was proposed to explain the structural organization for the material at multiple length scales. The function of surfactant and co-solvent in the structure forming process were also investigated. Although surfactant did not direct the macropore formation, it mediated nanoparticles growth and hence mesoporosity of the material through a nanoparticles assembly mechanism.

6.2. Future work

The synthesis of mesoporous alumna material has received more attention due to its potential uses as catalysts, catalyst supports and adsorption media. However, there is still a lot of work needed to develop an ideal alumina material that satisfies industrial requirements. In this work, thermal stability of mesoporous alumina has been characterized under elevated temperatures. As a catalyst candidate, another property of interest is the acidity of the material. It is of importance to characterize the acidity of mesoporous alumina using different instrumental methods. For example, solid state ^{27}Al NMR technique could be used to characterize the material with certain probe molecules linked on its catalytic surface. The acidic sites or the distribution of different coordinated aluminum atoms in the material could be determined. This points the direction on how to develop a material with better catalytic performance by optimizing the reaction conditions.

Hierarchically structured alumina has been synthesized with or without the mediation of a surfactant. A formation mechanism was proposed to explain structural organization at multiple length scales. However, more experimental evidences are needed to validate the speculations made in formulating the mechanism. Since a high reactivity of aluminum alkoxide, it is difficult to detect the hydrolysis or the formation process of the material. An

indirect method would be appropriate to gain more information in structural organization. More correlations could be constructed by investigating the relationship between reaction conditions and characterization results for the material.

The synthesis of hierarchically structured alumina is providing a good substrate to put active sites on. Since the material potentially has an enhanced diffusive property, a better catalytic performance would be expected for it. Works that could be carried on include the investigation of possibility to link functional groups onto the surface of the material and the following catalyst testing for a specific reaction.